DISSERTATION

SATURATED HIGH REPETITION RATE SOFT X-RAY LASERS

Submitted by

Yong Wang

Department of Electrical & Computer Engineering

In partial fulfillment of the requirements

For the Degree of Doctor of Philosophy

Colorado State University

Fort Collins, Colorado

Spring 2007

COLORADO STATE UNIVERSITY

APR, 2, 2007

WE HEREBY RECOMMEND THAT THE DISSERTATION PREPARED UNDER OUR SUPERVISION BY **YONG WANG** ENTITLED **SATURATED HIGH REPETITION RATE SOFT X-RAY LASERS** BE ACCEPTED AS FULFILLING IN PART REQUIREMENTS FOR THE DEGREE OF DOCTOR OF PHILOSOPHY.

Committee on Graduate Work

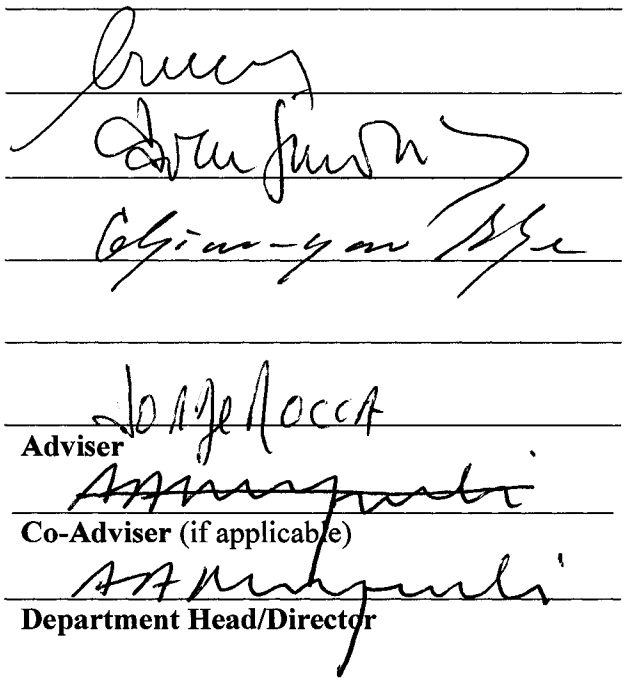

Adviser

Co-Adviser (if applicable)

Department Head/Director

ABSTRACT OF DISSERTATION

SATURATED HIGH REPETITION RATE SOFT X-RAY LASERS

This dissertation resulted in the demonstration of tabletop soft x-ray lasers operating at 5 Hz repetition rate with average powers of 1-5 μW in numerous transition of the $4d^1S_0$-$4p^1P_1$ nickel-like and the $3P^1S_0$-$3S^1P_1$ neon-like ion isolectronic sequences with wavelengths ranging from 32.6 nm to 13.2 nm. The lasers operate in the gain-saturate regime necessary for efficient laser energy generation. Lasing at shorter wavelengths was also observed in transitions of the same nickel-like ion isolectronic sequence, with amplification in the 11.9 nm line of nickel-like Sn approaching gain saturation, and progressively reduced gain for wavelengths as low as 10.9 nm for nickel-like Te. The results were obtained by heating plasmas of selected materials with picosecond duration optical laser pulses of only 1J energy impinging at grazing incidence angles optimized for maximum energy deposition. The grazing incidence pumping geometry takes advantage of the pump beam refraction into the plasma to efficiently deposit a large fraction of its energy into a pre-selected plasma region with optimum electron density for amplification. The soft x-ray lasers were characterized in term of small signal gain, output pulse energy, pulse duration, beam divergence, and spatial coherence. Streak camera measurements for the 13.9 nm nickel-like Ag and 13.2 nm nickel-like Cd laser showed that the laser pulses have a duration of about 5 ps.

To further improve the characteristics of these high repetition rate table-top soft x-ray lasers in terms of peak spectral brightness, short pulse duration, defined

polarization, and spatial coherence, we investigated the seeding of the soft x-ray amplifiers with high harmonic pulses generated in a gas cell using the same pump laser. Amplification of pulses from the 25^{th} harmonic pulses of the Ti:sapphire laser in a 32.6 nm line of Ne-like Ti laser amplifier by nearly two orders of magnitude was demonstrated to generate highly monochromatic laser pulses that were measured to approach full spatial coherence. Based on experimental measurements of the main parameters of the seeded soft x-ray laser pulses the peak spectral brightness is estimated to be $\sim 2\times10^{26}$ photons/(s mm^2 $mrad^2$ 0.01% bandwidth). This scheme for the generation of sub-picosecond soft x-ray laser pulses should be scalable to produce extremely bright lasers at very short wavelength.

These high repetition rate short wavelength lasers will make possible a variety of new studies of surfaces and materials, and enable the development of unique metrology and processing tools for industry. As an example of the potential of these compact lasers as intense sources of soft x-ray light for applications the nickel-like cadmium and silver lasers were used as illumination sources in a table-top high resolution microscope that achieved a spatial resolution better than 38 nm.

Yong Wang
Electrical & Computer Engineering Department
Colorado State University
Fort Collins, CO 80523
Spring 2007

Table of Contents

Chapter 1, Introduction

1.1 Motivation for the Development of Soft X-ray Lasers

Since the time of the invention of the Maser [1] there has been great interest in the generation of intense coherent beams of electromagnetic radiation at shorter and shorter wavelengths. The development of the first optical Lasers in 1960 was an enormous step forward and one of the most important scientific and technological advances of the 20th century [1-3]. Shortly after the realization of the first laser it was envision that lasers operating at x-ray wavelengths would be possible, and theoretical and experimental efforts were started with this goal.

Soft x-ray (SXR) lasers, sometimes also described as Extreme Ultraviolet Lasers (EUV), produce electromagnetic radiation in the 3-50 nm region of the spectrum. These photons are about 10-100 times more energetic than those produced by optical lasers, but still significantly less energetic than those used in medical corresponding to the x-ray radiation that is used for radiology in medical applications. Soft x-ray lasers generate bright highly monochromatic, that can have a high degree of spatial coherence. This laser action is normally realized in highly ionized plasmas. It should be mentioned however that recently the first "free electron" laser operating at soft x-ray wavelength was demonstrated to operate down to 13 nm [4], and efforts are underway to build accelerator based x-ray lasers at much shorter wavelengths [5]. In this dissertation, only plasma-based soft x-ray lasers are described. The first generation of soft x-ray lasers where laboratory size devices, many excited by the same kilojoule energy lasers used to conduct nuclear fusion research [6-8]. These

devices were capable of producing laser shots at repetition frequencies of the order of one shot per hour. Subsequent work increased the repetition rate of gain saturated soft x-ray lasers to a shot every several minutes, and in a reduce footpace [9-11]. Great progress in the development of high repetition rate, high average power soft x-ray lasers was achieved using fast discharge excitation of a capillary plasmas [12-16]. These discharge pumped lasers produced unsurpassed average powers of milliwatts at 46.9 nm, and allowed for numerous applications. However there is a need for high average power lasers at shorter wavelengths. The focus of the work conducted for this dissertation consists in the development of compact "table-top" soft x-ray lasers of the type require to implement scientific applications in a small laboratory at wavelengths below those of the extremely compact capillary discharge lasers.

Soft x-ray coherent light has unique properties that make it of interest for applications. These include its short wavelength that makes it possible to "see" and "write" smaller features; high absorption for most of materials, which make them ideal for surface studies; good degree of coherence for applications such as interferometry and holography; and a photon energy that allows it to interact with inner shell electrons enabling element specific applications.

The above mentioned characteristics enable the implementation of important applications such as nano-scale imaging and patterning. The direct observations of nanoscale structures with light-based microscopes have been hampered by the relatively long wavelength of light. Researchers have had to deduce many aspects of nanostructures more indirectly using conventional electron microscopy or scanning-tunneling or atomic-force microscopy. Soft x-ray microcopy offers an alternative and

complementary approach to high resolution imaging, and makes possible the acquisition of nano-scale resolution images without requiring significant sample preparation. Its high degree of monochromaticity allow the full use of diffractive optical elements, zone plate lenses, that make possible to reach 15 nm resolution when used in combination with sufficiently short wavelength light. High-brilliance tunable synchrotrons sources have allowed the implementation x-ray microscopes to achieve element-specific imaging, thus providing insight into structure composition of magnetic nanostructures and other samples of interest [17]. A 5 Hz repetition rate 13.2 nm wavelength tabletop soft-x-ray lasers developed as part of this thesis has allowed the development of a table-top microscope that takes advantage of the high brightness, high mono-chromaticity, and directionality of the illumination to obtain images with sub-38 nm resolution [18].

Another application of interest is the metrology necessary for the implementation of EUV lithography as a tool for the fabrication of the next generation of computer chips. As transistor features continue to become smaller in size (eg. 32 nm around year 2009- 2010), the semiconductor industry must look to adopt new methods of copying the sophisticated patterns required for the high-volume manufacture of integrated circuits. In order to satisfy the future demand for even smaller feature sizes, EUV lithography is showing the most promise. The development of high reflectivity (~70%) multilayer reflective coatings at wavelengths around 13.5 nm has determined the wavelength chosen by industry for the lithography of the future generation of computer chips. Compact bright light sources emitting at wavelengths in the vicinity of 13.5 nm are required to perform the

necessary metrology and in-situ alignment of the optics, and inspection for defects on the masks. Of particular interest is a sufficiently high coherence to allow for interferometry measurements. A compact high-coherence soft x-ray laser with a high repetition rate operation is one of the promising candidates for this purpose.

A long term goal for the development of compact x-ray lasers at shorter wavelength is the possibility to perform high resolution biological imaging using light in the so-called water window of the spectrum, the region between the carbon and oxygen K-edges (wavelengths from 4.4 nm to 2.3 nm), where a high contrast ratio between carbon and water exists, open the opportunity for high resolution imaging. A more near applications of soft x-ray lasers is their use in spectroscopy. A discharge pumped table-top soft x-ray operating at 46.9 nm, a wavelength longer than those corresponding to the soft x-ray lasers discussed in this dissertation, is currently employed very successfully to produce single ionization of nanoclusters for their study by mass spectroscopy [19, 20]. Shorter wavelength compact lasers will open other spectroscopy opportunities, such as the interaction with inner shell electrons in numerous elements, allowing for element specific spectroscopy.

These and other applications motivates the work in the development of a new generation of more compact soft x-ray lasers capable to operate at repetition rates of several Hz. The next section briefly summarized other methods to produce coherent soft x-ray radiation. Of particular interest is high harmonic generation, that as discussed in Chapter 5, was used to seed for the first time in this work a soft x-ray laser amplifier pumped heating a solid target.

1.2 Methods of Generating Soft X-ray Sources

There are several alternative and often complementary methods to generate intense beams of soft x-ray radiation that can be used for applications. These include synchrotron radiation, and high harmonic generation. Synchrotron radiation is generated when relativistic charge particles are accelerated (undergo a change of direction) in a magnetic field to almost the speed of light. As the electrons are deflected through magnetic fields they create extremely bright light. Synchrotron light is unique in its intensity and average brilliance and it can be generated across the range of the electromagnetic spectrum: from infrared to x-rays. The light is channeled down "beam lines" to experimental workstations where it is used for research. Synchrotron is very powerful soft x-ray source, can provide tunable x-ray light to very short wavelengths with high brightness, and when properly filtered has a high spatial coherence [17]. However it also has some disadvantages: the very large size and the very high cost of the facilities.

High-brightness radiation at discrete wavelengths, $\lambda_N = \lambda_0/N$ (N an odd integer), with λ_N down to ~ 2 nm, can be produced by high harmonic generation (HHG) [21-23]. The harmonics result from the strong non-linear interaction between the electric field of the incident optical laser pulse and the individual atoms. Laser intensities and pulse durations are just at the limits of ionizing the neutral atoms. Harmonic generation from ions is also possible [24]. The resultant harmonics add in phase in the direction of the firing pulse, leading to the appearance of intense high harmonics in a relatively narrow forward radiation cone. High-harmonic generation provides a table-top size light source with unique properties: soft x-ray wavelengths,

ultrashort time duration, coherence, high repetition rate (1 kHz). However compared with soft x-ray lasers, the single pulse energy from HHG is low.

A much higher energy per pulse, in particular cases up to millijoules, can be produced by the direct laser amplification of soft x-ray light in a population inversion produced in a dense plasma by collisions between free plasma electrons and multiply ionized atoms. The amplifying medium can be excited by either a fast discharge or a high power laser. In the case of laser pumped electron collision soft x-ray laser a common way to produce and heat the plasma is to impinge onto the target with a sequence of two pulses. The first is a relatively long pre-pulse (~100-500 ps duration), which creates a plasma that is allowed to expand to reduce electron density gradients. This pre-pulse is followed by an intense picosecond pulse that rapidly heats the plasma to heat the electrons that will produce the population inversions by electron impact excitation. Very recently it was shown that the pumping energy necessary for lasing could be significantly reduced by directing the short pulse onto the target at grazing incidence [25, 26]. This inherently traveling wave pumping geometry takes advantage of the refraction of the pump beam to increase the path length of the rays in the gain region of the plasma, thereby increasing the fraction of the pump energy absorbed in that region. Soft x-ray lasers are generally limited to single pass or double pass amplification of the spontaneous emission (ASE). Soft x-ray lasers generated by heating solid targets can have rather low spatial coherence. To overcome this limitation, seeding of the soft-x-ray-laser amplifier with a high harmonic of an optical laser has been developed as part of this dissertation [27]. This scheme has the advantage of producing extremely bright lasers at very short

wavelengths with full temporal and spatial coherence. In this case the laser pulse duration can be significantly shorter (subpicosecond) and also it is possible to obtain an increase in peak brightness.

1.3 Principles of Soft X-ray Laser Amplification

Lasing at short wavelengths in extreme ultraviolet (EUV) and soft x-ray regions of the spectrum is normally achieved in hot and dense plasmas. While several soft x-ray laser excitation mechanisms have been investigated [28-30], the most successful has been electron impact excitation [31, 32]. Temperatures of several hundred electron volts to above 1 keV are required to collisionally ionize and excite atoms to the required energy levels. As these are well above the binding energies of outer electrons, the atoms are necessarily ionized to a high degree. Upper state lifetimes are typically measured in picoseconds, and at high plasma density the collisional re-distribution of populations is also fast. Therefore to achieve the maximum possible amplification the energy delivery (pumping) must be fast. As a result high power optical lasers or fast high power discharger are generally employed to create and heat the plasma [9, 10, 33-34]. Due to the relatively small value of the stimulated emission cross sections at soft x-ray wavelengths, high gain lasing requires a high density of excited state ions, thus mandating a high density plasma. Preferred electron configurations to implement collisional lasers are those corresponding to neon-like (10 electrons), and nickel-like (28 electrons) ions, which tend to have a large fraction of the plasma ions in a desired ionization state over a broad range of plasma temperatures and densities.

The short lifetime of hot dense plasmas limits the effectiveness of cavity end mirrors. Therefore, in general these are high gain single pass lasers, though some double and triple pass amplification experiments exceptions [35]. Lacking multipass mode control, unseeded short wavelength lasers are typically far from diffraction limited. Temporal coherence lengths, set largely by ion Doppler line broadening, are typically of the order of 10^4 wavelengths.

The pumping power necessary to produce short wavelength lasers scales as $1/\lambda^4$. A EUV/soft x-ray laser amplifier is schematically shown in Fig 1.1.

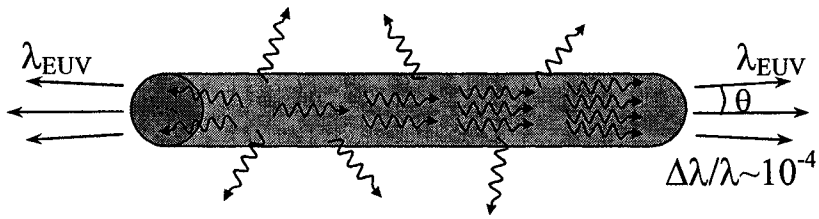

Figure 1.1 Schematic of a plasma column with a population inversion that generates EUV/ Soft X-ray Laser radiation.

The required pump power P, that must be delivered to the lasing medium (plasma) in order to maintain the inverted population density, can be estimated by [17]:

$$P = \frac{h\nu n_u FV}{\tau} \qquad (1.1)$$

where $n_u F$ is the inverted population density, n_u is the density of atoms (ions) in the upper states and F is the density inversion factor, V is the plasma volume, and $h\nu$ is the photon energy that would be emitted by spontaneous emission in a transition of

lifetime τ. In fact this is a lower limit on the required power, as the pumping is far from 100% efficient, $n_u F$ is distributed among several ionization stages, many energy states, and a general investment in thermal energy. Observing that $\tau = 1/A_{ul}$, A_{ul} is Einstein A coefficient, for spontaneous emission. Writing the population inversion as a function of the gain length product GL, where

$$G = \Delta N \cdot \sigma \tag{1.2}$$

$$G = n_u F \cdot \frac{\lambda^2 A_{ul}}{8\pi\Delta\nu} = \frac{\lambda^3 n_u F A_{ul}}{8\pi c(\Delta\lambda/\lambda)} \tag{1.3}$$

ΔN is population inversion density and σ is cross section. The required power per unit volume of plasma becomes:

$$\frac{P}{V} = \frac{8\pi c^2 h(\Delta\lambda/\lambda)G}{\lambda^4} \tag{1.4}$$

so that in terms of the gain-length product, with $V = AL$, the required power per unit area (intensity) is

$$\frac{P}{A} = \frac{8\pi c^2 h(\Delta\lambda/\lambda)GL}{\lambda^4} \tag{1.5}$$

Thus to maintain a population inversion density with a given gain-length product and a linewidth $(\Delta\lambda/\lambda)$ determined by the ion temperature, in the case of Doppler broadening, the requisite laser intensity scales as $1/\lambda^4$; in the case of Natural broadening, it scales as $1/\lambda^5$ [31]. This very rapid scaling of required pump

intensity with lasing wavelength provides a significant challenge for the achievement of laser action at soft x-ray wavelengths.

1.4 Population Inversion Mechanisms

Several population inversion mechanisms were proposed as early as in the 1960's to produce lasing at soft x-ray wavelengths [29]. These mechanisms are briefly summarized below.

a. Photoionization and resonant photopumping

These two population inversion mechanisms for x-ray amplification have in common that the excitation of the laser upper level population involves the use of high energy photons. The generation of large population inversions following the selective x-ray photoionization of inner shell electrons was originally proposed by Duguay and Rentzepis in 1967 [29].

The generation of population inversions by this mechanism is possible because at photon energies just above the threshold for inner shell photoionization the cross section is an order of magnitude larger for inner-shell electrons as compared to outer-shell electrons. This scheme has the potential advantage of leading to relatively compact lasers with wavelengths shorter than 1.5 nm. In principle, it can allow for operation at a low plasma temperature of less than 1 eV with consequently small Doppler broadenings and large gain coefficients. The incoherent x-ray photons that pump the laser media would be normally produced by a nearby plasma created by heating a target made of a high-Z material such as gold with an intense ultrashort

laser pulse. However, no demonstration of a photoionization laser at x-ray wavelengths has yet been realized. Nevertheless, the development of compact lasers capable of producing high peak power laser increases the likelihood that this type of x-ray laser will be realized in the future.

b. Collisional recombination

This population inversion mechanism was first proposed by Gudzenko and Shelepin in 1965 [28]. The first report of large amplification at soft x-ray wavelengths by plasma recombination, corresponds to an experiment realized by Suckewer et al. in 1984 [36]. After that, recombining plasmas pumped by table-top lasers has produced amplification in transitions to the ground state with gains up to g×l=6.5 at wavelengths as short as 13.5 nm [37, 38]. Evidence of amplification by plasma recombination has also been reported in plasmas created by compact electrical discharges [39]. In this scheme, the laser upper level is populated following the recombination of ions with a charge Z+1 with an electron, through a three-body interaction described as collisional or three-body recombination:

$$A^{Z+1} + 2e \rightarrow A^{Z^*} + e \qquad (1.6)$$

This type of process is the inverse of collisional electron ionization. It preferentially populates highly excited bound levels A^{Z^*} of the ion of charge Z, favoring the generation of population inversion [40]. As the reaction above suggests, the collisional recombination rate is proportional to the square of the electron density. The recombination rate is also extremely sensitive to the electron temperature [41].

Therefore, the generation of large population inversion by recombination requires a dense and relatively cold plasma.

c. Collisional electron excitation

This mechanism of excitation of soft x-ray lasers resembles that of some of the most widely utilized visible and ultraviolet ion lasers, the cw argon ion and krypton ion lasers [42, 43], in which the laser upper levels are predominantly excited by direct electron impact collision from the ground state of the ion stage of interest. In the initial implementation of these lasers, the generation of a population inversion occurs in a quasi-cw regime, aided by the very favorable radiative lifetime ratio between the laser upper and lower levels. The upper levels are metastable with respect to radiative decay to the ground state, and the laser lower levels are depopulated by strong dipole-allowed transitions.

This method involves the excitation of closed shell ions. This technique makes use of ionization bottlenecks associated with closed electron shell Ne-like or Ni-like ions to ensure a high density of lasing ions. For example, if the target is made of Silver (Ag), which has 47 electrons, the ionization process strips off 19 electrons, leaving 28, which correspond to the electron configuration of Nickel atoms. This close shell ion is difficult to ionize. This is a significant advantage because it results in a high relative abundance of the lasing ions over a wide range of plasma parameters. Ne-like ions are also very stable, closed-shell ions. The laser upper levels are mostly produced by collisions with plasma electrons, but also receive some contribution by cascading down from higher excited states, and by recombination of

overly ionized F-like ions. In steady state the population inversion is maintained by rapid radiative decay of the lower lasing level.

The first successful demonstration of lasing at soft x-ray wavelengths utilizing this approach was realized at Lawrence Livermore National Laboratory and involved the 3p–3s transitions in Ne-like Se and Ne-like Y [44]. Subsequent experiments demonstrated lasing in Ni-like ion transitions [45].

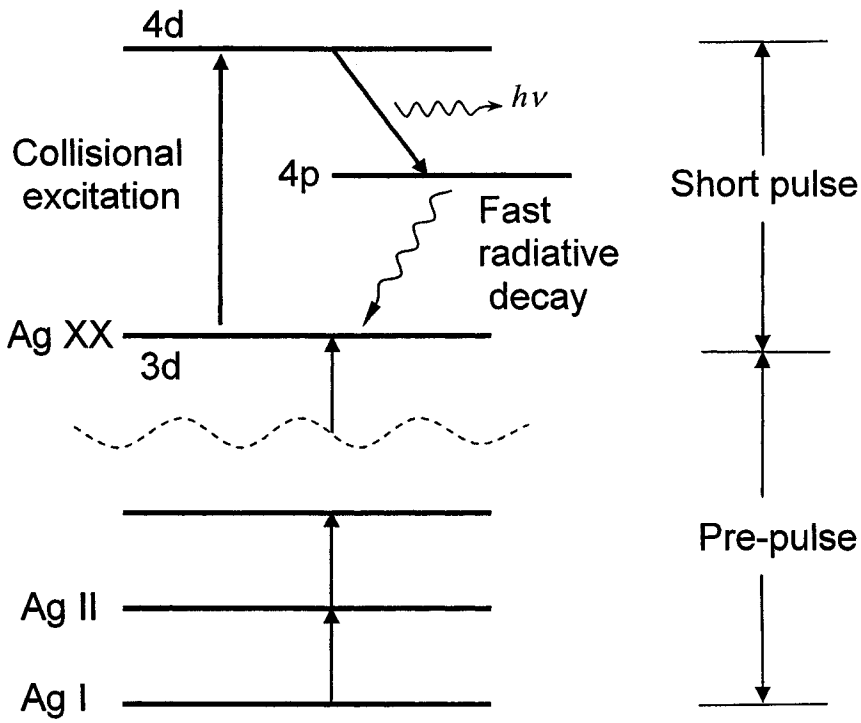

Figure 1.2 Energy level diagram of Ni-like Ag

Less pump energy is required by using two pump pulses, one of about a nanosecond and another in the picosecond range. Figure 1.2 shows the energy level diagram of a Ni-like Ag collisional laser. The pre-pulse is a relatively modest intensity nanosecond duration pulse that pre-forms a plasma to the desired ionization

stage. The plasma is then allowed to expand for 1-2 ns, creating a larger plasma with more gentle density gradients. The arrival of the short pulse rapidly heats the plasma collisionally exciting the Ne-like or Ni-like ground state ions to higher excited states. Differences in collisional excitation rates among the various excited states provide the desired population inversion. The more gentle density gradients reduce refraction in the plasma, increase the potential lasing volume, and permits a more efficient use of the energy from the picosecond heating pulse.

d. Transient collisional excitation

The optical pump laser energy necessary to pump collisional lasers can be greatly reduced with the use of picosecond duration short heating pulse to create large transient population inversions [9]. In the transient inversion scheme [46], a population inversion is formed as a result of differences between the rates of collisional pumping into the upper and lower laser levels. If a plasma of suitable lasant ions can be rapidly heated with a timescale shorter than the collisional and radiative relaxation processes, a very large transient population inversions can be created for a time period of several picoseconds, and before further significant ionization occurs. Over timescales longer than a few picoseconds, relaxation processes become important and the plasma enters the more "traditional" quasi-steady-state (QSS) regime. A smaller population inversion may then also be formed, over a longer timescale, relying on the same collisional excitation processes but also as a result of the favorable rates of radiative decay of the upper laser levels relative to the lower laser levels.

In practice, the implementation of the transient inversion scheme involves a combination of pre-pulse and short heating pulses. The pre-pulse is of relatively low intensity (~ 10^{12} W. cm^{-2}) and performs a column of plasma, heated to produce an sufficiently high abundance of lasant ions. This pre-plasma expands hydro-dynamically, reducing electrical density gradients, and once the lasant ion fraction is optimized, the high intensity picosecond pulse (~ 10^{15} W.cm^{-2}) rapidly heats the plasma to electron temperatures typically above 500 eV range.

Transient inversion soft x-ray lasers have significant advantages over collisionally pumped soft x-ray lasers operating in the QSS regime in terms of the pump energy required for operation. QSS x-ray lasers utilize the same, relatively long pulse (0.1–1.0 ns) for both creation and excitation of the desired ion stage. In both cases the long duration low energy prepulse is also used to reduce the density gradients. The difference between the two schemes resides in the consequences of using a much shorter heating pulse in the transient scheme. Since the optimum collision rate into the upper laser level occurs at a higher electron temperature than allows a significant steady state fraction of Ni-like (or analogously Ne-like) lasant ions to exist, the single pump pulse thus has two strongly conflicting roles to play. By using a heating pulse of much shorter duration in the transient inversion scheme, with each of the two pulses specifically tailored to its role of either creating an abundance of lasant ions or rapid heating, the energy in the pump pulses is much more efficiently used.

The pump energy required to saturate Ni-like lasers has been improved by nearly an order of magnitude using the picosecond transient inversion techniques

combined with a true traveling wave illumination that allows the pump pulse to propagate at the same speed as the amplified soft x-ray laser pulse [46].

The transient inversion collisional scheme has undergone the extensive development. The first gain-saturated operation for Ne-like ion sequence conducted in Ti (λ=32.6 nm), Fe (25.5 nm), Ge (19.6 nm) employed pump energies well above 10 J [9]. However the Ni-like ion sequence, that scales down in wavelength more rapidly as a function of the nuclear charge Z, became the center of the interest. Gain-saturated operation for elements such as Mo, Pd, Ag has been obtained with a total pump energy of only 7 J [11]. The spectral range between the 12 and 15 nm has been extremely investigated due to efficient optical elements available (reflectivity up to 70%).

In an alternative approach of the collisional excitation mechanism the atoms are ionized by tunnel ionization in the high electric field of the driving laser. The electrons produced by optical field ionization using a circularly polarized beam retain the energy acquired during the laser pulse, providing an excellent match with the cross sections necessary to excite the laser upper levels by electron collisions from the ion ground state. Optical field driven soft x-ray lasers operating at 10 Hz repetition rate driven by highly intense Ti:Sa pulses of less than 1 J have been demonstrated in Pd-like Xe at 41.8 nm and in Ni-like Kr at 32.8 nm [47, 48].

1.5 Implementation of Collisional Soft X-ray Lasers

Kilo-joule energy lasers were required for the first generation of laboratory size soft x-ray lasers. New opportunities for the efficient pumping of table-top soft x-

ray lasers aroused from the development of compact, very high power ultrafast optical lasers based on the technique of chirped-pulse amplification (CPA) [49] and fast electrical discharges in capillary tubes [12-16].

Significant effort has been placed in the development of high repetition rate soft x-ray lasers for applications [14-16, 48, 50-52]. A pumping method consisting of a fast electrical discharge in a capillary tube has been proposed and successfully developed [13]. Capillary discharge lasers operating at 46.9 nm in Ne-like Ar offer the highest average power (3.5 mW) among all compact coherent soft X-ray sources. The chirped-pulse amplification technique developed in the late 1980s opened new opportunities for the development of compact high repetition rate soft x-ray lasers This technique gets around the problem of self focusing of very intense beams on solid state laser amplifiers by expanding a very short pulse before it travels through the amplifiers and then compressing it to its original pulsewidth using a grating compressor. The chirped pulse amplification technique presently allows for the generation of Ti:sapphire laser pulses with several tens of terawatts from tabletop systems operating at repetition rates of typically 10 Hz.

Using chirp pulse amplification pump lasers saturated operation at a repetition rate of one shot every several minutes has been obtained at several wavelengths between 13.9 and 33 nm by transient collisional electron excitation of targets at normal incidence with 3-10 J of short pulse pump energy [9, 11]. Different pumping configurations have been investigated to further reduce the necessary pumping energy and enable operation at higher repetition rate. Excitation of a Mo target with 150 fs, 300 mJ pulses impinging at 60 degrees from normal incidence resulted in the

appearance of the 18.9 and 22.6 nm laser lines of Ni-like Mo [53]. Longitudinal pumping at 10 Hz produced non-saturated amplification at 18.9 nm in Ni-like Mo [54]. Recently, it has been demonstrated that the energy deposition efficiency of the short pulse can be significantly increased by directing it at grazing incidence [25, 26, 55]. This inherently traveling wave pumping geometry takes advantage of the refraction of the pump beam to increase the path length of the rays in the gain region of the plasma, thereby increasing the fraction of the pump energy absorbed in that region. Pumping of the 18.9 nm line of Ni-like Mo with 150 mJ of total pumping energy from a 10 Hz laser was reported to generate a gain-length product of ~ 15 [55], As part of the present work the use of 1 J heating pulses resulted in laser operation in the gain-saturated regime and in the generation of 150 nJ soft x-ray laser pulses [25]. Several important applications, including the metrology necessary for of extreme ultraviolet lithography at 13.5 nm create significant interest in the development of high average flux soft x-ray lasers at shorter wavelengths [17].

This dissertation discusses the demonstration and characterization of high repetition rate table top soft x-ray lasers in transitions of Ni-like and Ne-like ions. Saturated amplification of lasers operating at 5 Hz repetition rates at wavelengths between 32.6 nm and 13.2 nm was demonstrated. Average powers >1 μW were obtained using picosecond laser heating pulses with an energy of only 1 J by optimizing the angle of incidence for maximum energy deposition. Lasing was also observed for shorter wavelength transitions of the same isoelectronic sequence, with amplification in the 11.9 nm line of Ni-like Sn approaching gain saturation, and progressively reduced gain for wavelengths as low as 10.9 nm for Ni-like Te [56-58].

To further improve the characteristics of these high repetition rate table-top soft x-ray lasers we investigated the seeding of the soft x-ray amplifiers with high harmonic pulses generated in a gas cell using the same pump laser. Amplification of pulses from the 25th harmonic pulses of the Ti:sapphire laser in a 32.6 nm line of Ne-like Ti laser amplifier by nearly two orders of magnitude was demonstrated to generate highly monochromatic laser pulses that were measured to approach full spatial coherence. Based on experimental measurements of the main parameters of the seeded soft x-ray laser pulses the peak spectral brightness is estimated to be $\sim 2\times10^{26}$ photons/(s mm^2 mrad^2 0.01% bandwidth).

These high repetition rate soft x-ray lasers will enable new applications in science and the development of unique metrology and processing tools for industry.

1.6 Outline of this Dissertation

The remainder of this thesis is outlined below. Chapter 1 describes the motivation of this work and discusses the principles of soft x-ray laser amplification, including difference possible laser excitation mechanisms. Emphasis is placed in the transient collisional scheme used to obtain the results discussed in the following chapters.

Chapter 2 describes the experimental techniques employed to obtain the results. These include the details of the grazing incidence pumping geometry employed to pump the lasers, the Ti:Sapphire chirped-pulse-amplification pump laser system used, and soft x-ray laser diagnostics setup. Chapter 3 describes the demonstration of soft x-ray lasers in transitions of Ni-like and Ne-like x-ray lasers

with variable materials at wavelengths ranging from 32.6 nm to 10.9 nm, with saturated output down to 13.2 nm. Measurements of the gain, and results of the optimization of the lasers in terms of the time delay between pump pulses, pump pulse duration, grazing incidence angle are presented. Chapter 4 describes measurements conducted to characterize the output of the Ni-like x-ray laser beam. This includes measurements of the beam divergence, spatial coherence, and the determination of the soft x-ray laser pulse duration using a fast streak camera.

Chapter 5 describes the demonstration of a Ne-like Ti soft x-ray laser amplifier seeded by high harmonic pulses from the Ti:Sapphire laser. This technique results in the generation of highly monochromatic soft x-ray pulses of low divergence, extremely high spectral brightness and nearly full spatial coherence. Chapter 6 provides a summary and includes a brief discussion of the use of these lasers in high resolution microscopy as an example of the significant potential of these high repetition rate soft x-ray lasers in applications.

Reference:

[1] A. L. Schawlow and C. H. Townes, "Infrared and Optical Masers," Phys. Rev. 112, 1940-1949, (1958)

[2] T. Maiman, "Stimulated Optical Radiation in Ruby," Nature (London) 187, 493 (1960).

[3] A. Javan, W. R. Bennett, Jr., and D. R. Herriott "Population Inversion and Continuous Optical Maser Oscillation in a Gas Discharge Containing a He-Ne Mixture," Phys. Rev. Lett. 6, 106–110 (1961)

[4] recent results of Tesla FEL:

http://zms.desy.de/press/pressreleases/2006nbsp/pr_070906/index_eng.html

[5] SLAC-PUB-6541 "Short Wavelength FELs Using the SLAC Linac."

[6] D. L. Matthews, P. L. Hagelstein, M. D. Rosen, M. J. Eckart, N. M. Ceglio, A. U. Hazi, H. Medecki, B. J. MacGowan, J. E. Trebes, B. L. Whitten, E. M. Campbell, C. W. Hatcher, A. M. Hawryluk, R. L. Kauffman, L. D. Pleasance, G. Rambach, J. H. Scofield, G. Stone, and T. A. Weaver "Demonstration of a Soft X-Ray Amplifier," Phys. Rev. Lett. 54, 110–113 (1985)

[7] B. J. MacGowan, S. Maxon, P. L. Hagelstein, C. J. Keane, R. A. London, D. L. Matthews, M. D. Rosen, J. H. Scofield, and D. A. Whelan, "Demonstration of soft x-ray amplification in nickel-like ions," Phys. Rev. Lett. 59, 2157–2160 (1987)

[8] A Carillont, M J Edwardsf, M GrandeP, M J de C Henshawl, P Jaeglet, G Jamelott, M H Key, G P Kiehn, A Klisnickt, C L S Lewis, D O'Neillfl, G J Pertll, S A Ramsden, C M E Regany, S J Rose, R Smith and O Willi, "Soft x-ray amplification in aluminium recombining plasma produced from a thin coated fibre," J. Phys. B: At. Mol. Opt. Phys. 23, 147-163 (1990)

[9] P. V. Nickles, V. N. Shlyaptsev, M. Kalachnikov, M. Schnürer, I. Will, and W. Sandner, "Short Pulse X-Ray Laser at 32.6 nm Based on Transient Gain in Ne-like Titanium," Phys. Rev. Lett. 78, 2748–2751 (1997)

[10] J. Dunn, A. L. Osterheld, R. Shepherd, W. E. White, V. N. Shlyaptsev, and R. E. Stewart, "Demonstration of X-Ray Amplification in Transient Gain Nickel-like Palladium Scheme," Phys. Rev. Lett. 80, 2825–2828 (1998)

[11] J. Dunn, Y. Li, A. L. Osterheld, J. Nilsen, J. R. Hunter, and V. N. Shlyaptsev, "Gain Saturation Regime for Laser-Driven Tabletop, Transient Ni-Like Ion X-Ray Lasers," Phys. Rev. Lett. 84, 4834–4837 (2000)

[12] J. J. Rocca, V. Shlyaptsev, F. G. Tomasel, O. D. Cortázar, D. Hartshorn, and J. L. A. Chilla, "Demonstration of a Discharge Pumped Table-Top Soft-X-Ray Laser," Phys. Rev. Lett. 73, 2192–2195 (1994)

[13] J. J. Rocca, D. P. Clark, J. L. A. Chilla, and V. N. Shlyaptsev, "Energy Extraction and Achievement of the Saturation Limit in a Discharge-Pumped Table-Top Soft X-Ray Amplifier," Phys. Rev. Lett. 77, 1476–1479 (1996)

[14] B. R. Benware, C. D. Macchietto, C. H. Moreno, and J. J. Rocca, "Demonstration of a High Average Power Tabletop Soft X-Ray Laser," Phys. Rev. Lett. 81, 5804–5807 (1998)

[15] C. D. Macchietto, B. R. Benware, and J. J. Rocca, "Generation of millijoule-level soft-x-ray laser pulses at a 4-Hz repetition rate in a highly saturated tabletop capillary discharge amplifier," Opt. Lett. 24, 1115 (1999)

[16] S. Heinbuch, M. Grisham, D. Martz, and J.J. Rocca, "Demonstration of a desk-top size high repetition rate soft x-ray laser," Opt. Express 13, 4050 (2005)

[17] D.T. Attwood. Soft X-Rays and Extreme Ultraviolet Radiation: Principles and Applications. Cambridge University Press. (Cambridge, England, 1999)

[18] G. Vaschenko, C. Brewer, F. Brizuela, Y. Wang, M. A. Larotonda, B. M. Luther, M. C. Marconi, J. J. Rocca, C. S. Menoni, E. H. Anderson, W. Chao, B. D. Harteneck, J. A. Liddle, Y. Liu, and D. T. Attwood "Sub-38 nm resolution tabletop microscopy with 13 nm wavelength laser light." Opt. Lett. 31, 1214 (2006)

[19] F. Dong, S. Heinbuch, J. J. Rocca, and E. R. Bernstein, "Dynamics and fragmentation of van der Waals clusters: $(H_2O)_n$, $(CH_3OH)_n$, and $(NH_3)_n$ upon ionization by a 26.5 eV soft x-ray laser" J. Chem. Phys. 124, 224319 (2006)

[20] S. Heinbuch, F. Dong, J. J. Rocca, and E. R. Bernstein "Single photon ionization of van der Waals clusters with a soft x-ray laser: $(CO_2)_n$ and $(CO_2)n(H_2O)_m$," J. Chem. Phys. 125, 154316 (2006)

[21] T. Ditmire, T. Donnelly, R. W. Falcone, and M. D. Perry, "Strong X-Ray Emission from High-Temperature Plasmas Produced by Intense Irradiation of Clusters," Phys. Rev. Lett. 75, 3122–3125 (1995)

[22] Ivan P. Christov, Margaret M. Murnane, and Henry C. Kapteyn, "High-Harmonic Generation of Attosecond Pulses in the "Single-Cycle" Regime," Phys. Rev. Lett. 78, 1251–1254 (1997)

[23] Jeffrey L. Krause, Kenneth J. Schafer, and Kenneth C. Kulander, "High-order harmonic generation from atoms and ions in the high intensity regime," Phys. Rev. Lett. 68, 3535–3538 (1992)

[24] David M. Gaudiosi, Brendan Reagan, Tenio Popmintchev, Michael Grisham, Mark Berrill, Oren Cohen, Barry C. Walker, Margaret M. Murnane, Henry C. Kapteyn, and Jorge J. Rocca, "High-Order Harmonic Generation from Ions in a Capillary Discharge," Phys. Rev. Lett. 96, 203001 (2006)

[25] V.N. Shlyaptsev, J. Dunn, S. Moon, R. Smith, R. Keenan, J. Nilsen, K.B. Fournier, J. Kuba, A.L. Osterheld, J.J. Rocca, B. Luther, Y. Wang, M. Marconni, Proc. of SPIE 5197 Soft X-Ray Lasers and Applications V (SPIE, Bellingham, WA, 2003), 221 (2003)

[26] R. Keenan, J. Dunn, V.N. Shlyaptsev, R. Smith, P.K. Patel, D.F. Price Proc. of SPIE 5197 Soft X-Ray Lasers and Applications V (SPIE, Bellingham, WA, 2003), 213 (2003)

[27] Y. Wang, E. Granados, M. A. Larotonda, M. Berrill, B. M. Luther, D. Patel, C. S. Menoni, and J. J. RoccaD. "High-Brightness Injection-Seeded Soft-X-Ray-Laser Amplifier Using a Solid Target," Phys. Rev. Lett. 97, 123901 (2006)

[28] G. A. Gudzenko and L. A. Shelepin, Zh. Eksp. Teor. Fiz. 45, 1445 (1963) [Sov. Phys. JETP 18, 998 (1964)]

[29] M. A. Duguay and P. M. Rentzepis, "Approaches to vacuum ultraviolet and x-ray lasers,"Appl. Phys. Lett. 10, 350 (1967)

[30] A. G. Molchanov, Sov. Phys. Usp. 15, 124 (1972)

[31] J. J. Rocca, "Table-top soft x-ray lasers," Review of Scientific Instruments, 70, 3799 (1999)

[32] H. Daido, "Review of soft x-ray laser researches and developments," Rep. Prog. Phys. 65, 1513–1576 (2002)

[33] J. J. Rocca, O. D. Corta´zar, B. Szapiro, K. Floyd, and F. G. Tomasel, "Fast-discharge excitation of hot capillary plasmas for soft-x-ray amplifiers," Phys. Rev. E 47, 1299 (1993)

[34] J. J. Rocca, O. D. Corta´zar, F. G. Tomasel, and B. T. Szapiro, "Efficient generation of highly ionized calcium and titanium plasma columns for collisionally excited soft-x-ray lasers in a fast capillary discharge," Phys. Rev. E 48, R2378 (1993)

[35] Natale M. Ceglio, David P. Gaines, James E. Trebes, Richard A. London, Daniel G. Stearns, "Time-resolved measurement of double-pass amplification of soft X rays," Applied Optics 27, 5022 (1988)

[36] S. Suckewer, C. H. Skinner, H. Milchberg, C. Keane, and D. Voorhees, "Amplification of stimulated soft x-ray emission in a confined plasma column," Phys. Rev. Lett. 55, 1753 (1985)

[37] Y. Nagata, K. Midorikawa, S. Kubodera, M. Obara, H. Tashiro, and K. Tokoda, "Soft-x-ray amplification of the Lyman-α transition by optical-field-induced ionization," Phys. Rev. Lett. 71, 3774 (1993)

[38] D. Korobkin, C. H. Nam, S. Suckewer, and A. Golstov, "Demonstration of Soft X-Ray Lasing to Ground State in Li III," Phys. Rev. Lett. 77, 5206 (1996)

[39] J. J. Rocca, M. C. Marconi, B. T. Szapiro, and J. Meyer, Proc. SPIE 1551, 275 (1991)

[40] D. R. Bates and A. Dalgarno, in Atomic and Molecular Processes, edited by D. R. Bates (Academic, New York, 1962), p. 245.

[41] F. V. Bunkin, V. I. Der Zhiev, and S. I. Yakovlenko, "Prospects for light amplification in the far ultraviolet," Sov. J. Quantum Electron, 11, 981 (1981)

[42] W. B. Bridges, "Ionized gas lasers," in Handbook of Laser Science and Technol. Sec. 2, Vol. II. edited by M. J. Weber (Chemical Rubber Corp., Boca Raton, 1982)

[43] M. A. Dunn and J. N. Ross, "The argon ion laser," Prog. Quantum Electron. 4, 233 (1976)

[44] D. L. Matthews et al., Phys. Rev. Lett. 54, 110 (1985); M. D. Rosen, P. L. Hagelstein, D. L. Matthews, E. M. Campbell, A. U. Hazi, B. L. Whitten, B. MacGowan, R. E. Turner, and R. W. Lee, ibid. 54, 106 (1985).

[45] B. J. MacGowan, S. Maxon, P. L. Hagelstein, C. J. Keane, R. A. London, D. L. Matthews, M. D. Rosen, J. H. Scofield, and D. A. Whelan, "Demonstration of soft x-ray amplification in nickel-like ions," Phys. Rev. Lett. 59, 2157–2160 (1987)

[46] P. J. Warwick, K. A. Janulewicz, M. P. Kalachnikov, A. Klisnick, C. L. S. Lewis, W. Sandner, and P. V. Nickles, "Transient Inversion Soft X-Ray Lasers," IEEE J. Sel. Topics Quantum Electron., vol. 5, 6, 1447, (1999)

[47] B. E. Lemoff, G. Y. Yin, C. L. Gordon III, C. P. J. Barty, and S. E. Harris, "Demonstration of a 10-Hz Femtosecond-Pulse-Driven XUV Laser at 41.8 nm in Xe IX" Phys. Rev. Lett. 74, 2574 (1995)

[48] S. Sebban, R. Haroutunian, Ph. Balcou, *et al*, "Saturated Amplification of a Collisionally Pumped Optical-Field-Ionization Soft X-Ray Laser at 41.8 nm," Phys. Rev. Lett. **86**, 3004, (2001) and S. Sebban, T. Mocek, D. Ross, *et al.* "Demonstration of a Ni-Like Kr Optical-Field-Ionization Collisional Soft X-Ray Laser at 32.8 nm," Phys. Rev. Lett. 89, 253901 (2002)

[49] D. Strickland and G. Mourou, "Compression of amplified chirped optical pulses" (first paper on CPA), Opt. Commun. 56, 219 (1985)

[50] C. D. Macchieto, B. R. Benware, J. J. Rocca, "Generation of millijoule-level soft-x-ray laser pulses at a 4-Hz repetition rate in a highly saturated tabletop capillary discharge amplifier," Opt. Lett. 24, 1115 (1999)

[51] D.V. Korobkin, C.H. Nam, S. Suckewer, A. Goltsov, "Demonstration of Soft X-Ray Lasing to Ground State in Li III," Phys. Rev. Lett. **77**, 5206 (1996)

[52] K.A. Jenulewicz, A. Lucianetti, G. Pruebe, W. Sadner and P.V. Nickles. "Saturated Ni-like Ag x-ray laser at 13.9 nm pumped by a single picosecond laser pulse," Phys. Rev. A 68, 051802, (2003)

[53] R. Tommasini, J. Nilsen, E. E. Fill, "Investigations on 10-Hz sub-Joule fs-laser pumped neon- and nickel-like x-ray lasers," Proc. of SPIE 4505, 85 (2001)

[54] T. Ozaki, R. A. Ganeev, A. Ishizawa, T. Kanai, H. Kuroda, "Highly Directive 18.9 nm Nickel-like Molybdenum X-Ray Laser Operating at 150 mJ Pump Energy," Phys. Rev. Lett. **89,** 253902 (2002), and R. Li and Z. Z. Xu "Highly efficient transient collisional excitation X-ray laser in Ni-like Mo ions," Journal de Physique IV, 11 (PR2) 27 (2001)

[55] R. Keenan, J. Dunn, P. K. Patel, D. F. Price, R. F. Smith, V. N. Shlyaptsev, "High-Repetition-Rate Grazing-Incidence Pumped X-Ray Laser Operating at 18.9 nm," Phys. Rev. Lett., 94, 103901 (2005)

[56] B. M. Luther, Y. Wang, M. Larotonda, D. Alessi, M. Berrill, M. Marconi, V. Shlyaptsev, J. J. Rocca, "Saturated high-repetition-rate 18.9-nm tabletop laser in nickellike molybdenum," Opt. Lett. 30, 165 (1999).

[57] Y. Wang, M. A. Larotonda, B. M. Luther, M. C. Marconi, D. Alessi, M. Berrill, V. N. Shlyaptsev, and J. J. Rocca, "Demonstration of saturated high repetition rate

tabletop soft X-ray lasers at wavelengths down to 13.9 nm," Phys. Rev. A., vol. 72, p. 053807, 2005.

[58] J. J. Rocca, Y. Wang, M. A. Larotonda, B. M. Luther, M. Berrill, and D. Alessi, "Saturated 13.2 nm high-repetition-rate laser in nickellike cadmium." Opt. Lett. 30, 2581-2583 (2005).

Chapter 2, Grazing Incidence Pumping of Transient Collisional Soft X-ray Lasers

2.1 Introduction

This chapter introduces the concept of grazing incidence pumping, which can improve the efficiency of laser pumped soft x-ray lasers by delivering heating laser energy into optimum electron density for amplification. Soft x-ray laser pumping geometry and implementation are also described. A high power laser system is required to create hot plasma to generate population inversion. In this chapter, the details of Ti:Sapphire chirped pulse amplification (CPA) pump laser system will be described.

2.2 Concept of Grazing Incidence Pumping

In our experiment, the gain medium is a plasma column, created by a sequence of two laser pulses. We use 120 ps, 350 mJ pulse as pre-pulse to create a pre-formed plasma, and use 8 ps, 1 J short pulse as heating pulse at a grazing incidence angle (Fig. 2.1). Ne-like and Ni-like targets with selected material were shot to generate plasma for different wavelength. The grazing incidence pumping (GRIP) uses refraction of the short laser pump in the pre-formed plasma to deliver the laser energy into a specific electron density region where the population inversion takes place.

The grazing incidence pumping scheme is proposed to dramatically improve the efficiency of laser-pumped x-ray lasers. From the Figure 2.1, the pre-pulse is a 120 ps long pulse that hits a solid, polished target at normal incidence. This pulse

ablates the target, creates and heats the plasma. After a selected time delay, that allows the plasma to expand and reduce the electron density gradients, a grazing incidence picosecond pulse heats a selected portion of the plasma, which has optimum density for amplification. Refraction of the pump beam into the plasma couples the beam with a predefined optimum gain region. This is possible due to the fact that light coming at an angle is refracted at an electron density given by this expression:

$$\theta = (n_e / n_c)^{1/2} \qquad (2.1)$$

where n_e is the maximum electron density within the amplification region and n_c is the critical density at the wavelength of the pump.

This allows a very efficient energy deposition into the region of maximum gain. And therefore reduces the energy requirement for the pump beams, compared with normal incidence scheme.

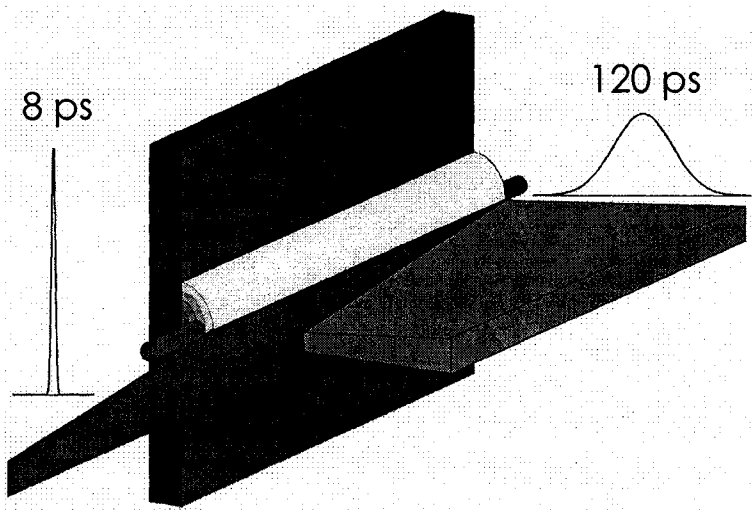

Figure 2.1 Grazing incidence pumping geometry

In laser pumped EUV and soft X-ray lasers, grazing incident angle can increase the interaction length between plasma and laser.

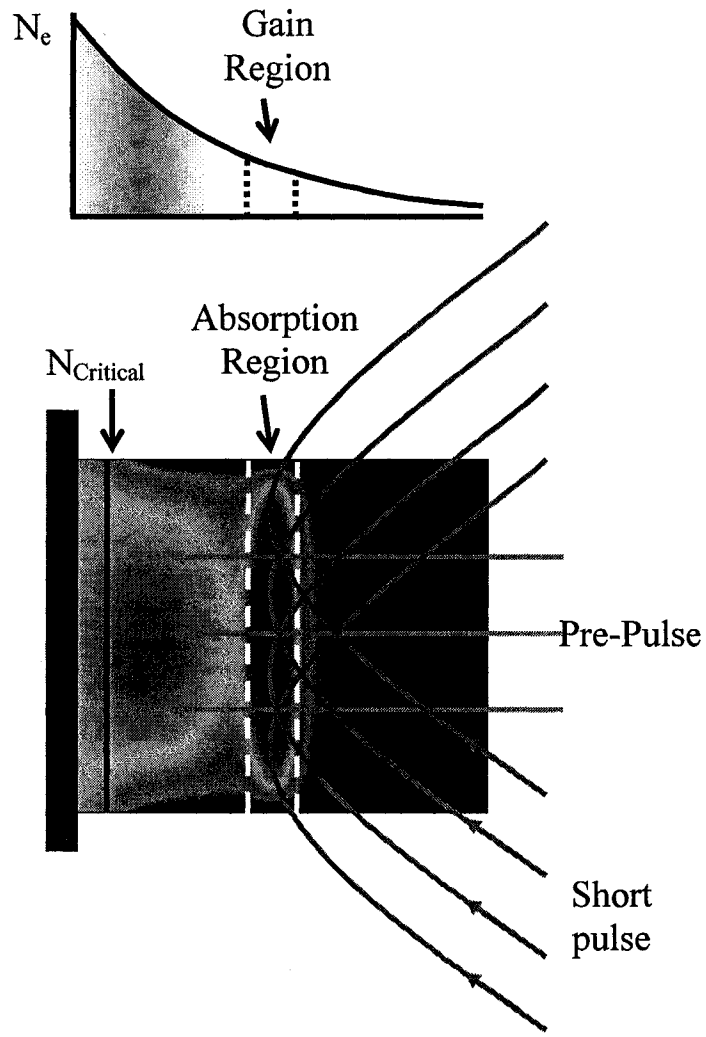

Figure 2.2 Grazing incidence pumping geometry increases interactive length of the pump beam

From Figure 2.2, grazing incidence allows for efficient heating of plasma region of selected electron density. The output soft x-ray laser can be optimized by changing this angle [1]. If grazing incidence angle is too big, the short pulse will go through from high density plasma where the density gradient is too steep so the refraction angle is high, and the efficiency of energy extraction became low. If the

grazing incident is too small, the pump beam energy is deposited in a region where the electron density is lower than the optimum value for maximum output intensity. The plasma density is not high enough so that the gain is also low. That's why we did a lot of work to optimize the grazing incidence angle for different target (details in Chapter 3).

The above discussion is illustrated in Fig. 2.3 by model simulation results for the specific case of the 14.7 nm Ni-like Pd laser for which we present experimental results in chapter 3. These results were obtained using a 1.5 D hydrodynamic/atomic physics code with multicell radiation transport and beam refraction developed at Colorado State University by Mark Berrill. The simulation compares normal incidence and 20° grazing incidence irradiation of a 4 mm long Pd plasma heated by a 1 J pulse of 8 ps duration focused to an intensity of 8×10^{13} $W.cm^{-2}$. The plasma is assumed to be created by a 350 mJ prepulse of 120 ps duration impinging at normal incidence onto the target. In the case of normal incidence pumping the picosecond pulse rapidly heats the region near the critical density, generating a transient gain with a peak gain coefficient of about 200 cm^{-1} at a distance of about 10 μm from the target, where the value of the electron density is close to 2×10^{21} cm^{-3}. However in this region the amplified soft X-rays refract out of the high gain region in only several hundred micrometers, inhibiting amplification to large intensities. In contrast, at 20° grazing incidence angle the pump beam energy is coupled into the region of the plasma with $N_e=2\times10^{20}$ cm^{-3}, where the peak small signal gain is computed to be 80 cm^{-1} and the refraction length L_r is larger than the 4-mm target length, allowing amplification to intensities that exceed the gain saturation intensity.

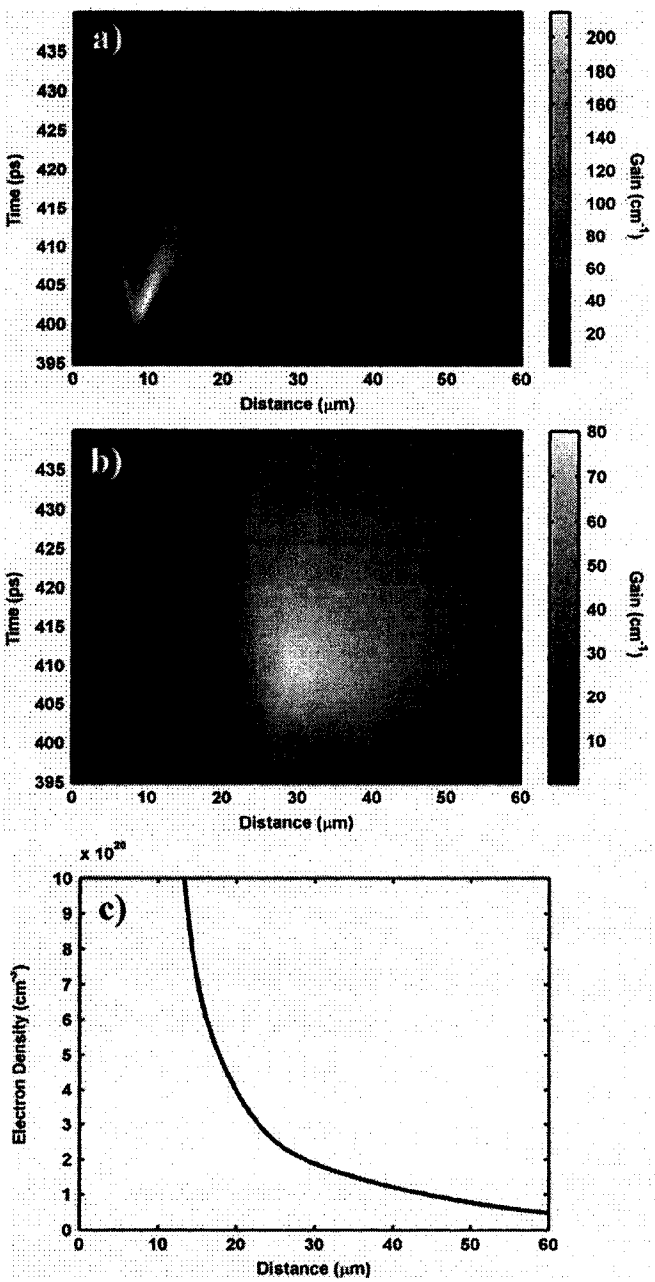

Fig. 2.3. Simulated gain maps for a Ni-like Pd 14.7-nm laser at the moment of peak gain for (a) normal incidence irradiation, (b) 20° grazing incidence irradiation, and (c) simulated electron density profile of the prepulse at the moment of the short pulse arrival. At normal incidence the region of large gain coefficient coincides with large density gradients that rapidly refract the beam out of the narrow gain region. For a pump angle of 20° the beam heats the plasma where $N_e=2\times10^{20}$ cm^{-3}, creating large gain in a region where reduced refraction allows the beam to effectively propagate and amplify. The plasma is assumed to be created by a 120-ps normal incidence prepulse with an intensity of 2.4×10^{12} $W.cm^{-2}$, and heated after a 300-ps delay by an 8-ps duration, 800-nm wavelength, pulse focused to an intensity of 8×10^{13} $W.cm^{-2}$, both line foci are 30 μm-wide FWHM.

The simulations show that for the case of the grazing incidence pumped lasers discussed below the fraction of the pump energy deposited into the gain region is of the order of 20%–30%, significantly greater than the 5%–8% corresponding to the normal incidence pumping case. This significantly reduces the amount of pump energy required for lasing in the gain-saturated regime, making possible the development of high repetition rate table-top lasers.

2.3 Soft X-ray Laser Pumping Geometry and Implementation

The soft x-ray lasers were pumped by an 800 nm Ti:Sapphire CPA laser system, consisting of a mode-locked oscillator and three stages of chirped-pulse amplification, that is described in detail in next section. After three stages amplifiers, 2 J, 120 ps laser pulses at 5 Hz take place. We use a beam-splitter placed at the output of the third amplifier stage directs 20 percent of the laser energy to the pre-pulse arm at 120 ps pulse width, while the rest was compressed to 6-8 ps in a vacuum grating compressor. From 350 mJ, 120 ps prepulse, we also split an additional pre-pulse with 10 mJ energy that preceded the short pulse by 5.3 ns.

The gain medium plasma was formed by irradiating target at near normal incidence with a sequence of an early prepulse of 120 ps duration and ~10 mJ energy, followed after about 5 ns by a main prepulse of the same duration and ~350 mJ energy, which in turn was followed after a selected delay by a 6-8 ps duration heating pulse of ~ 1 J energy impinging at an optimized grazing incidence angle.

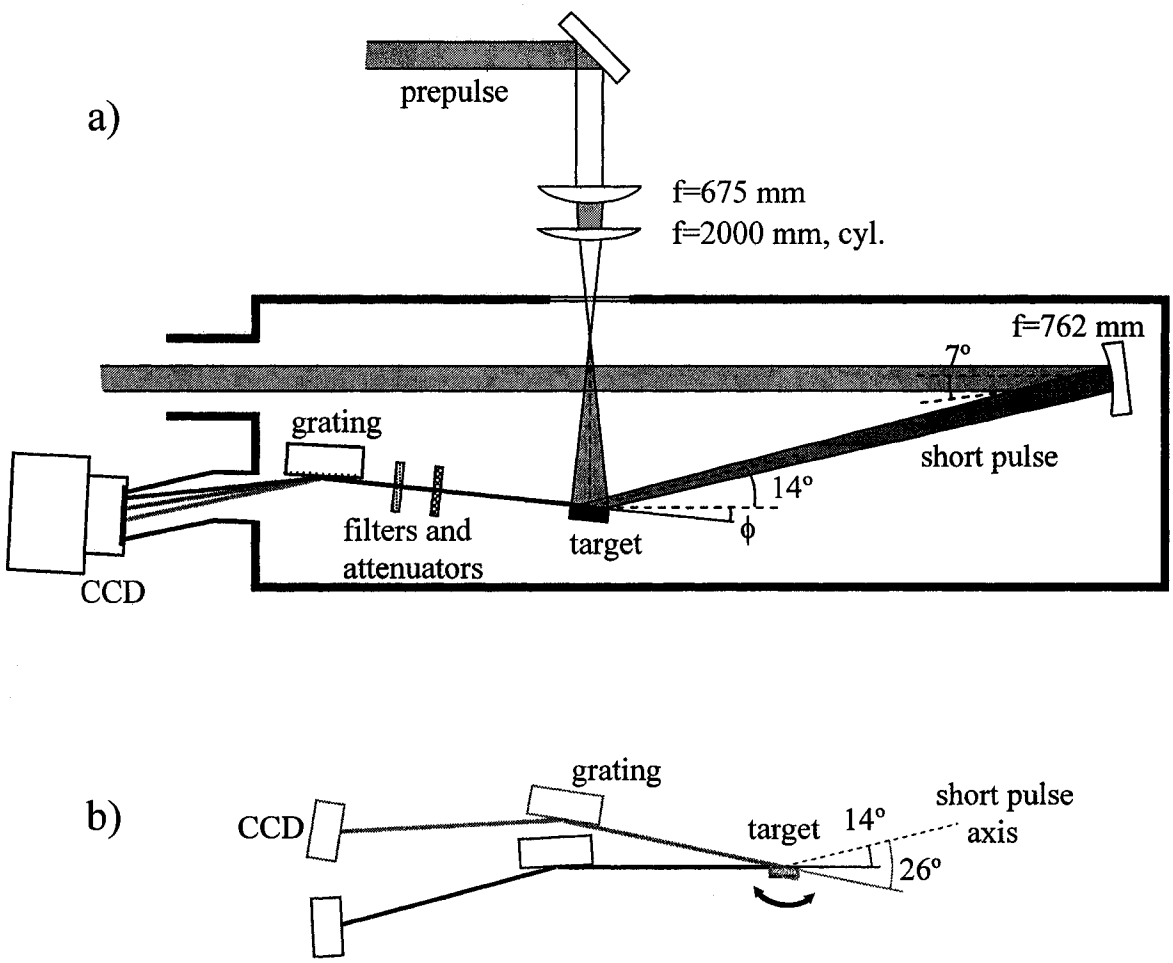

Figure 2.4 (a) Schematic illustration of the pumping configuration and detection system. (b) Diagram of target and detection system rotation used to access different grazing incidence angles.

The target irradiation configuration is shown in Fig. 2.4 (a). The two pre-pulses are combined and focused onto the target surface using the combination of an f= 67.5 cm focal length spherical lens and an f=200 cm focal length cylindrical lens to generate a 30 μm × 4.1 mm FWHM line focus. The short pulse was focused into a line of similar dimensions, using a multilayer-coated f=76.2 cm parabolic mirror placed at 7° from normal incidence. This allows the short pulse to impinge onto the target at 14° grazing incidence when the target is placed at normal incidence respect

to the pre-pulse arm. To obtain grazing incidence angles greater than 14° the target was rotated about its center while maintaining the same prepulse and short pulse beam paths [Fig. 2.4 (b)]. For example, to set a grazing incidence pumping angle of 23° the target was tilted by 9°. The overlap of the two line foci on target was monitored imaging the target onto a CCD. For each grazing incidence angle the astigmatism of the beam was adjusted such that the FWHM length of the line focus on the target would always equal 4.1 mm. For instance at 14° grazing incidence an astigmatic beam with a 1 mm FWHM major axis is required in order to form a 4.1 mm FWHM long line focus upon its intersection with the target plane. To maintain the same line focus length for operation at 26° the FWHM of the major axis of the astigmatic beam must be increased to 1.75 mm. This was accomplished by adjusting the distance (~8 cm) between a pair of f=+2 m and f=-2 m cylindrical lenses placed immediately before the compressor (Fig. 2.10). This pair creates a variable cylindrical lens with a focal length range from 20 to 100 m.

The grazing incidence nature of the experiment results in a line focus that changes in width as a function of target length. In general the change in the line focus width along the target depends on the distance the beam propagates from the time it hits one edge of the target until it hits the other edge, L (given by the cosine of the grazing incidence angle multiplied by the target length). In the limit case of normal incidence pumping the beam width is the same over the entire target while in the case of zero degree grazing incidence (longitudinal pumping) the change in the beam width is determined by the Rayleigh length of the beam and the length of the target. To characterize the line focus on the target surface we measured the change in the

beam width as a function of the distance from the waist. The waist was measured to have a FWHM of 31 μm which increases to a FWHM of 41 μm at the edge of the target, 2 mm away from the waist. Therefore this effect causes an increase of ~ 30 % in the focal width at the edge of the target with respect to the center for all angles used. Model simulations indicate the corresponding change of pump intensity results in associated gain coefficient variation of less than 10%. It should be noticed that line focus width also changes as the target is rotated to access different grazing incidence angles. However, since in our case the propagation distance only changes from L= 3.88 mm to L= 3.60 mm as the angle is increased from 14° to 26°, the line focus width changes only by ~ 3% as the target is rotated [2].

The spectrally resolved on-axis plasma emission was recorded using a spectrograph composed of a 1200 l/mm gold-coated variably spaced spherical grating placed at 24.7 cm from the end of the target and a back-illuminated 1 inch^2 CCD detector positioned at 48 cm from the target. The effective grating area is 26 mm×46 mm, on a blank size 30 mm×50 mm×10 mm. For each grazing incidence angle used the grating was placed in the corresponding target plane at 3° grazing incidence. The dispersion direction was contained in a plane normal to the target surface. Measurements were conducted to evaluate the change of the grating collection efficiency caused by the increase in plasma refraction associated with the variation in grazing incidence angle. For this purpose the variation of the collected soft x-ray laser intensity as a function of grating position was measured displacing the grating in the direction normal to the target plane. For the case of 26° grazing incidence angle corresponding to maximum refraction, the maximum laser output signal was obtained

displacing the grating by 1 mm from its original location in plane of the target. For this displacement, which corresponds to a change in grating incidence angle on the grating of 0.23 degrees, the laser signal strength increased by 7 percent. The change in grating diffraction efficiency associated with such small angle variations can be neglected. Therefore we can expect errors in soft x-ray laser intensity measurements associated with the variation of the collection efficiency to be less than 10 percent. Combinations of Zr or Al filters and meshes of measured transmissivity positioned to avoid Moire patterns were used to reach attenuation factors up to 1500. To increase the accuracy of the determination of the soft x-ray laser output energy the trasmissivity of the filters used was measured using synchrotron radiation [3].

2.4 Pumping Laser System

2.4.1 Introduction of chirped pulse amplification (CPA) system

To obtain short wavelength soft x-ray laser, a very high power laser system is required to reach the high intensity needed to create the hot plasma required. A severe limitation when amplifying intense pulses is that when the power density increases, the pulse damages the optics it passes through. A major breakthrough came with the chirped-pulse-amplification technique in 1985 [4]. The concept involves starting with a short pulse of low intensity, then stretch the pulse in time in a controlled way. The peak intensity is thus reduced and it is possible to increase the energy in the pulse further without damaging optics. The final step is to recompress the pulse to the original time duration.

The implementation of this concept is illustrated in Fig. 2.5. First the short pulse is generated in a mode-locked oscillator. Next, the pulse is stretched in a dispersive delay line or "pulse stretcher". The delay line is arranged such that the time it takes for the pulse to pass through is dependent on frequency. The low-frequency components will pass through faster than the high. In contrast to a transform-limited pulse, where all frequency components arrive at once, this pulse has an instantaneous frequency that depends on time, a chirp. Unlike self-phase modulation, no frequency components are added, they are just rearranged, and the time averaged spectrum is thus the same. After the stretcher, the low-frequency components comes at the leading edge of the pulse while the high-frequency components arrive later, it has a positive chirp. The stretched pulse can be obtained in several ways, most common by a pair of anti-parallel gratings [5]. Typically the pulse can be stretched a few thousand times in time, reducing the intensity by the same factor.

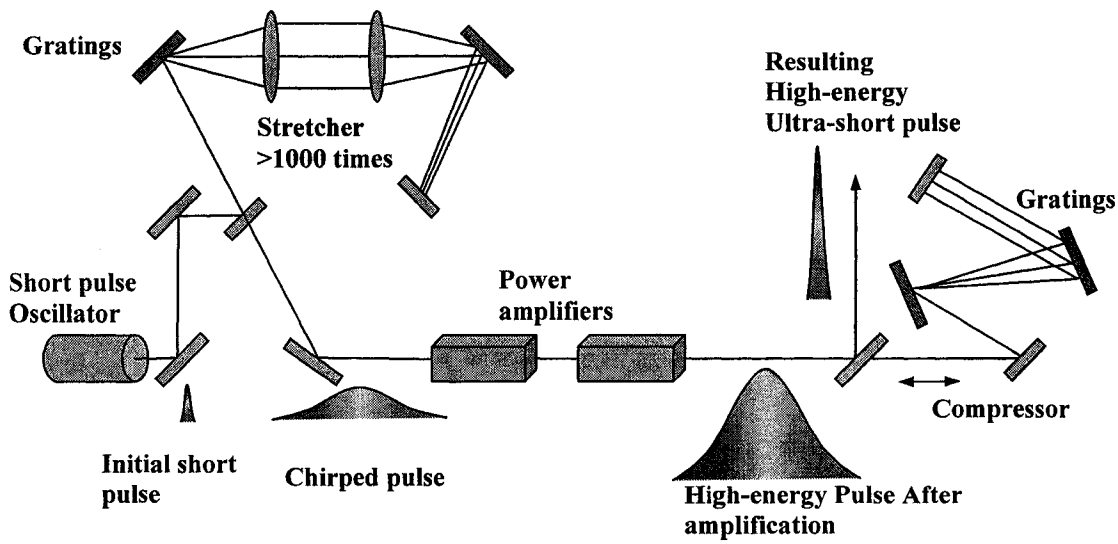

Figure 2.5 Schematic representation of a chirp pulse amplification laser system

After amplification, the pulse is recompressed. It passes optics with negative dispersion compensating the positive dispersion of the stretcher. The high frequencies must pass through this optics faster than the low. A pair of parallel gratings can be used for this purpose. They can also compensate for additional chirp acquired from passing through optics in the amplifier chain. To be able to recompress the pulse to the original time duration all frequencies must be equally amplified. The successfulness of this method relies on a crystal being able to amplify such large bandwidth. However, often it is not possible to get back exactly the original pulse-duration.

2.4.2 Description of Ti:Sapphire CPA pump laser system

Our experiments were conducted using a 800 nm Ti:sapphire pump laser system consisting of a mode-locked oscillator and three stages of chirped-pulse amplification. In this setup a Kerr mode-locked Ti:sapphire laser oscillator produces nanojoule pulses of about 30 fs duration that are stretched to about 180 ps by a grating stretcher. The stretched pulsed are subsequently amplified in a chain of three Ti:sapphire amplifiers pumped by frequency doubled Nd:YAG lasers. Eight passes through the first stage amplifier increases the pulse energy to about 2 mJ, while the pulse width narrows to about 120 ps. Further amplification to 2 J takes place in a five-pass second stage bow-tie amplifier and a final three-pass amplifier that is pumped by a 5 J frequency doubled Nd:YAG laser. A beam-splitter placed at the output of the third amplifier stage directs 20 percent of the laser energy to the pre-pulse arm (120 ps pulses), while the rest was compressed to 6-8 ps in a vacuum grating compressor. While this pump laser can operate at a repetition rate of 10 Hz in the present

experiments the third stage amplifier was operated at 5 Hz to improve the pump beam mode quality.

a. Oscillator

There are several techniques to achieve mode locking by inserting an active or passive component into the cavity. The Kerr-lens mode locking is a passive technique that is often used in Ti:sapphire lasers [6]. This technique is based on the optical Kerr effect. Suppose the light inside the cavity has a Gaussian intensity distribution transverse to the direction of propagation, the Ti:sapphire crystal will act as lens due to self-focusing. To induce this nonlinear effect, a high intensity is needed. A low intensity beam does not get focused. Thus a high intensity results in collimating the beam while this does not happen for low intensity. Now suppose some modes incidentally are phase locked and interfere constructively forming a pulse that has higher intensity than the modes with random phases (continuous light). The high-intensity pulse is focused and thereby collimated with the Kerr effect, while the continuous light is not focused. The unfocused light can thus be blocked, and suffer from losses while the focused part do not have such losses. The modes in phase, forming a high-intensity pulse, will further increase its intensity while low intensity continuous light decreases. Eventually only modes oscillating in phase, creating the intense mode-locked pulse, survive.

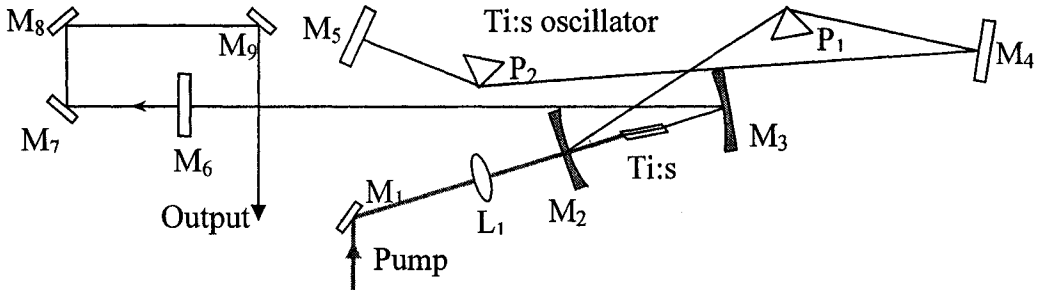

Fig. 2.6 Schematic diagram of Ti:Sapphire oscillator

Figure 2.6 is a diagram of a Mode-locked oscillator (KM Labs) [7]. The Ti:sapphire Laser we used can provide either CW or Mode-locked laser, centered at 780-800 nm. The Ti:Sapphire has been shown to be the most attractive gain medium for laser operation in the near-infrared spectral region. The broad gain bandwidth of Ti:Sapphire means that in addition to a large tuning range it is especially well suited to ultra-short pulse generation. However, the output laser pulse is broadened because of the frequency chirp which originates from within the laser cavity and is due primarily to the presence of self-phase modulation (SPM) and group velocity dispersion (GVD) within the Ti:Sapphire gain medium. For generating narrow pulse width, two prism sequence shown in the Fig. 2.6 (P1 and P2) can overcome the pulse-broadening.

Using a 17% output coupler (M6 in Fig. 2.6), the laser typically requires ~4.0W 532nm pump power, in a clean TEM00 mode, for mode-locked operation. Alignment of the laser is easier if a laser with pump power ~5.5W is used. We use 5W from a Nd:YVO_4 532 nm (2HG) laser as pump source (Coherent-Verdi) [8].

For aligning the oscillator, the pump beam is focused at the entrance face of the crystal by adjusting the position of lens (L1). The fluorescence collimated by the curved mirror (M2) should pass through both prisms (P1, P2) and the end-mirror should retroreflect the fluorescence. The prism orientations should both be adjusted for "minimum deviation" of the fluorescence light. Retroreflecting the fluorescence with the end mirrors, and repeated readjustments, brightens the fluorescence and leads to lasing.

The beam should be overlap at both ends of the cavity; i.e. look at the fluorescence at one end of the cavity, while blocking and unblocking the beam at the other end to observe the retroreflected fluorescence. Another useful place to look for fluorescence overlap is between the two prisms, nearest the cavity subassembly.

During the initial alignment, it is useful to turn-up the pump power full power, but not more than 6 Watts. The laser will start lasing much more easily if "overpumped." Turn the pump laser down to ~5 W as soon as we obtain lasing. Repeated adjustments of the end mirrors can be useful to optimize the output power. If the long-cavity proves unsuccessful, it may be necessary to start from a short-cavity layout and slowly extend the laser cavity to its full length.

Generally we don't need realign the oscillator everyday, if the CW output power is normal, we can just touch the second prism to trigger the laser to mode-locking mode. The normal output mode-locking power is 700 mW, at 88 MHz.

b. Stretcher and compressor

In CPA systems the seed pulse from oscillator is temporally stretched when it passes through a positive delay line consisting of a diffraction grating and a concave spherical mirror (pulse stretcher). After the amplification the chirped pulse is recompressed when it passes through a negative delay line consisting of a pair of two parallel gratings (pulse compressor) [5, 9]. In our CPA system the mode-lock laser pulses are stretched from about 30 fs to 180 ps before the pulses are amplified.

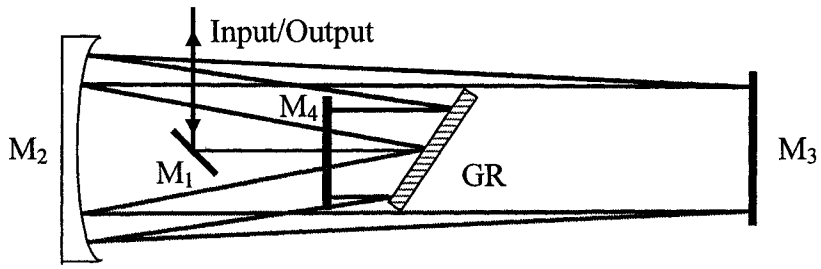

Fig. 2.7 Schematic diagram of Stretcher. M1: 45^0 mirror for 800 nm, M2: concave spherical mirror for 800nm, M3, M4: 0^0 mirrors for 800nm, GR: diffraction grating.

Figure 2.7 is an schematic diagram of the pulse stretcher, that makes use of a 1200 lines/mm diffraction grating. This stretcher can extend short pulses by 6000 times, from 30 fs to 180 fs. After stretcher, the 88 MHz train of 180 ps pulses is converted into a 10 Hz train by a Pockel-cell. The 3 nJ pulses are amplified in a series of three amplifiers. After the first stage amplifier, the pulse duration increases to 120 ps due to gain narrowing. As discussed below, the two final amplifiers increase the energy to 2 J, so finally we can get 2 J output energy.

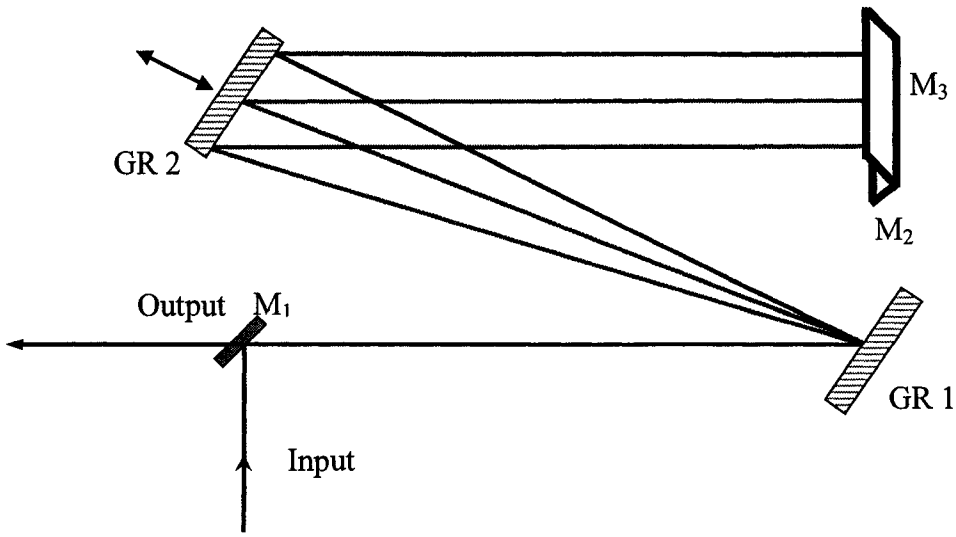

Fig. 2.8 Schematic diagram of compressor, M1: 45° mirror for 800nm center wavelength, GR1, GR2: Gratings, M2, M3: 45° roof mirrors for 800nm to change height from 7" to 10"

A vacuum compressor is used to compress pulses back to original pulse width (see Fig. 2.8). Laser pulses are compressed down to ~ 50 fs. However, for most experiments, the pulses were compressed down to 6-8 ps. The optimum pulse width for the excitation of the soft x-ray lasers is discussed in the next chapter.

c. Amplification stages

The stretched pulses are selected by Pockel-cell and the frequency is changed from 88 MHz to 10 Hz and sent to the first stage amplifier.

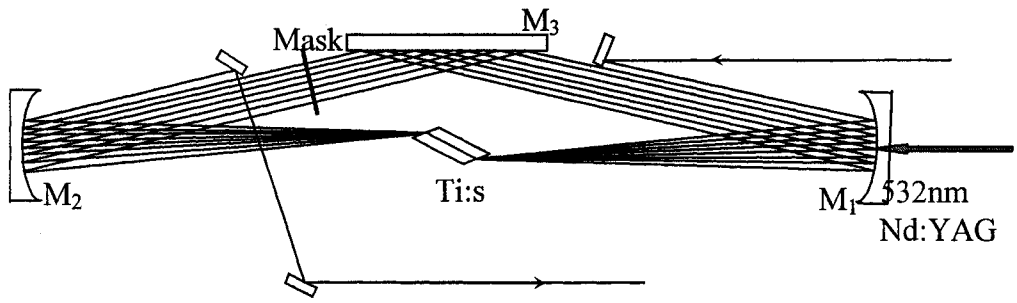

Fig. 2.9 Schematic diagram of first stage amplifier

The first stage amplifier is a multi-pass Ti:Sapphire laser (Fig 2.9). We use multi-pass amplifier because its simplicity in construction and alignment. The stretched pulses are amplified to an energy of 2 mJ in this multi-pass amplifier pumped by a fraction of the 532-nm radiation from a Q-switched Nd:YAG laser. After the first stage amplifier, the pulse is amplified in a five-pass bow tie arrangement in a second Ti:sapphire crystal (Fig. 2.10). The amplifier is longitudinally pumped from the both ends with remaining frequency-doubled output from the first Q-switched Nd:YAG laser. The total pump energy in the second amplifier is 0.75 J. Although energies as high as 200 mJ have been obtained from this amplifier, the typical output energy is 150 mJ after a spatial filter and a pockel-cell.

The final Ti:sapphire amplifier is an 25-mm diameter × 25-mm thick Ti:sapphire crystal, which is pumped by the doubled output from a Nd:YAG (Positive Light) laser chain. The Nd:YAG laser chain starts with a Q-switched Nd:YAG oscillator (Quanta-Ray), which produces 400-mJ pulses of 1.064-mm radiation at 10 Hz. After passing through two stage amplifiers, the output energy for each leg can attain to 2.5 J, frequency is 5 Hz, at 532 nm.

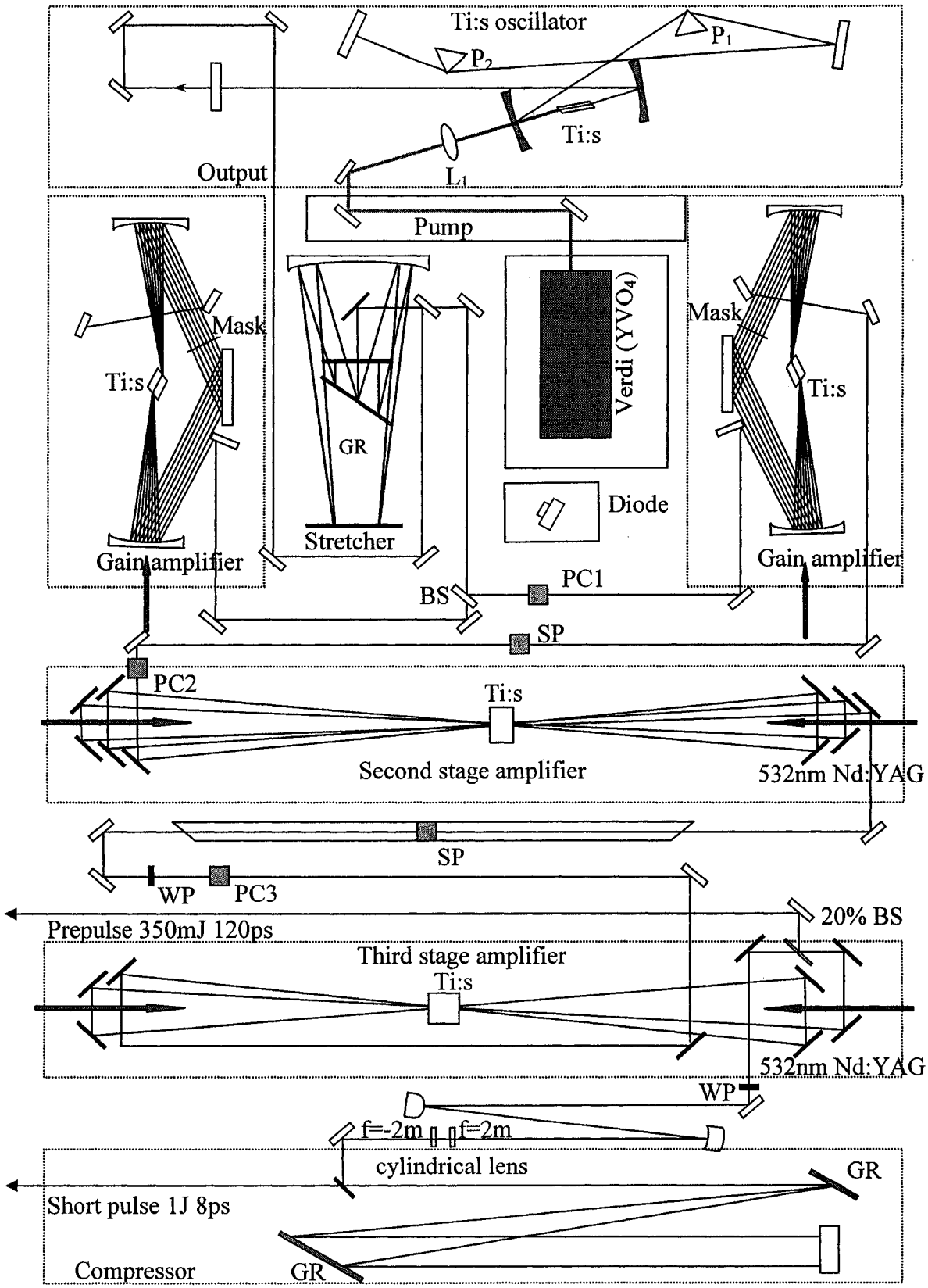

Fig. 2.10 Schematic diagram of Ti:Sapphire laser pump laser system

In Figure 2.10, P1, P2: are Prisms, PC1~PC3: Pockel Cell, SP: Spatial filter, WP: wave plate, GR: grating, BS: Beam splitter.

While this pump laser can operate at a repetition rate of 10 Hz in the present experiments the third stage amplifier was operated at 5 Hz to improve the pump beam mode quality. So this system can be fired at 5Hz for hours every day.

The diagram of the entire pump laser system is shown in Figure 2.10. The output beam from the stretcher is divided by a 50% beam splitter and sent to two first stage amplifiers. One is used as the first stage in a chain of three amplifiers, and the other can provide synchronize low power trigger beam for some experiments. From the system diagram, we can tell the second stage amplifier is five-pass Ti:Sapphire laser, and the third stage amplifier is three-pass amplifier. After third stage, a 20 % beam splitter is used to send beam to target chamber as pre-pulse, the energy is about 350 mJ. The rest 80% energy is sent to compressor to compress to 6~8 ps and send to target chamber as short pulse. The compressed short pulse energy is about 1 J.

References

[1] B. M. Luther, Y. Wang, M. A. Larotonda, *et al.* "High repetition rate collisional soft x-ray lasers based on grazing incidence pumping," IEEE, JQE, 42, 4 (2006)

[2] Y. Wang, M. A. Larotonda, B. M. Luther, M. C. Marconi, D. Alessi, M. Berrill, V. N. Shlyaptsev, and J. J. Rocca, "Demonstration of saturated high repetition rate tabletop soft X-ray lasers at wavelengths down to 13.9 nm," Phys. Rev. A. 72, 053807, (2005)

[3] Advanced Light Source, Lawrence Berkeley National Laboratory, courtesy Eric Gullikson.

[4] D. Strickland and G. Mourou. "Compression of amplified chirped optical pulses," Opt. Commun., 55, 447, 1985.

[5] O. E. Martinez, "Design of high-power ultrashort pulse amplifiers by. expansion and recompression," IEEE J. Quantum Electron. QE-23, 59 (1987).

[6] D. E. Spence, P. N. Kean, and W. Sibbett, "60-fsec pulse generation from a self-mode-locked Ti:sapphire laser," Opt. Lett. 16, 42 (1991).

[7] http://www.kmlabs.com/

[8] http://www.coherentinc.com/

[9] E. B. Treacy, "Optical pulse compression with diffraction gratings," IEEE J. Quantum Electron. QE-5, 454 (1969).

Chapter 3, Demonstration of High Repetition Rate Soft X-ray Lasers at Wavelengths between 10.9 and 32.6 nm.

3.1 Introduction

For generating high density and high temperature plasma, we developed ultra-short and ultra-high intensity lasers using the chirped pulse amplification technique which was introduced in chapter 2. This technique has provided us with new fields of x-ray laser development because the shorter wavelength x-ray lasers need high-intensity and short-pulse pumping which can overcome the strong depopulation of the population inversion. In this chapter, the author would like to describe the high repetition rate Ni-like and Ne-like soft x-ray lasers at wavelength from 10.9 nm to 32.6 nm, with saturated output down to 13.2 nm. We measured the gain feature of Ni-like x-ray laser, and give the details about how we optimized x-ray lasers, including scanning delay time between pump pulses, changing pulse duration, grazing incidence angle, using 3 pump pulses, continuous work at 5 Hz high repetition rate.

3.2 Ni-like Mo X-ray Laser at 18.9 nm

Our initial experiments focused in demonstrating lasing at high repetition rate in the 18.9 nm laser line of Ni-like Mo (molybdenum). The pumping geometry is schematically illustrated in Fig. 2.4. A line focus plasma was first formed by irradiating a 2 mm thick, 4 mm wide polished Mo slab target at near normal incidence

with an intensity of 2.4×10^{12} W/cm^2 obtained by focusing the long duration prepulse into a 4.1 mm full-width at half-maximum (FWHM) long 30 μm FWHM wide line.

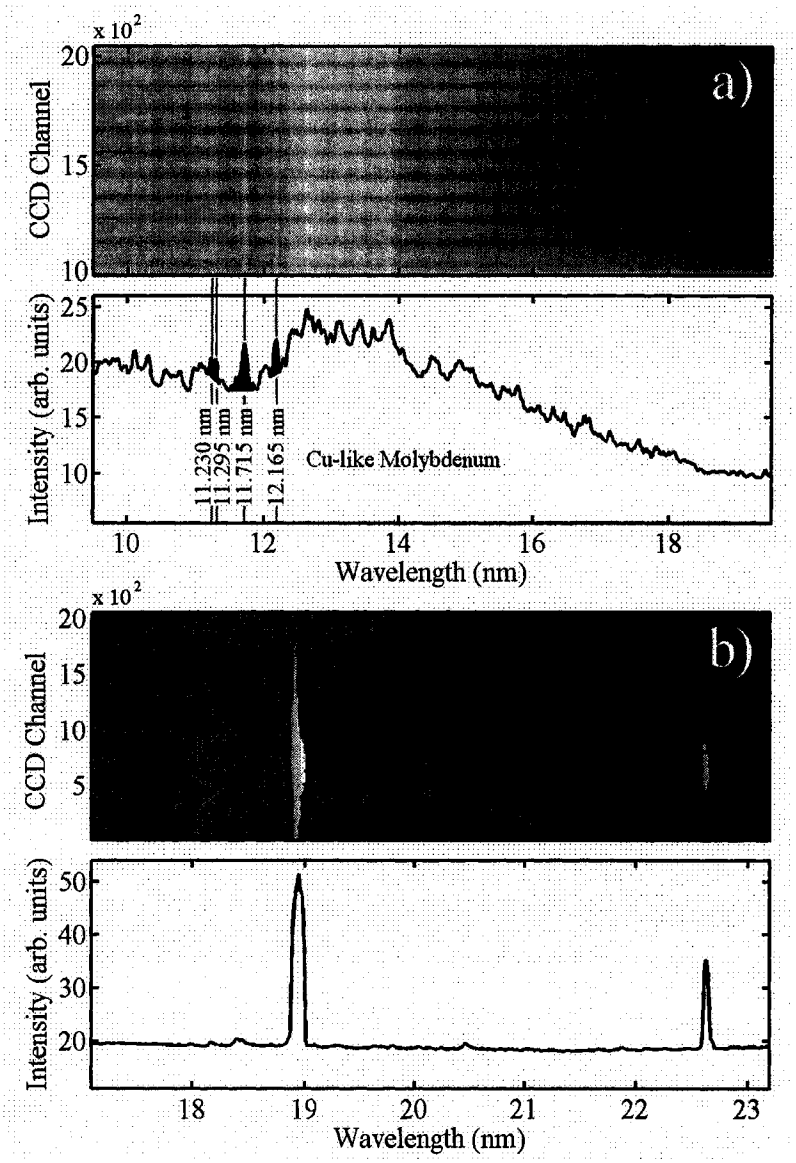

Figure 3.1 (a) Axial spectra of a 4 mm long Mo plasma excited by a 320 mJ, 120 ps duration pulse. Cu-like Mo lines are observed to be dominant. (b) Spectra obtained using a ~ 960 mJ, 8.1 ps short pulse 700 ps after the pre-pulse. Strong lasing is observed in the 18.9 nm 4d $^1S_0$ – 4p $^1P_1$ and in the 22.6 nm 4f $^1P_1$ – 4d $^1P_1$ lines of Ni-like Mo.

Figure 3.1 (a) shows on-axis spectra obtained irradiating 4 mm Mo target with a single 320 mJ laser pre-pulse, covering the 10 to 19 nm region. Several of the strongest lines correspond to Cu-like Mo are observed [1], an indication that the pre-plasma is likely to also contain a significant concentration of Ni-like ions. Figure 3.1(b) shows a typical spectrum obtained when the 4 mm long Mo target was also irradiated with a 930 mJ, 8.1 ps FWHM short pulse 700 ps after the pre-pulse. Strong laser emission is observed in both the 18.9 nm $4d^1S_0 - 4p^1P_1$ and the 22.6 nm $4f^1P_1 - 4d^1P_1$ lines of Ni-like Mo. Lasing was observed in plasmas generated using short pulse line widths as broad as 50 μm FWHM and as narrow as 18 μm FWHM. However, the best results in terms of output intensity and shot-to-shot reproducibility were obtained using 30 μm FWHM widths for both of the pulses. The laser output obtained utilizing the narrower line focus was significantly more erratic. Lasing was observed for heating pulse width ranging from 1.8 to 12 ps. The characterization of the laser reported herein was conducted using 8.1 ps pulses. Lasing at 18.9 nm was observed with pumping energies as low as 140 mJ for the pre-pulse and 310 mJ for the short pulse.

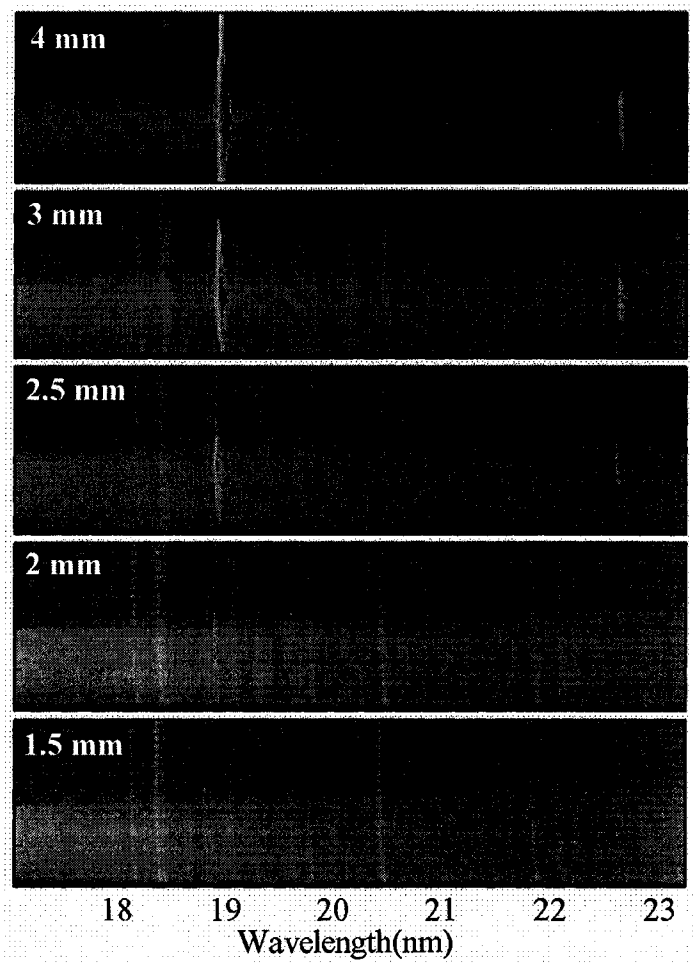

Figure 3.2 Rapid Mo laser line intensity growth with plasma length from 1.5 mm to 4 mm. Signals on the left are laser lines at 18.9 nm and signals on the right are laser lines at 22.6 nm.

Gain measurement:

The gain of soft x-ray laser is usually diagnosed by measuring the laser output as a function of lasing medium length. To measure gain, a target with steps ranging from 1.5 mm to 4 mm in length was used. Two laser lines are observed at 18.9 nm and 22.6 nm. Figure 3.2 shows the results obtained irradiating the target with a 350 mJ pre-pulse and a ~ 1 J short pulse separated by 700 ps. The intensity of the 18.9 nm Ni-like Mo line is observed to increase by nearly three orders of magnitude when the

target length is varied between 1.5 mm, the minimum length for which the line was observed, and 4 mm.

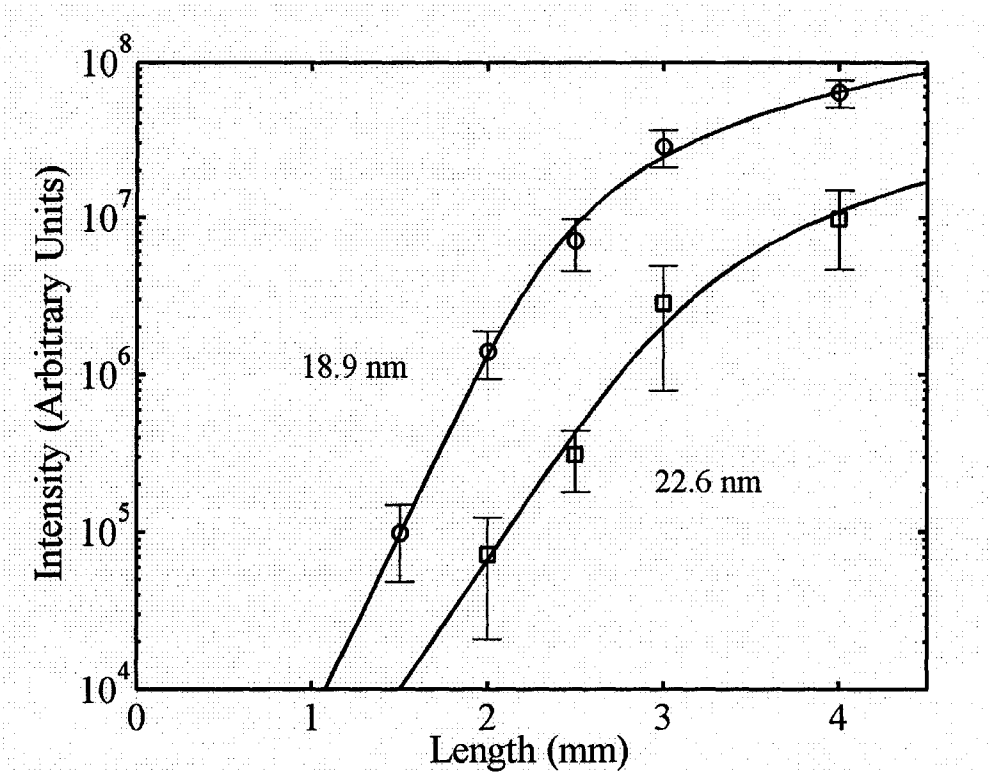

Figure 3.3 Variation of the output intensity of the 18.9 nm and 22.6 nm laser lines of Ni-like Mo as a function of plasma length. Each of the points is an average of ten or more laser shots.

The solid lines in Fig. 3.3 are fits of the data with the expression by Tallents *et al* [2], for the variation of the line intensity with the plasma length taking into account gain saturation. The resulting small signal gain coefficient for the 18.9 nm line is 58 cm^{-1}. The gain-length product reaches $g \times l = 15.5$, a value that corresponds to saturated operation in collisional laser systems. The energy of the most intense 18.9 nm laser pulses was initially estimated from the CCD counts to exceed 250 nJ. However, an accurate measurement of the transmissivity of the thin film filters (Al) used in the experiments employing synchrotron radiation [3] showed that these filters

are significantly more absorbent than what was initially estimated based on published optical constants. This suggests that the energy for the 18.9 nm wavelength Ni-like Mo laser pulses we reported in Ref. [4] for the case of grazing-incidence pumping at 14° grazing incidence is likely to be underestimated. We conducted a new Ni-like Mo laser experiment at a grazing-incidence pumping angle of 20° using 1 J of short pulse (~ 8 ps duration) excitation and the calibrated filters. A series of shots made using a 4 mm long Mo slab target yielded an average 18.9 nm laser pulse energy of 1 μJ, with the most intense pulses reaching 1.4 μJ. The results demonstrate the feasibility of the development of a >10 μW average power table top laser at this wavelength using 10 Hz pumping.

Assuming a laser pulse width equal to the duration of the gain divided by $(g\times l)^{1/2}$ (~ 4 ps) and a gain region of 20 micrometer diameter, the 18.9 nm laser beam intensity can be calculated to reach the computed gain saturation intensity of 8×10^{10} W/cm^2 when the pulse energy reaches 1 μJ. The 22.6 nm line was measured to amplify with a smaller gain coefficient of 41.1 cm^{-1}, and to reach a gain-length product of $g\times l = 13.5$.

3.3 Demonstration of Ni-like X-ray Lasers from 16.5 to 10.9 nm

3.3.1 The Ni-like Mo results were isoelectronically scaled to shorter wavelengths

Figure 3.4 shows on-axis spectra corresponding to plasmas generated with 4 mm long targets of Ru (Z=44), Pd (Z=46), Ag (Z=47), Cd (Z=48), and Sn (Z=50) irradiated at a grazing incidence angle of 20°, Sb (Z=51) and Te (Z=52) targets irradiated at an increased grazing incidence angle of 23°. The time delay between the

two pulses was 500 ps for Ru, Pd, Ag and Cd, and 150 ps for Sn, 100 ps for Sb and 75 ps for Te. The targets were polished slabs with thickness of 1 mm for Ru, and Pd, and 2 mm for Ag, Cd and Sn. The Sb and Te targets consisted of a 1 μm thick film of these materials deposited on a polished Cu slab target using an intermediate Ti adhesion layer. To demonstrate lasing in Ni-like Sb and Ni-like Te we reduced the FWHM length of the short pulse line focus to 3.5 mm to increase the irradiation intensity up to 1.2×10^{14} W/cm^2.

Strong lasing was obtained in the 4d-4p lines of the Ni-like ions at 16.5, 14.7, 13.9, 13.2 nm, and 11.9 nm, while significantly weaker laser output was observed for the 11.4 nm, and 10.9 nm lines of Ni-like Sb and Te respectively. The divergences in the direction parallel to the target were observed to range from 7-10 milliradians. Figure 3.5 shows these results are in good agreement with the computed Z scaling of the main pre-pulse and short pulse pump energies necessary for strong lasing with 20 degrees grazing incidence pumping. The computations were conducted by V. N. Shlyaptsev using the code RADEX [5]. The model includes 1D expansion of laser produced plasma under transverse prepulse and grazing incidence main pulse, atomic kinetics, the refraction of the main pump pulse, and refraction of x-ray radiation pulse and its amplification computed taking into account the saturation of the amplified spontaneous emission (ASE) signal. The computations predict that with the pump energies used in the experiment strong lasing should be obtained in all the elements investigated up to Sn, for which the available pump energy starts to fall short of the predicted required amount. Extension of the results to λ=7.97 nm in Ni-like Nd (Z=60) is estimated to require ~ 7 J of short pulse pump energy.

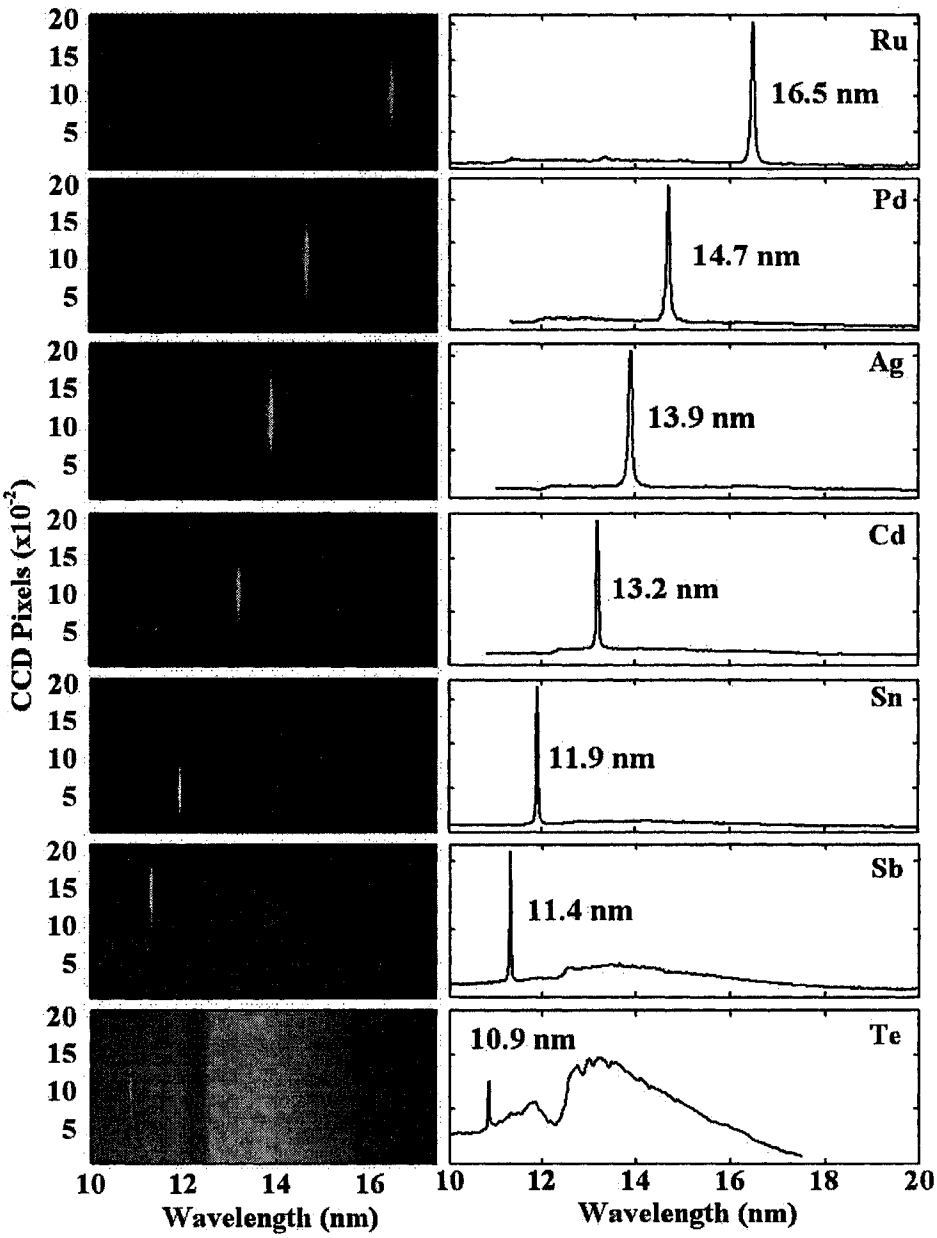

Figure 3.4 Single shot on-axis spectra of 4 mm line focus plasmas showing lasing in the $4d^1S_0$- $4p^1P_1$ transition of the Ni-like ions at wavelengths ranging from 16.5 to 10.9 nm. The laser lines completely dominate the spectrum.

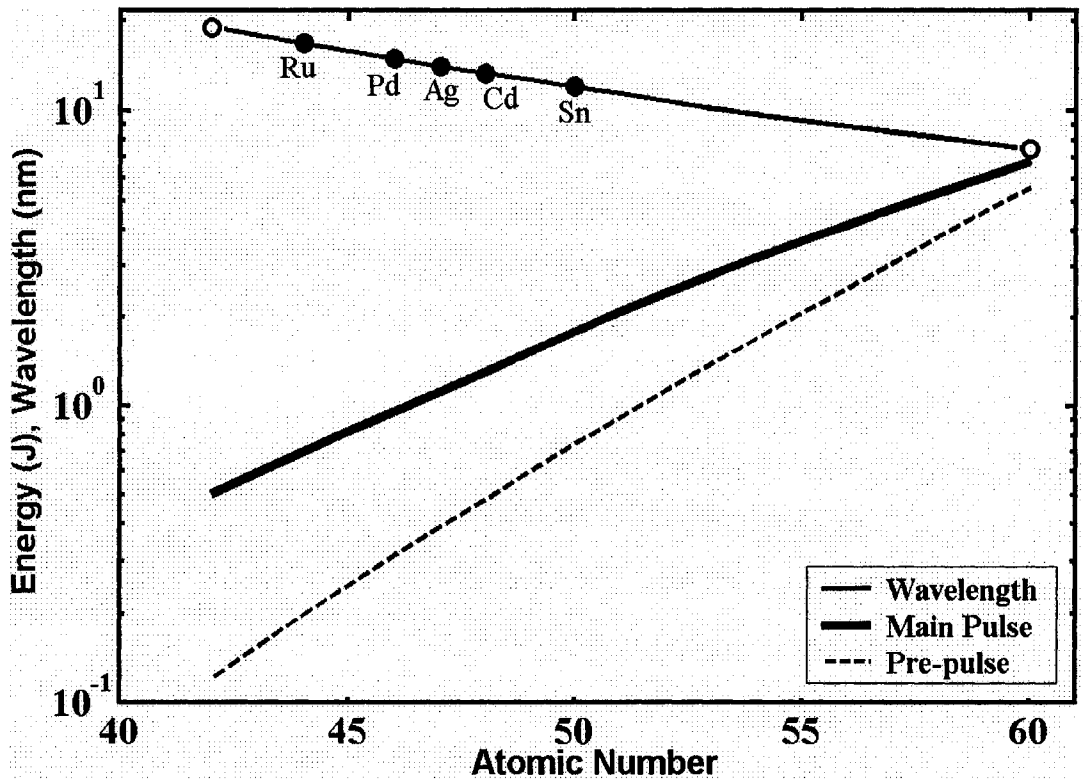

Figure 3.5 Computed main pulse and pre-pulse pump energies necessary to pump the $4d^1S_0$- $4p^1P_1$ laser transition of Ni-like ions as a function of atomic number Z. The calculations are for a main pulse grazing incidence angle of 20 degrees and 30 μm line focus width. The pump pulse durations are those used in the experiment.

3.3.2 Gain measurement of Ni-like x-ray lasers

Figure 3.6 (a-d) shows results of gain measurement for Ni-like Pd, Ag, Cd and Sn. We used target that increases in length by steps of 0.5 mm, ranging from 1.5 mm to 4 mm. Gain measurements were conducted by monitoring the variation of the laser line intensity as a function of target length. For all curves, laser intensity is observed to increase rapidly as a function of target length, until it rolls off into saturation. The solid line corresponds to a fit of the data with an analytical expression that describes the variation of the amplified spontaneous emission as a function of plasma length

taking into account the effect of gain saturation [2]. The resulting small signal gain coefficient for Ag laser is 67.5 cm^{-1} and g×l=16.8. Similar gain-length products were measured as g×l=16.1 for Pd, and 17.6 for Cd. Higher Z elements (Sn) showed progressively lower amplification. The laser pulse energy was estimated from the counts on the CCD taking into account the quantum efficiency of the detector and the losses. The energy of the most intense Ag and Pd shots obtained with a 4 mm target are estimated to exceed 0.6 μJ. Assuming the laser pulse width is that predicted by model computations, ~5 ps, and an exit beam diameter corresponding to the width of the pump beam ~20 μm, this pulse energy corresponds to a laser intensity of about 3.8×10^{10} W/cm^2, that exceeds the computed saturation intensity of $5–7 \times 10^9$ W/cm^2.

Figure 3.6 (d) shows the variation of the Ni-like Sn (11.9 nm) laser line intensity as a function of plasma column length. The data was obtained using a main prepulse energy of ~350 mJ and a short pulse energy of ~1 J at a grazing incidence angle of 23°, at the optimum delay of 100 ps. The fit corresponds to a gain coefficient of 50 cm^{-1}, and a gain length product of g×l=14.3, the value for which the onset of gain saturation effects are observable. The most intense 11.9 nm laser pulses were measured to have an energy of ~230 nJ.

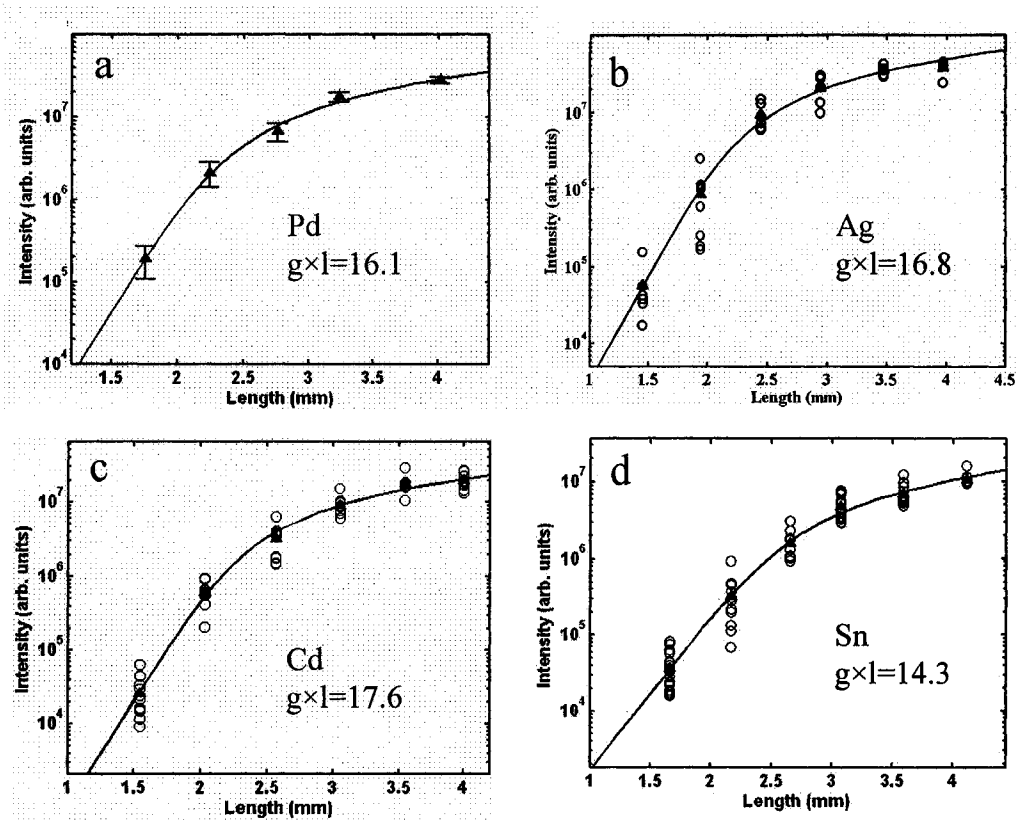

Figure 3.6 Intensity versus target length for the laser line of Ni-like Pd(a), Ag(b), Cd(c), and Sn(d). The solid triangles represent the average of the points shown. A fit of the data gives a gain-length product of g×l=16.1 for Pd, 16.8 for Ag, 17.6 for Cd, and 14.3 for Sn.

3.4 Ne-like X-ray Lasers at 30 nm Range

While a major driver in x-ray laser development has been the demonstration of practical laser at shorter wavelengths, there are also applications that can benefit from compact lasers operating in the 30 nm spectral region which include for example the metrology of optics for astronomical studies.

We have demonstrated transient high repetition rate Ne-like soft x-ray lasers in Ti, V, and Cr [6]. As results, high average power x-ray laser operation was

obtained for the first time to our knowledge in the $2p^5 3p\,^1S_0 \rightarrow 2p^5 3s\,^1P_1$ transitions of Ne-like Ti and V at 32.6 nm and 30.4 nm respectively. We also observed strong lasing in the corresponding line in Ne-like Cr at 28.6 nm, and in the 30.1 nm $2p^5 3d\,^1P_1 \rightarrow 2p^5 3p\,^1P_1$ line of Ne-like Ti which inversion relies on strong re-absorption of the 2.335 nm resonant transition linking the $3d\,^1P_1$ laser upper level to the ion ground state [7].

Figure 3.7 shows on-axis spectra corresponding to 4 mm long plasmas of Ti, V and Cr irradiated at a grazing incidence angle of 20°. In the Ti experiment the energy of the picosecond short pulse was 1 J and the pre-pulse was 0.35. In the V and Cr experiments the energy of the main pre-pulse was increased to 0.52 J at expense of the energy of the picosecond short pulse, which in these cases was ~ 0.9 J. In all cases, the $3p\,^1S_0 \rightarrow 3s\,^1P_1$ line of the Ne-like lasers was observed to clearly dominate the spectra. In the case of Ti, lasing was also observed in the 30.1 nm $3d\,^1P_1 \rightarrow 3p\,^1P_1$ line of the Ne-like ion. The intensity of this line was in general weaker than that of the 32.6 nm line, but approached it for short time delays (~ 450 ps) between the pre-pulse and the short pulse [6].

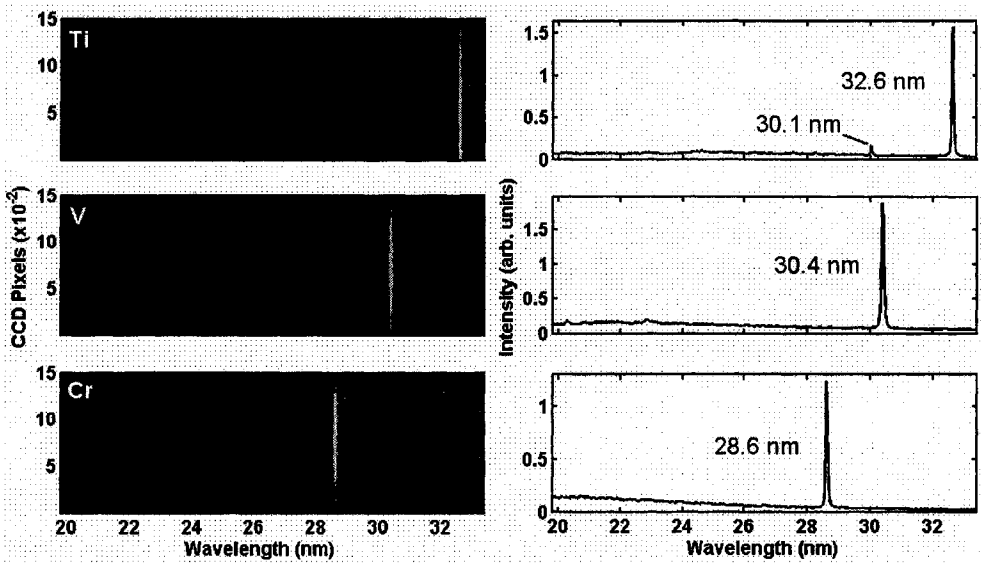

Fig. 3.7. Single shot on-axis spectra of 4 mm long line focus plasmas showing lasing in the $2p^53p^1S_0 \rightarrow 2p^53s^1P_1$ transition of Ne-like Ti, V and Cr ions. In all three cases, this laser-line dominates the spectrum.

3.5 Optimization

Measurements were done to improve the soft x-ray laser output energy and some of the other laser beam characteristics. For improving short pulse and pre-pulse foci, in these experiments, we varied the line focus width from 18 μm to 50 μm, and found that 30 μm foci was optimum for the laser pump energy we had available. The length is also an important factor, which was scanned from 3 mm to 4 mm by changing the separation between the cylindrical lenses before compressor to control the astigmatism of the beam, and finally we decided to use 4 mm FWHM.

Many other factors can change the laser output characteristics: the delay time between pulses, the grazing incidence angle, short pulse duration, and the ratio of energies between the two prepulses. Below we discuss the effect of these parameters on the laser output intensity.

3.5.1 Delay time between pre-pulse and short pulse

Delay time between pre-pulse and short pump pulse is a very important factor to determine the laser output beam energy and quality. Figure 3.8 shows the output intensity of Ni-like x-ray laser as a function of delay between the 350 mJ pre-pulse and the ~ 1 J short pulse, for Pd, Ag, Cd and Sn with 4 mm target. Strong lasing was observed to take place for a broad range of time delays. However, the range gets smaller with increasing nuclear charge Z. From Pd (Z=46) to Sn (Z=50), the range changes from 600 ps to 150 ps. Model computations show that for short time delay, the electron density profile is too steep for effective amplification, while at long time delay, the plasma temperature and degree of ionization decreases as a result of the plasma expansion, dropping the degree of ionization significantly below that necessary for lasing. For the Ni-like Mo laser, we observed a broad range of time delays for strong lasing, which is about 790 ps [4]. This time window for lasing is significantly broader than that observed in the experiment by Keenan *et al.* (~ 50 ps) [8]. The larger pump energy in our Ni-like Mo experiment can be expected to give origin to an enlarged gain region which results in the increased laser output pulse energy we observed.

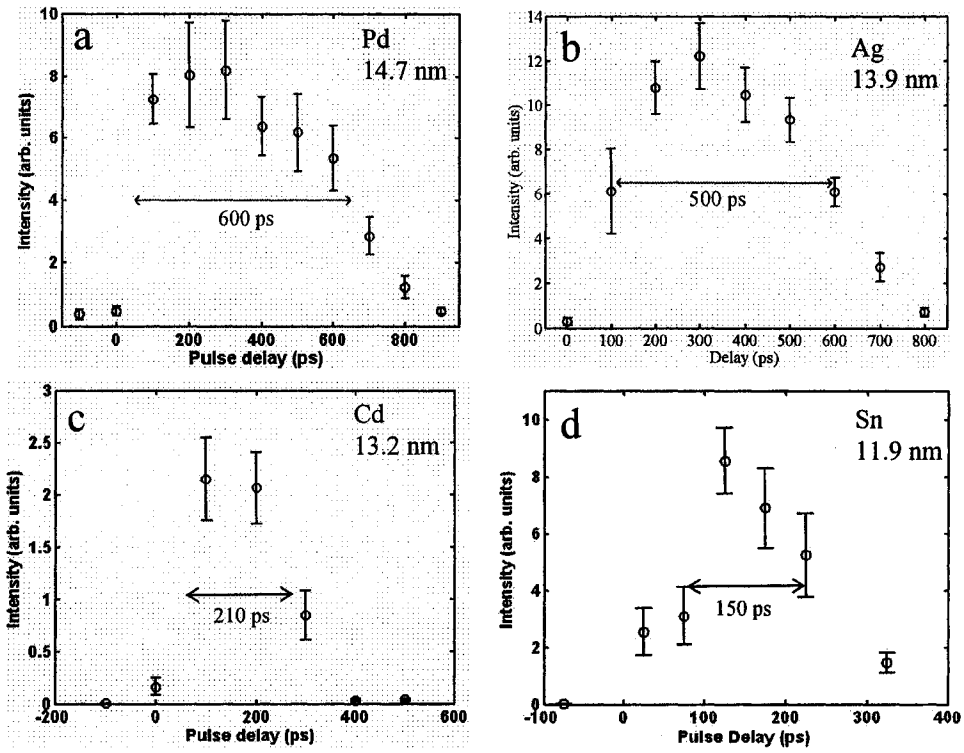

Figure 3.8 Measured intensity of the soft x-ray laser output as a function of time delay between the 120 ps pre-pulse and the 8 ps grazing incidence pulse for Ni-like Pd(a), Ag(b), Cd(c), and Sn(d). The FWHM of the time span in which strong laser is achieved is indicated.

Fig. 3.9 shows how the optimum delay between pump pulses for lasing in the 4d-4p transition of Ni-like ions decreases as Z increases. The optimum delay drops from 700 ps for Ni-like Mo (Z=42) [4, 9] to 100 ps for Sn (Z=50) [10]. This is consistent with the fact that the high degrees of ionization necessary for lasing in higher Z ions are reached only in the early stages of the pre-pulse plasma expansion. Therefore, for lasing in higher Z ions the optimum delay that results from the tradeoff between increased Ni-like ion fraction for maximum gain coefficient (longer delay) and decreased electron density gradients for reduced refraction loss occurs at short delays.

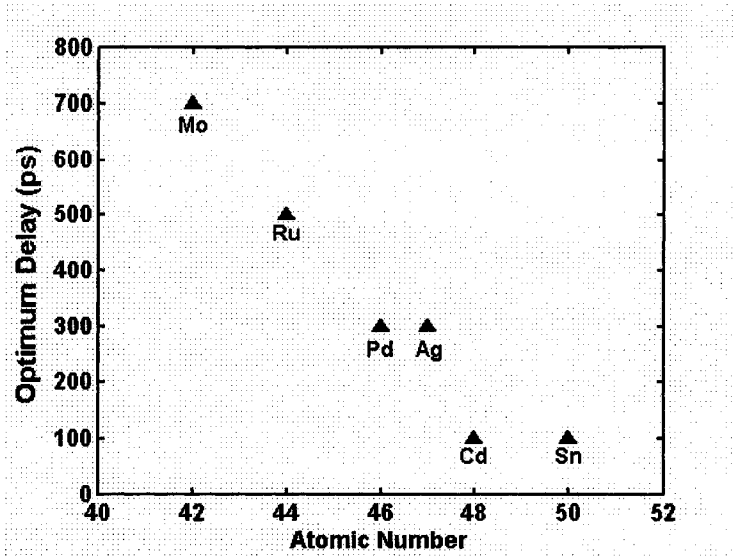

Figure 3.9 Measured optimum delay between the 120 ps, ~350 mJ pre-pulse and the 8 ps, ~1 J short pulse, for $4d\ ^1S_0 \rightarrow 4p\ ^1P_1$ lasers on the different Ni-like ions; Z=42 (Mo), Z=44 (Ru), Z=46 (Pd), Z=47 (Ag), Z=48 (Cd) and Z=50 (Sn).

3.5.2 Grazing incident angle optimization

The selection of the short pulse grazing incidence angle that maximizes the pump beam energy deposition in the gain region is key to improve the soft X-ray laser efficiency. Figure 3.10 shows the variation of Ni-like Cd laser output intensity as a function of the grazing incidence angle of the short pump pulse. As the angle of incidence, θ, is incremented, the electron density of the plasma region in which refraction couples the pump beam increases as $n_e = \theta^2 \times n_{ec}$, where n_{ec} is the critical density. At the lower angles refraction couples the pump beam into a plasma region at which the density is lower than optimum for amplification by transient collisional excitation. The maximum laser output intensity was observed at an angle of 23°, for

which the plasma density is 2.8×10^{20} cm^{-3}. The same grazing incidence angle was measured to be optimum for Ni-like Pd and Ag.

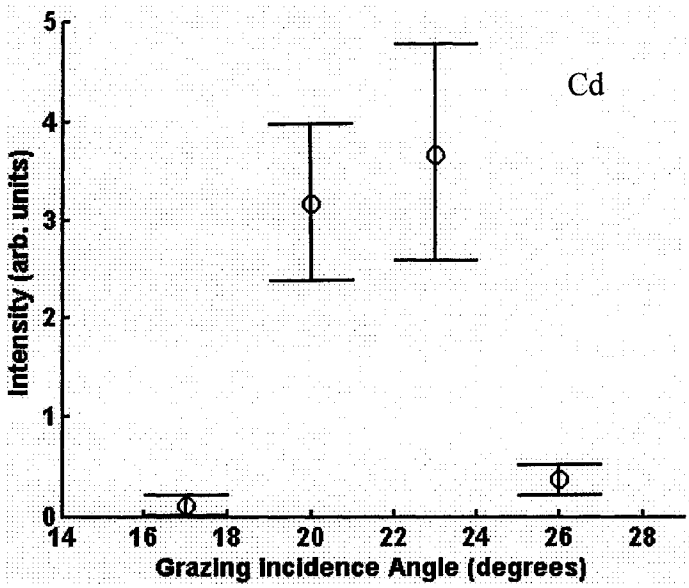

Figure 3.10 Variation of the intensity of the 13.2 nm line of Ni-like Cd as a function of grazing incidence angle of the 8 ps beam onto the target.

Similar measurements of the laser output energy as a function of angle were conducted for Ne-like ions. Fig. 3.11 shows the variation of Ne-like soft x-ray laser output intensity as a function of the angle of incidence of the short pulse beam for Ne-like Ti, V, and Cr. At an incidence angle of 17° lasing was observed for the $3p^1S_0$-$3s^1P_1$ lines of the Ne-like ions of all three species. However, at this angle the pump beam is deposited in a region where the electron density is lower than the optimum value for maximum soft x-ray laser output intensity. The output intensity of all three Ne-like ion lasers was observed to increase significantly for an angle of 20°, for which refraction helps to couple the pump beam into a region of high electron density (2×10^{20} cm^{-3}). However, at the steeper angle of incidence of 23° a significant fraction of the beam energy is absorbed in a higher density region where the electron density

gradients are too steep for optimum amplification, and the laser output energy is observed to decrease. Also contributing to a lower laser output at this angle is the shorter duration of the gain and the increased mismatch between the velocity of the traveling wave of the pump and the speed of light in the plasma.

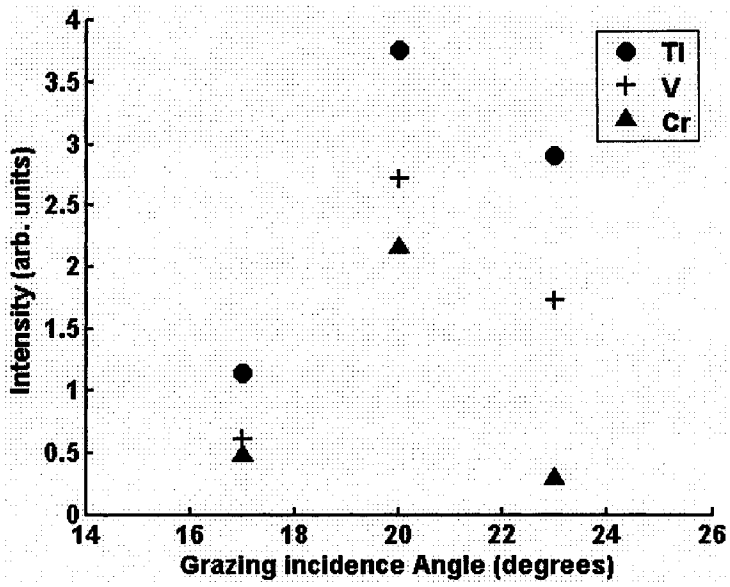

Figure 3.11 Variation of output laser intensity as a function of grazing incidence angle for Ne-like Ti, V and Cr. Each point represents the mean of 15 or more consecutive laser shots. In all three cases the laser operates best at 20 degrees. At this angle the standard deviation of each data set ranges from 14% to 38% of the mean.

For the $3d^1P_1 \rightarrow 3p^1P_1$ Ti line at 30.1 nm, the laser is very weak at incidence angle of 17°, and lasing was observed to be strong for 20° and 23° grazing incidence angle for optimum [6]. As discussed in last section, the 30.1 nm laser line relies on strong re-absorption of the 2.335 nm transition linking the $3d^1P_1$ laser upper lever to the ion ground state for inversion. Therefore amplification in this line requires a large density of Ne-like ground state ions which increase the trapping of the 2.335 nm line, explaining the fact this line is very weak at the lower plasma density corresponding to the 17 degrees grazing incidence angle.

3.5.3 Short pulse duration

Another important parameter is width of the short pump pulse. The variation of the laser output energy with pump pulse length was measured for select of these lasers.

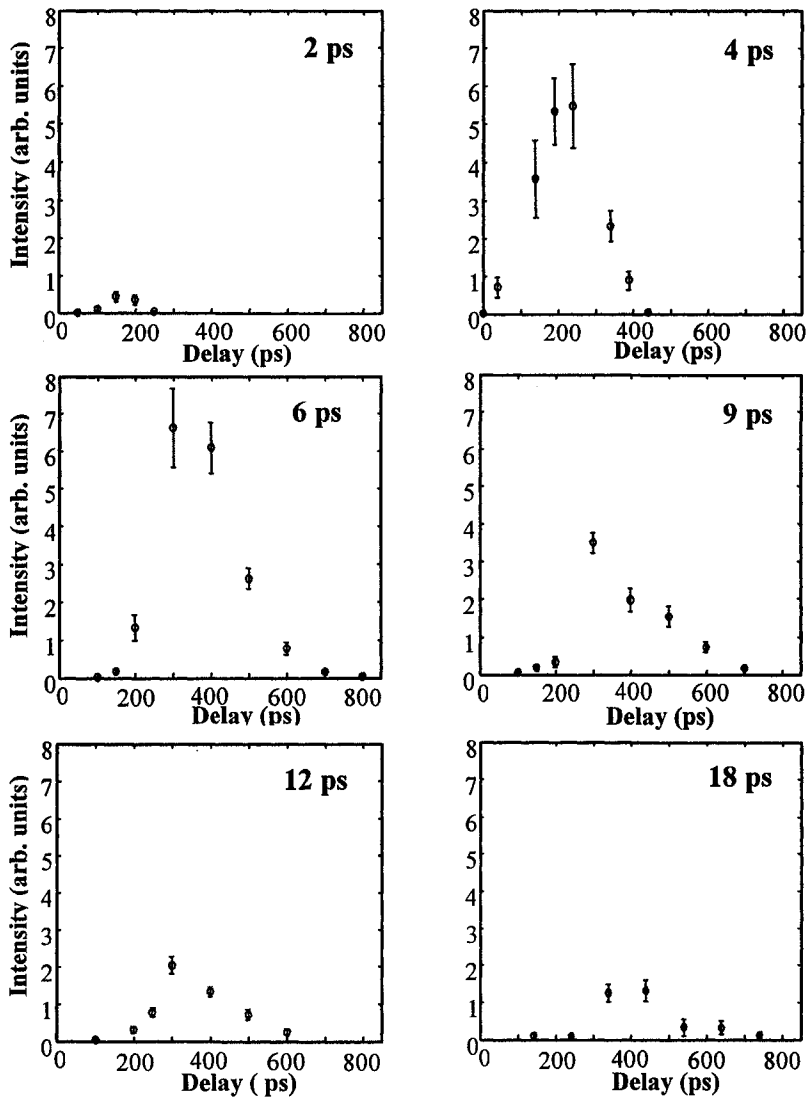

Figure 3.12 Variation of output laser intensity as a function of short heating pulse durations for Ni-like Ag (13.9 nm). Each point represents the mean of 10 or more consecutive laser shots.

Figure 3.12 shows the effect of the short pulse length in the line intensity of the 13.9 nm of Ni-like Ag for pulse width between 2 and 18 ps. The short pulse pump energy was kept constant at 1 J.

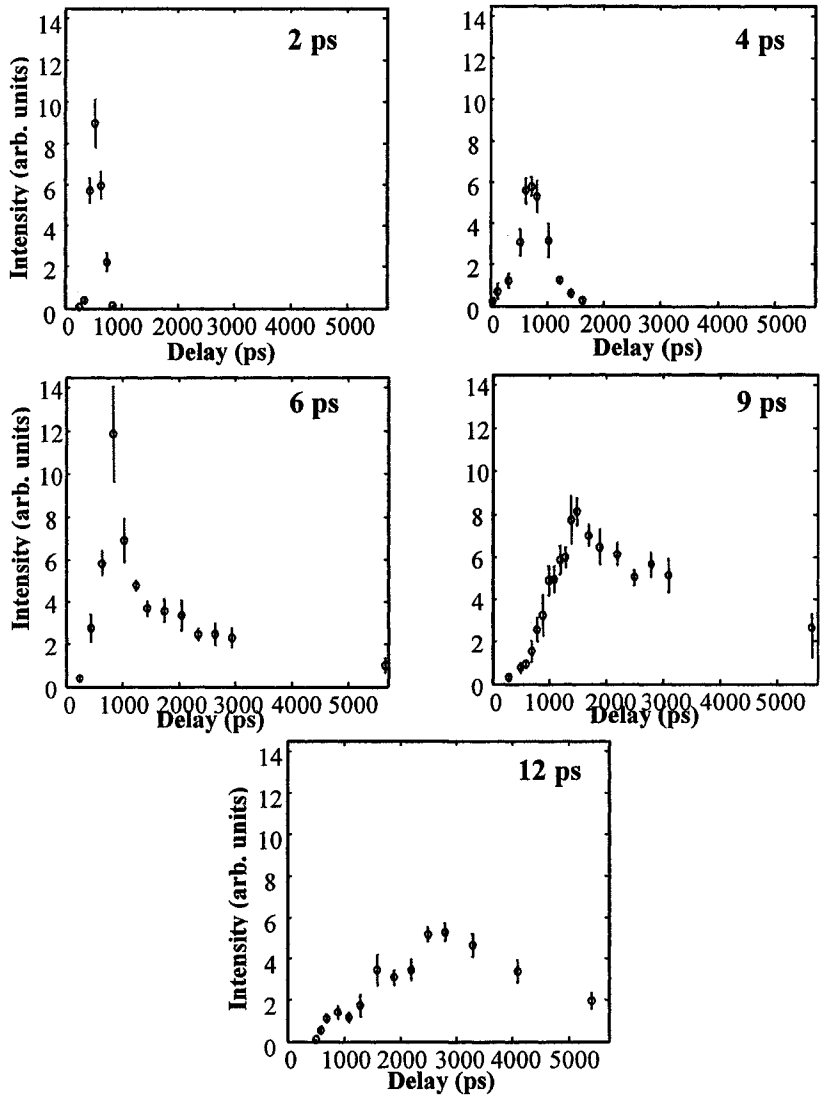

Figure 3.13 Variation of Ni-like Mo laser (18.9 nm) intensity as a function of time delay between pre-pulse and short pulse for different duration of the short pulses.

To conduct these experiments, the pump laser pulse width was set by adjusting the position of the second grating position in compressor.

For the 13.9 nm laser line of Ni-like Ag, the optimum pulse width was determined to be 6 ps. The time delay between the 300 mJ pre-pulse and the short heating pulse is observed to increase from 150 ps for 2 ps pump pulse to 400 ps for 18 ps pump pulse.

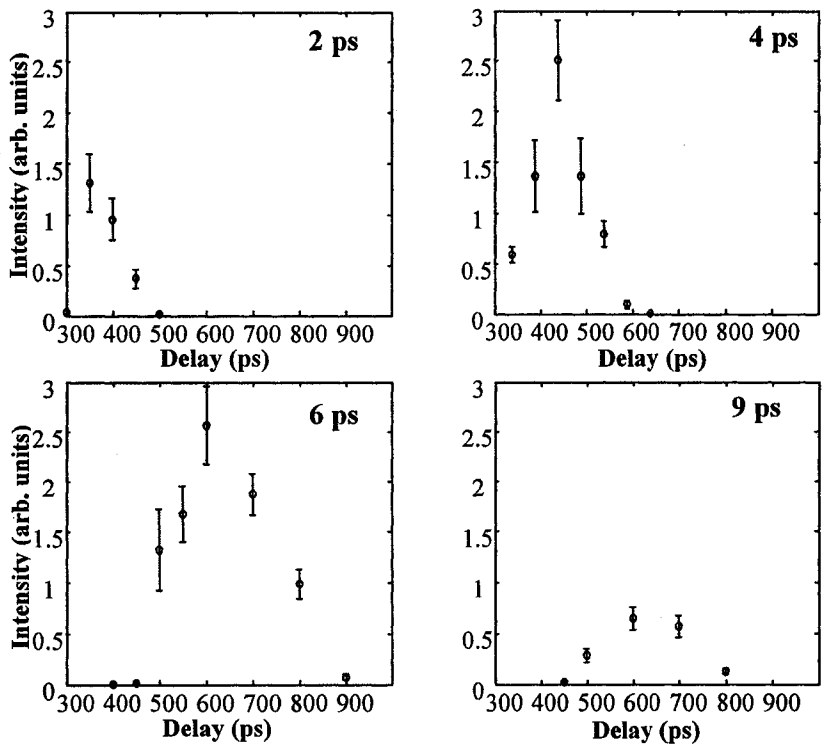

Figure 3.14 Variation of Ne-like Ti laser (32.6 nm) intensity as a function of short pulse durations.

We also conducted similar measurements for Ni-like Mo laser at 18.9 nm (Fig. 3.13) and Ne-like Ti laser lines at 32.6 nm (Fig. 3.14). The optimum pump pulse durations for laser intensity are also around 6 ps (for short pulse). In general, it can be concluded that duration of 6 ps for the short pulse is adequate to pump a great variety of Ni-like and Ne-like laser transition.

For all the factors we tested to get best laser output, we made a table to show the best conditions for all Ni-like materials (table 3.1).

Table 3.1 Optimum pump parameters for different Ni-like x-ray laser line

Target material	Wavelength (nm)	Delay time (ps)	Delay range (ps)	Incident angle (degrees)	Pulse duration (ps)
Ti	32.6	600	250	20	6
V	30.4	450	200	20	*
Cr	28.6	450	200	20	*
Mo	18.9	700	500	20	6
Ru	16.5	500	300	23	*
Pd	14.7	300	300	23	*
Ag	13.9	300	300	23	6
Cd	13.2	150	200	23	*
Sn	11.9	100	100	23	*
Sb	11.4	75	50	23	*
Te	10.9	50	<50	23	*

*. Not measured.

3.6 Continous Operation at 5 Hz Repetition Rate

Prolonged repetitive operation of pulsed lasers at optical wavelengths has been available for several decades and has made possible the implementation of numerous applications requiring intense pulses of coherent infrared, visible, and ultraviolet light. To extend and develop these applications at shorter wavelength requires high repetition rate operation of soft x-ray laser amplifiers in the gain-saturation regime. A renewable gain medium that can allow for the un-interrupted generation of long series of laser shots is essential.

Capillary discharge lasers based on the excitation of a gas by a fast discharge current pulse were the first soft x-ray lasers to achieve prolonged operation in the gain-saturated regime at a repetition rate of up to 10 Hz [11, 12]. This made possible

the use of a Ne-like Ar laser emitting at 46.9 nm in several applications [13]. Soft x-ray lasers based on optical field ionization of gaseous targets emitting at wavelengths longer than 30 nm have also been demonstrated to operate repetitively in the gain-saturated regime [14, 15]. Several other experiments have demonstrated soft x-ray laser amplification at multi-Hz repetition rates, but without achieving the gain-saturated amplification levels necessary to produce significant average powers [16, 17].

In the transient collisional lasers discussed above, the number of laser shots that can be obtained heating the same target surface depends on the material. While for Ni-like Mo up to 20 to 30 laser shots can be obtained without moving the target in between shots, for Ni-like Ag or Ni-like Cd the laser output intensity is observed to degrade after only 2-3 shots on the same target surface. This quick degradation raises the question whether these materials are suitable for extended continuous operation particularly in the 13 – 14 nm EUV wavelength range where many studies have utilized the high average brightness of synchrotrons.

To provide a solution to this problem we developed a solid helicoidal target that is continuously rotated and advanced to renew the target surface between shots. This method will allow for uninterrupted soft x-ray laser output at a repetition rate of 10 Hz for a period of hours. An average power of 2 μW and high average spectral brightness of 1.3×10^{13} photons mm^{-2} $mrad^{-2}$ s^{-1} $(0.01\%\ BW)^{-1}$ at 13.9 nm was obtained. More than 2×10^4 laser shots were obtained at 5 Hz repetition rate from a single target with a useful spiral perimeter length of 96 cm rotated at a tangential

speed of 0.2 mm s^{-1}. An increase of the number of laser shots supported by the target to about 5×10^4 was achieved by reducing the tangential rotation velocity to 0.1 mm s^{-1} at the expense of reducing the soft x-ray laser average power by about 20 percent. This set up will allow for uninterrupted saturated operation of laser-pumped table-top collisional soft x-ray lasers at a repetition rate of 10 Hz for period of about two hours.

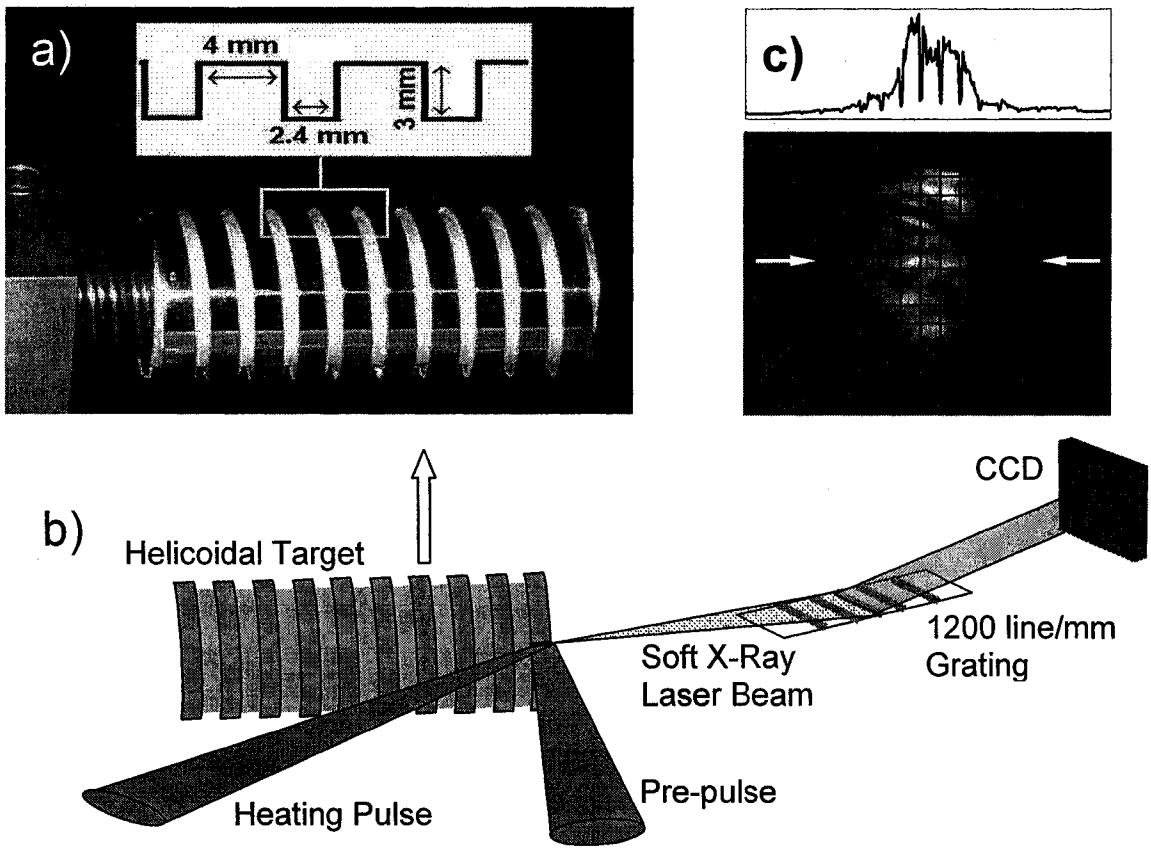

Figure 3.15 a). Schematic diagram of helicoidal soft x-ray laser target for high repetition rate soft x-ray laser operation. b) photograph of the helicoidal target. For optimized operation at 5 Hz repetition rate in the 13.9 nm line of Ni-like Ag the target was rotated at a tangential velocity of 0.2 mm s^{-1}. c) far-field image of the Ni-like Cd laser, with an intensity profile obtained at the indicated position. The square structure is produced by the supporting mesh of the Zr filter.

A schematic diagram and a photograph of the rotating target are shown in Fig. 3.15. The target consists of a solid cylindrical body 30 mm in diameter and 63 mm in length which outer surface was machined to constitute a helicoid of rectangular cross section having a 4 mm wide top surface and a 6 mm period. The target was made of electrolytic copper and was electroplated with a ~20 μm thick silver coating. It was mounted on a motorized screw having a pitch designed to continuously rotate and advance the target while making the horizontal position of the 4 mm wide stripe look stationary to the pump laser beam. A stepper motor was used to rotate the screw and advance it respect to a stationary nut, renewing the target surface irradiated by the pump beam.

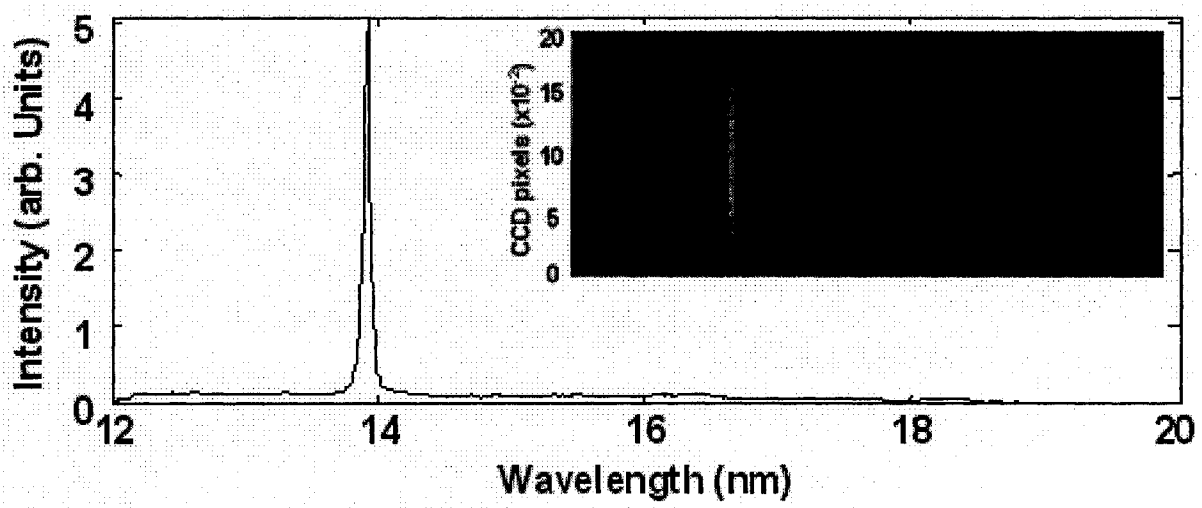

Figure 3.16 Spectrum of the emission from a Ni-like Ag laser operating at 5 Hz repetition rate using the rotating helicoidal target. The 13.9 nm line completely dominates the spectrum. The inset shows the image of the spectrum captured on the CCD.

Figure 3.16 shows a single-shot spectrum of the axial emission of a Ag plasma generated by heating the helicoidal target. The 13.9 nm line of Ni-like Ag is observed to completely dominate the spectrum. The most intense laser pulses were measured to

have an energy of 850 nJ. The laser intensity is very similar to that obtained using a flat polished Ag slab target (Fig 3.4), for which the measured gain-length product of 16.8 and observed output intensity indicate operation in the gain-saturated regime [10]. The beam quality is illustrated by the far field pattern shown in Fig 3.15 (c). To record the shot to shot intensity variations of the laser output pulse at 5 Hz repetition rate we reduced the necessary CCD readout time by binning of the pixels of the detector array and limiting the detector area read after each shot. Shooting a second shot onto the same silver target surface resulted in a decreased laser output intensity. Full recovery of the laser intensity was observed when the target was rotated to displace the ablated target surface by at least 40 μm. This induced us to select a tangential target velocity of 0.2 mm s^{-1} for soft x-ray laser operation at 5 Hz repetition rate. An increase of the rotation velocity beyond this point did not cause any significant increase in laser output energy. In contrast a reduction of the tangential velocity to 0.1 mm s^{-1}, which doubles the numbers of shots than can obtained from a single target at the expense of partially overlapping the target regions directly irradiated by the laser beam in two contiguous shots , was observed to reduce the soft x-ray laser output energy per pulse by about 20 percent.

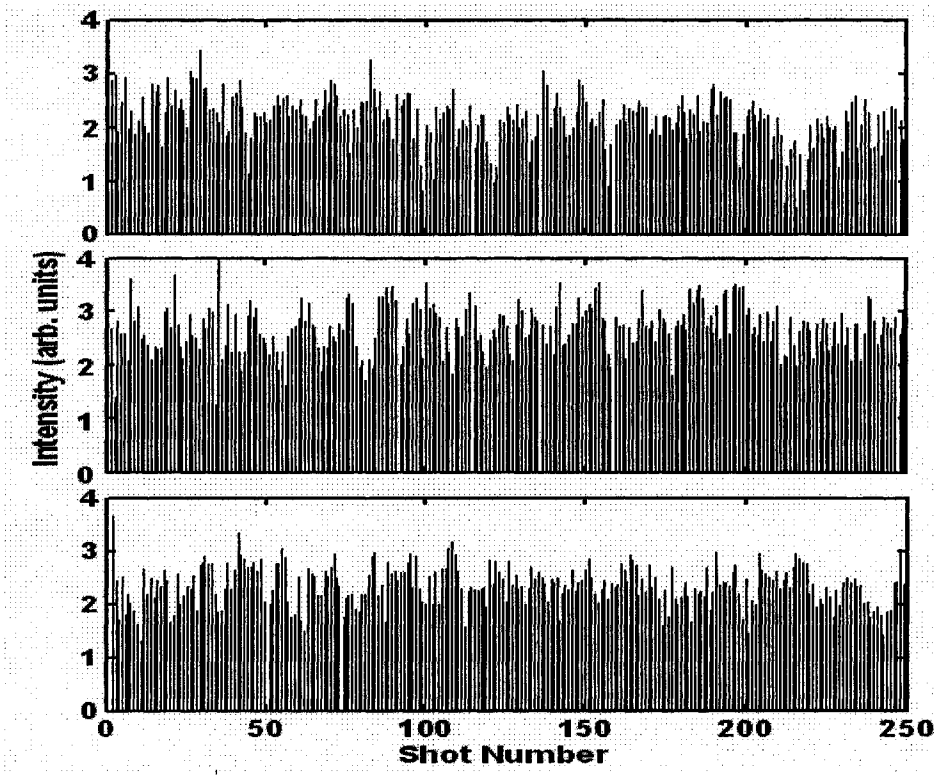

Figure 3.17 Three contiguous series of 250 laser shots at 5 Hz repetition for a λ=13.9 nm Ni-like Ag laser obtained at 5 minute intervals. The average power is about 2 μW.

Figure 3.17 shows three contiguous series of 250 laser shots each obtained at intervals of 5 minutes. The average laser pulse energy for the three series is 400 nJ, corresponding to an average power of 2 μW, and the shot to shot variation is characterized by an standard deviation of 19%. Longer series of shots showed a continuous decrease of the output pulse energy after the first ~ 250 shots. The decrease in laser pulse energy was traced to degradation of the laser beam wavefront and line focus quality due to the thermal loading of the replica diffraction gratings of the pulse compressor. As illustrated in Fig. 3.17, an interval of 4-5 minutes between

each series of 250 shots allows for full recovery of the laser intensity. The use of master diffraction gratings should readily allow for uninterrupted operation of the 5 Hz laser for more than 5×10^4 laser shots, corresponding to more than two hours of continuous laser operation. The straightforward increase of the target length will allow for several hours of uninterrupted 10 Hz repetition rate laser operation and potentially double the average power to 4 μW using 0.2 mm s^{-1} speeds. Laser operation at other soft x-ray wavelengths can be readily obtained selecting a coating which allows lasing in transitions of other Ni-like of Ne-like ions. Similar results were obtained for the 13.2 nm line of Ni-like Cd by coating the target with Cd. A laser average output power of about 1 μW was generated in this line as the result of operation at 5 Hz repetition moving the target at 0.2 mm s^{-1}.

This x-ray laser source has a combination of both high average power and high average spectral brightness as a result of the 5 - 10 Hz repetition rate described here. The 2 μW average power operation is equivalent to 1.5×10^{11} photons/s, while the energy of the most intense pulses approaches 1 μJ. The estimated average brightness of the source, 1.3×10^{13} photons mm^{-2} $mrad^{-2}$ s^{-1} $(0.01\%\ BW)^{-1}$, is similar to that of some synchrotron bending magnets operating at the same photon wavelength. Simultaneously as a result of the measured short pulse duration of 5 ps (FWHM) for the 13.9 nm Ni-like Ag. A high peak power of 0.1 –0.2 MW and peak spectral brightness of about $0.5\text{-}1 \times 10^{24}$ photons mm^{-2} $mrad^{-2}$ s^{-1} $(0.01\%\ BW)^{-1}$ can be achieved. This peak spectral brightness exceeds by two to three orders of magnitude that of undulators operating at this wavelength.

3.7 Conclusion

In this chapter, the variation of soft x-ray laser output energy is discussed as a function of several parameters. A solid target scheme that allows for the first time to our knowledge the operation of high repetition rate laser-pumped transient collisional lasers emitting in the 100 eV photon range for periods of hours is described. The uninterrupted generation of high average power soft x-ray laser radiation will enable numerous applications.

References

[1] B. M. Luther, Y. Wang, M. A. Larotonda, D. Alessi, M. Berrill, J. J. Rocca, J. Dunn, R. Keenan, and V. N. Shlyaptsev, "High Repetition Rate Collisional Soft X-Ray Lasers Based on Grazing Incidence Pumping," IEEE, Quantum Electron., vol. 42, 1, (2006)

[2] G. J. Tallents, Y. Abou-Ali, M. Edwards, R. E. King, G. J. Pert, S. J. Pestehe, F. Strati, R. Keenan, C. L. S. Lewis, S. Topping, O. Guilbaud, A. Klisnick, D. Ros, R. Clarke, D. Neely, and M. Notley, in X-Ray Lasers, American Institute of Physics Conference Proceedings 641 (American Institute of Physics, Melville, N.Y., 2002), p. 291.

[3] Advanced Light Source, Lawrence Berkeley National Laboratory, courtesy Eric Gullikson.

[4] B. M. Luther, Y. Wang, M. Larotonda, D. Alessi, M. Berrill, M. Marconi, V. Shlyaptsev, and J. J. Rocca, "Saturated high repetition rate 18.9 nm table-top laser in nickel-like molybdenum," Opt. Lett., vol. 30, pp. 165–167, 2005.

[5] V. N. Shlyaptsev, A. V. Gerusov, A. V. Vinogradov, J. J. Rocca, O. D. Cortazar, F. Tomasel, and B. Szapiro, in Ultrashort Wavelength Lasers II, edited by S. Suckewer, SPIE Proc. Vol. 2012, pp. 99–110 (1993).

[6] D. Alessi, B. M. Luther, Y. Wang, M. A. Larotonda, M. Berrill, and J. J. Rocca, "High repetition rate operation of saturated tabletop soft x-ray lasers in transitions of neon-like ions near 30 nm," Opt. Express 13, 2093 (2005)

[7] J. Nilsen, "Analysis of a picosecond-laser-driven Ne-like Ti x-ray laser," Phys. Rev. A 55, 3271-3274 (1997)

[8] R. Keenan, J. Dunn, P. K. Patel, D. F. Price, R. F. Smith, and V. N. Shlyaptsev, "High repetition rate grazing incidence pumped x-ray laser operating at 18.9 nm," Phys. Rev. Lett. **94**, 103901 (2005)

[9] M. A. Larotonda, B. M. Luther,Y.Wang,Y. Liu, D. Alessi, M. Berrill, A. Dummer, F. Brizuela, C. S. Menoni, M. C. Marconi, V. N. Shlyaptsev, J. Dunn, and J. J. Rocca, "Characteristics of a saturated 18.9-nm tabletop laser operating at 5-Hz repetition rate," IEEE J. Sel. Topics Quantum Electron., vol. 10, 6, 1363–1367, (2004)

[10] Y. Wang, M. A. Larotonda, B. M. Luther, M. C. Marconi, D. Alessi, M. Berrill, V. N. Shlyaptsev, and J. J. Rocca, "Demonstration of saturated high repetition rate

tabletop soft X-ray lasers at wavelengths down to 13.9 nm," Phys. Rev. A., vol. **72**, p. 053807, (2005)

[11] B. R. Benware, C. D. Macchietto, C. H. Moreno, and J. J. Rocca, "Demonstration of a high average power tabletop soft x-ray laser", Phys. Rev. Lett. 81, 5804-5806 (1998)

[12] S. Heinbuch, M. Grisham, D. Martz, and J.J. Rocca, "Demonstration of a desk-top size high repetition rate soft x-ray laser," Opt. Express **13**, 4050 (2005)

[13] Several of these applications are discussed in: J. J. Rocca, M. Frati, B. Benware, M. Seminario, J. Filevich, M. Marconi, K. Kanizay, A. Ozols, I. A. Artiukov, A. Vinogradov, and Y. A. Uspenskii, "Capillary discharge tabletop soft X-ray lasers reach new wavelengths and applications," C. R. Acad. Sci. Paris, vol. 1, 1065-1081 (2000), and in references therein.

[14] S. Sebban, R. Haroutunian, P. Balcou, G. Grillon, A. Rousse, S. Kazamias, T. Marin, J. P. Rousseau, L. Notebaert, M. Pittman, J. P. Chambaret, A. Antonetti, D. Hulin, D. Ross, A. Klisnick, A. Carillon, P. Jaegle, G. Jamelot, and J. F. Wyart, "Saturated amplification of a collisionally pumped optical-field-ionization soft X-ray laser at 41.8 nm," Phys. Rev. Lett. 86, 3004-3007 (2001)

[15] S. Sebban, T. Mocek, D. Ross, L. Upcraft, P. Balcou, R. Haroutunian, G. Grillon, B. Rus, A. Klisnick, A. Carillon, G. Jamelot, C. Valentin, A. Rousse, J. P. Rousseau, L. Notebaert, M. Pittman, and D. Hulin, "Demonstration of a Ni-like Kr

optical-field-ionization collisional soft X-ray laser at 32.8 nm," Phys. Rev. Lett. **89**, art. 253901 (2002)

[16] D. V. Korobkin, C. H. Nam, S. Suckewer, and A. Golstov, "Demonstration of soft x-ray lasing to ground state in Li III," Phys. Rev. Lett. 77, 5206-5209 (1996)

[17] T. Ozaki, R. A. Ganeev, A. Ishizawa, T. Kanai, H. Kuroda, "Highly directive 18.9 nm nickel-like molybdenum X-ray laser operating at 150 mJ pump energy", Phys. Rev. Lett. **89**, art. 253902 (2002)

Chapter 4, Characterization of Soft X-ray Lasers

4.1Introduction

The characteristics of the beam produced by the soft x-ray lasers described in chapter 3 are important for their use in different applications. This chapter describes the measurement of the beam divergence, spatial coherence length and pulse width of the high repetition rate Ni-like lasers executed by grazing incidence pumping.

4.2 Soft X-ray Laser Beam Divergence

The soft x-ray laser beam divergence is determined by the respect ratio of the plasma amplification and by refraction effect.

The divergence was determined from the extent of laser beam. Figure 4.1 shows on schematic diagram of the setup used to determine the beam divergence. The distance from the target to grating was 248 mm, and that from grating to CCD camera was 235 mm, amounting to a total distance of 483 mm.

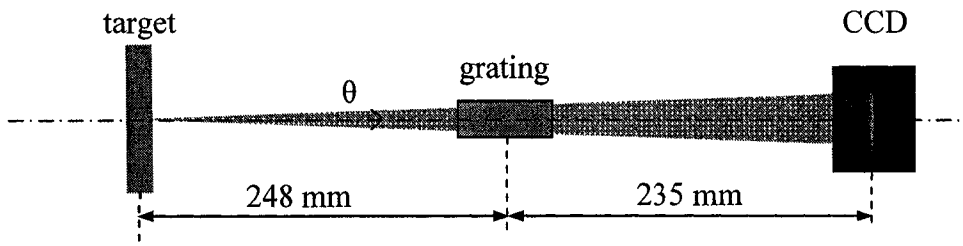

Figure 4.1 Schematic diagram of the set up used to measure the beam divergence in the direction parallel to the target.

Figure 4.2 shows an on-axis spectra of the Ni-like Ag laser generated by irradiating 4 mm long target. The extent of the 13.9 nm $4d^1S_0$-$4p^1P_1$ line in the

direction parallel to the target corresponds to a divergence of 9 milliradians. Divergence angle of direction perpendicular to the target is smaller, which is about 5 milliradians. Figure 3.4 shows single shot on-axis spectra corresponding to a 4 mm line focus plasmas showing lasing of the Ni-like ions for different wavelengths at direction parallel to the target.

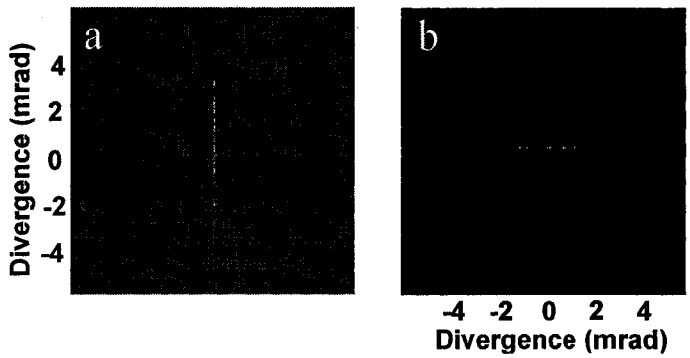

Figure 4.2 Divergence angle of 13.9 nm Ni-like Ag laser at both direction: a) 9 milliradians at direction parallel to the target, b) 5 milliradians at direction perpendicular to the target.

4.3 Measurement of the Spatial Coherence

4.3.1 Spatial coherence measurement of 18.9 nm Ni-like Mo

One of the fundamental properties of a laser is its ability to produce spatially coherent beams. This is often accomplished in the visible and ultraviolet regions of the spectrum with the aid of an optical resonator that permits the growth of only a single transverse "TEM00" mode. At shorter wavelengths, in the EUV and soft x-ray regions of the spectrum, optical resonators are of limited use due to the finite lifetime of the gain medium, limited reflectivity of available mirrors, and mirror damage. Short-wavelength light sources such as electron impact sources, synchrotron sources [1], x-ray lasers [2, 3], and free-electron lasers [4] to date generate only partially

coherent light. Pinhole spatial filtering has been used to achieve spatial coherence from otherwise incoherent sources, such as undulator radiation, but generally at a significant loss of available photon flux, and without imposing phase coherence across the radiation field.

The spatial coherence of the 18.9-nm radiation produced at 20 degree grazing incidence pumping was characterized by placing Young's double slits 5.5 cm from the Mo target. The laser beam profile at this location was found to have a width (FWHM) of approximately 500 μm. The double slits were prepared by laser drilling two 4-mm-long 5-μm-wide slits on 12.5 μm thick stainless steel substrates (National Aperture Inc., NH). Slit separations of 50 μm and 75 μm were used in the experiments. A diffraction grating was used to reduce the background plasma radiation and increase the signal-to-noise ratio of the recorded interference pattern [Fig. 2.4]. The slits were placed horizontally, perpendicular to the target surface and grating groove direction, generating interference in the vertical direction. The length of the slits (4 mm) was much longer than the laser beam diameter (~ 500 μm here). Therefore, the slits had minimal effect on the spatial extent of the spectral line. The intensity modulation observed along the length of the 18.9-nm laser line is an indication of the degree of spatial coherence between light illuminating each of the two individual slits.

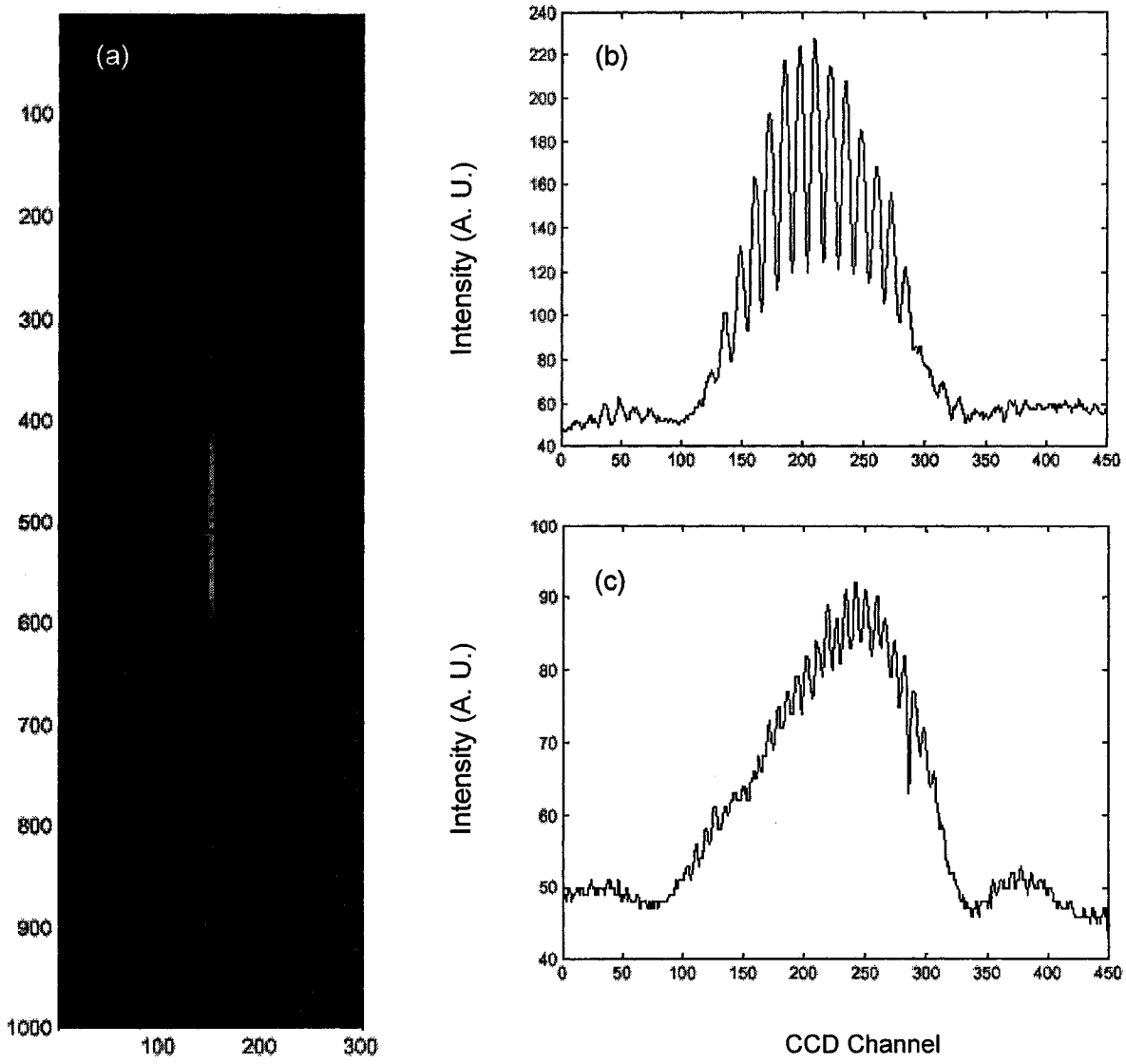

Figure 4.3 Results of Yong's interference experiment to determine the spatial coherence of the 18.9 nm Ni-like Mo line. (a) Interferogram obtained placing a slit pair with 50 μm separation at 5.5 cm from the exit of a 4-mm-long Mo target. (b) Lineout for the 50 μm separation slit pair obtained integrating the interference pattern in the direction perpendicular to the line. (c) Lineout for the slit pair with 75 μm separation. The asymmetry is due to the uneven illumination of the slit pair that was not centered on the beam axis.

As shown in Fig. 4.3 (a), this method produced a very clear interference pattern on the 18.9-nm laser line with a single laser shot, even though the slits blocked more than 90% of the photons. In fact, the gain-saturated operation of the

laser produced such a high photon flux level that the first-order spectral line of the 18.9-nm radiation saturated the CCD. Therefore, to measure the fringe visibility we used the line produced by the second order of the diffraction grating. The evaluation of the degree of spatial coherence using the double-pinhole or the double-slit technique follows the description of partially coherent radiation in terms of the mutual intensity and the complex coherence factor [5]. In an ideal double slit experiment where both slits are equally illuminated, the modulus of the complex coherence factor is equal to the fringe visibility, defined as $V = (I_{max} - I_{min}) / (I_{max} + I_{min})$, where I_{max} and I_{min} are the maximum and minimum intensities of the fringe pattern. Fig. 4.3 (a) shows the interference generated by the 18.9-nm laser line when a double slit with 50-μm separation was used. The horizontal lineouts for 50-μm and 75-μm slit separations are shown in Fig. 4.3 (b) and (c), respectively. From the fringe visibilities, the degree of spatial coherence is determined to be 0.4 between two slits separated by 50 μm and 0.1 for 75 μm separation.

Using the van Cittert–Zernike theorem [5] a near-Gaussian intensity profile, incoherent source of roughly 11 μm diameter (FWHM) would be needed to produce similar fringe visibilities with the same slit pairs at the same distance (5.5 cm) from the source. This is about 3× smaller than the 30 μm pump laser beam width. An additional characteristic of a pulsed light source closely related to the spatial coherence is the peak spectral brightness. With a measured divergence angle of about 9 mrad and approximating the pulse duration with the value we measured for the Ni-like Ag line using a streak camera, ~5 ps, the peak spectral brightness of this source is

estimated to be of the order of 1 x 10^{24} in units of photons s^{-1} mm^{-2} $mrad^{-2}$ within 0.01% spectral bandwidth.

4.3.2 Spatial coherence measurement of 13.2 nm Ni-like Cd

Spatial coherence measurement was also performed for Ni-like Cd laser at 13.2 nm. The experimental setup of the coherence measurements is illustrated in Fig. 4.4. It differs from the previous set up in that incorporates a 45 degrees Mo/Si multilayer mirror. A set of slit pairs with separations of 30, 50, and 75 μm was used in the experiments. The width of each individual slit was 5 μm. In the measurements the slits were placed at 105 mm from the laser target. A 0.2 μm thick self-supported Zr filter was used to block the Ti:sapphire laser and the visible/ultraviolet radiations from the plasma. The 45-degree folding mirror is coated with Mo/Si multilayer, which has ~50% reflectivity at 13.2 nm and a spectral bandwidth of ~1 nm (FWHM). The interferograms were recorded with an EUV sensitive CCD camera having a back-illuminated 2048 × 2048 array of 13 × 13 μm^2 pixels. The total path length from the double-slit to the CCD is 330 mm. The multilayer mirror and Zr filters sufficiently prevent most unwanted radiation from reaching the CCD and allow us to record clean interferogram in a single shot. Given the fact that the 13.2 nm laser line has a narrow linewidth of $\Delta\lambda<10^{-4}$ λ, although it strongly dominates the spectrum, it's still necessary to discriminate from a low level of background (typically 10% of the 13.2 nm radiation) in the CCD readouts originating from plasma radiation emitted at EUV wavelengths falling into the 1-nm bandwidth of the multilayer. Assuming the background radiation from the plasma to be isotropic, for each interferogram we recorded the background by moving the slit away from the soft x-ray laser beam path

and repeated the shot under the same experimental condition. We then obtained a clean interferogram by subtracting the background from the original one. This process also automatically removes the uniform thermal dark current of the CCD.

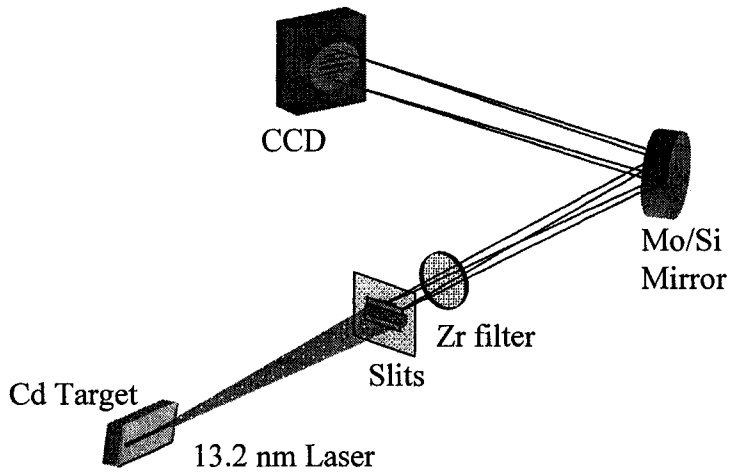

Figure 4.4 Young's double-slit experiment setup for measuring the spatial coherence of a 13.2 nm Ni-like Cd soft x-ray laser.

A typical interferogram recorded using a double slit with 30 μm separation is shown in Fig. 4.5 (a). The double-slit was placed horizontally, in the direction perpendicular to the target, thus diffraction and interference pattern occurred in the vertical direction. We integrated the interferogram along both horizontal and vertical directions. The vertical one (Fig. 4.5 (b)) can be seen as a lineout of the laser beam intensity profile, sampled by the slits. It provides useful information on beam size and divergence angle. The horizontally integrated one (Fig. 4.5 (c)) is the overall double-slit interference pattern, from which an 'average' fringe visibility can be obtained. The high fringe visibility in Fig. 4.5 (c) implies a high degree of spatial coherence for 30 μm separation.

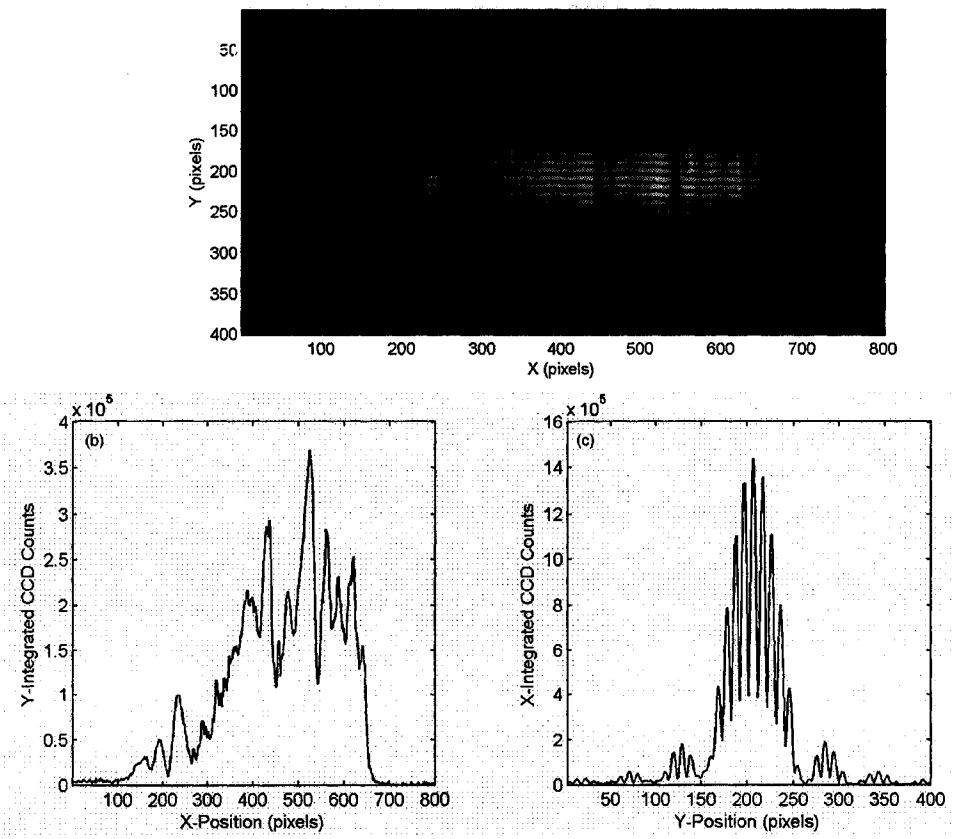

Fig. 4.5. (a) A typical two-slit interferogram recorded by the CCD for a 30 μm slit separation. The double-slit is placed horizontally (x-direction). (b) Integration of (a) in the vertical direction, which gives a lineout of the laser beam intensity profile. Intensity irregularities, or microstructures, are clearly observed. (c) Integration of (a) in the horizontal direction, which gives an 'average' interference pattern, whose fringe visibility is a measure of the spatial coherence.

A noticeable feature of the interferograms is the pronounced intensity irregularity, with many local intense spots in them. Those spots were observed in all the interferograms, regardless of slit orientation and Cd target length. Their peak intensities and positions changed randomly from shot to shot. Their presence causes complications on the analysis of the interferograms. For typical double-pinhole/slit

coherence measurements, the relationship between fringe visibility V and the spatial coherence factor μ_{12} is [5]:

$$V = \frac{2\sqrt{I_1 I_2}}{I_1 + I_2}|\mu_{12}| \qquad (4.1)$$

where I_1 and I_2 are the beam intensities at the two individual slits. The fringe visibility V can be directly obtained from the interferogram as $V = (I_{max}-I_{min})/(I_{max}+I_{min})$, where I_{max} and I_{min} are the intensity maxima and minima in the interferogram. Usually, the double-slit is positioned such that $I_1 \approx I_2$, which leads to the simple relationship $V = |\mu_{12}|$. However, in general cases when $I_1 \neq I_2$, Eq. (4.1) implies $V < |\mu_{12}|$, meaning measured fringe visibility would always underestimate the real degree of spatial coherence. As the difference between I_1 and I_2 becomes larger, the discrepancy between fringe visibility V and coherence factor will also become larger. In our experiments, the randomly located hot spots present in the beam microstructure make it practically impossible to position the slit so that $I_1 \approx I_2$ can be satisfied across the whole slit. The relative strength of I_1 and I_2 is also varying therefore the factor $2\sqrt{I_1 I_2}/(I_1 + I_2)$ can not be fully determined. The characteristic size of those spots at the double-slit plane, estimated by their sizes on the CCD and a simple geometric reduction, is around 100 μm. This is comparable to the slit separations used in the experiments. While two slits separated by 30 μm (the smallest separation used in experiments) may still sample those ~ 100 μm spots with roughly the same intensities, it is more likely that double-slits with 50 μm and 75 μm separations will see increasingly different intensities on individual slits. Such

intensity difference will cause visibility variation even though $|\mu_{12}|$ could still be essentially constant.

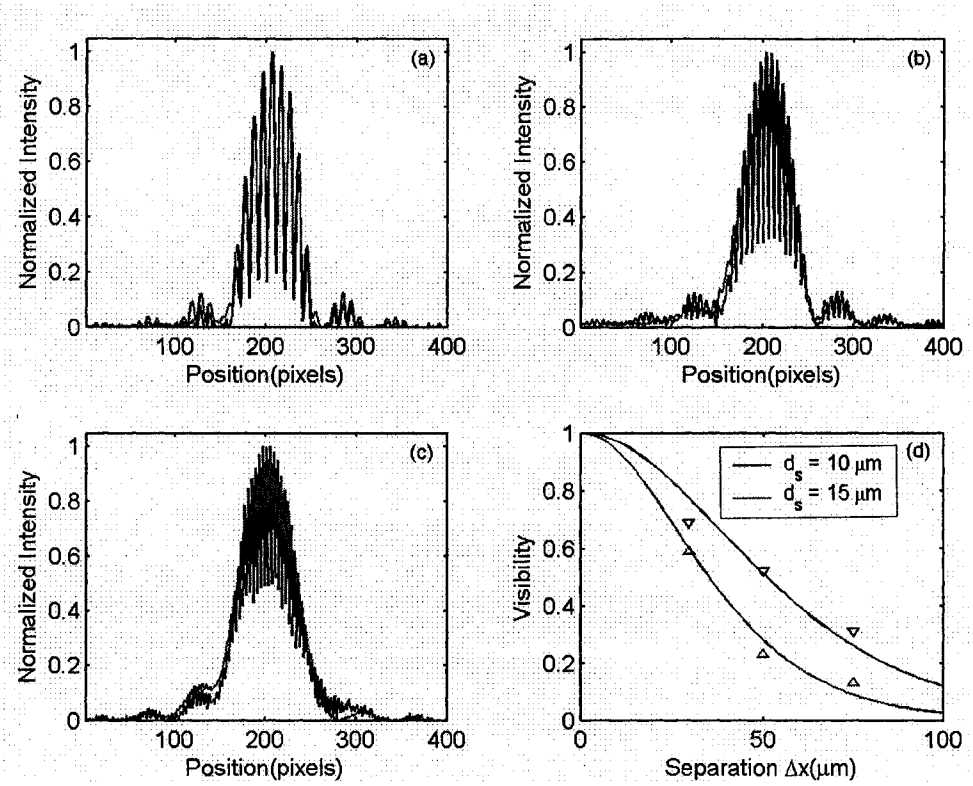

Fig. 4.6. Results of Young's interference experiment designed to determine the spatial coherence of the 13.2 nm Ni-like laser. (a-c) Interference fringes with average visibility (red), obtained by integrating the whole interferogram, and fringes with highest visibility (blue), picked by manually scanning the interferogram. For comparison the fringe patterns are normalized in intensity and overlap each other. The slit separations are (a) 30, (b) 50, and (c) 75 μm. (d) Fringe visibilities at different slit separations and theoretical predictions based on van Cittert-Zernike theorem with a parabolic-like intensity profile. The source size is 10 μm (blue, corresponding to highest visibilities in (a-c)) and 15 μm (red, corresponding to average visibilities).

Figure 4.6 illustrates the fringe patterns obtained using 4-mm-long target and horizontally placed (perpendicular to target surface) double-slits with separations of 30 (a), 50 (b), and 75 μm (c). For each separation, we first obtained an average fringe visibility (red lines) by integrating the whole interferogram. We then manually scanned the interferogram along the slit orientation and picked a small region where

the visibility is highest (blue lines in figure). The variation of fringe visibility with 30 μm double-slit is relatively small, where the best/average visibility is 0.69/0.59. The visibility variation becomes larger with 50 and 75 μm double-slits, where best/average visibility is 0.52/0.23 and 0.31/0.13, respectively. Although we could not rule out the possibility that spatial coherence factor is varying in space, we believe the highest visibility observed is a more accurate, while the average visibility underestimates it.

Having values of spatial coherence factor for different separations, we can again estimate the size of an equivalent incoherent source using van Cittert-Zernike theorem. Assuming the source has a parabolic-like intensity profile of $I=I_0\cosh^{-2}(x/a)$ [6], to produce similar spatial coherence at the double-slit plane, the source size (FWHM) is 10 μm (Fig. 4.6 (d), blue curve). For comparison, using the average visibility data (red Δ) results in a source size of 15 μm FWHM (red curve). The above results are for horizontally placed slits; vertically placed slits (parallel to target plane) gave similar results. The spatial coherence properties seem to be the same in both directions.

For applications such as interferometry and coherent imaging, highly coherent radiation is needed. The laser has a very narrow linewidth ($\Delta\lambda/\lambda<10^{-4}$), corresponding to a longitudinal coherence length of $\lambda^2/\Delta\lambda > 100$ μm, sufficient for most applications at this wavelength. To ensure high degree of spatial (transverse) coherence, adequate spatial filtering can be used [7]. Based on 430 nJ pulse energy and a 15 μm laser exit diameter predicted by a hydrodynamic model, and the measured laser pulse duration

of 5 ps [8], the laser's peak spectral brightness, a parameter closely related to a source's coherence properties and of particular value in imaging experiments, is ~ 3×10^{23} photons sec^{-1} mm^{-2} $mrad^{-2}$ within less than 0.01% spectral bandwidth. In this case, this value is slightly smaller than that computed for the 18.9 nm Ni-like Mo laser, but still exceeds the peak special brightness of modern synchrotron radiation facilities at similar wavelengths.

4.4 Measurement of the Laser Pulse Width

We measured the duration of the laser pulses corresponding to the $4d^1S_0 \rightarrow 4p^1P_1$ transitions of Ni-like Ag and Cd using a fast x-ray streak camera. The streak camera, developed at Kansas State University [9], can provide sub-picosecond temporal resolution when a sufficiently high voltage is applied between the photocathode and acceleration electron. However as discussed bellow for these measurements, the camera was operated at a reduced acceleration voltage would reduced the temporal resolution to 1.8±0.1 ps. The measurements were conducted for the optimum pumping angle at 23 degrees grazing incidence. The experiment layout used to obtain the measurement is schematically illustrated in Fig. 4.7. The soft x-ray laser pulses were generated heating 4 mm long polished slab targets of the lasing material (Ag or Cd) with a sequence of optical laser pulses generated with a 5 Hz table-top chirped-pulse amplification Ti:Sapphire laser system.

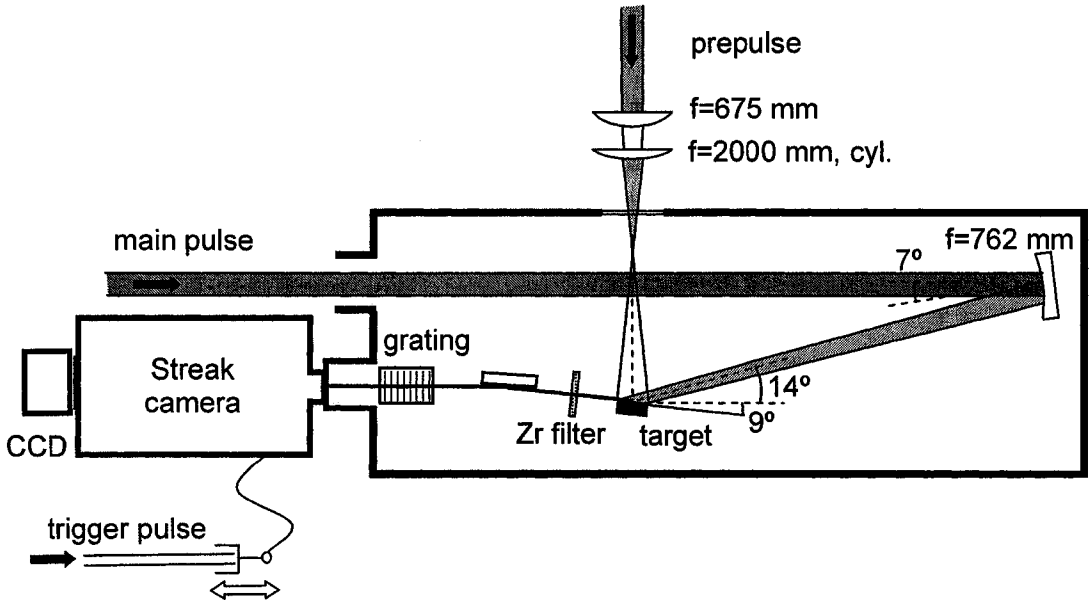

Figure 4.7 Schematic representation of the experimental set up used to measure the laser pulse width showing the soft x-ray laser pumping configuration and streak camera detection system.

The plasma emission was filtered with a 1500 Å thick Zr film and was reflected at grazing incidence by a borosilicate flat that directed it towards a 1200 l/mm gold-coated variably spaced ruling spherical grating that dispersed the light and sent the laser beam to the streak-camera slit. The fast streak camera used in the experiment is described in [9]. The experiments were conducted using a 1019 Å thick KBr photocathode film deposited onto a 1085 Å thick lexan film. High harmonic pulses from a Ti:sapphire laser of less than 30 fs duration were used to determine the resolution of the streak camera at the (-7 kV) photocathode acceleration voltages condition used in this experiment. The resolution was determined to be (1.8±0.1) ps. The temporal smearing produced by the grating can further degrade the resolution of the measurements [10, 11]. However, since the slit of the streak camera was placed 13 cm away from the image plane of the grating, its 25 μm width sampled only a

fraction of the wavefront, causing a negligible temporal smearing of 0.04 ps. The streak camera sweep was synchronized with the soft x-ray laser using a photoconductor switch triggered with a 0.2 mJ, 50 fs duration Ti:sapphire laser pulse generated by a multi-pass amplifier seeded by the same laser oscillator that seeds the soft x-ray laser pump beam and a separate grating pulse compressor. The photoconductive switch was mounted on a translation stage in order to control the delay between the sweep of the ramp and the arrival of the soft x-ray laser. The laser intensity reaching the photocathode was attenuated by slightly misaligning the center of the laser line generated by the grating respect to the center of the slit until space charge broadening was verified not to affect the measurement.

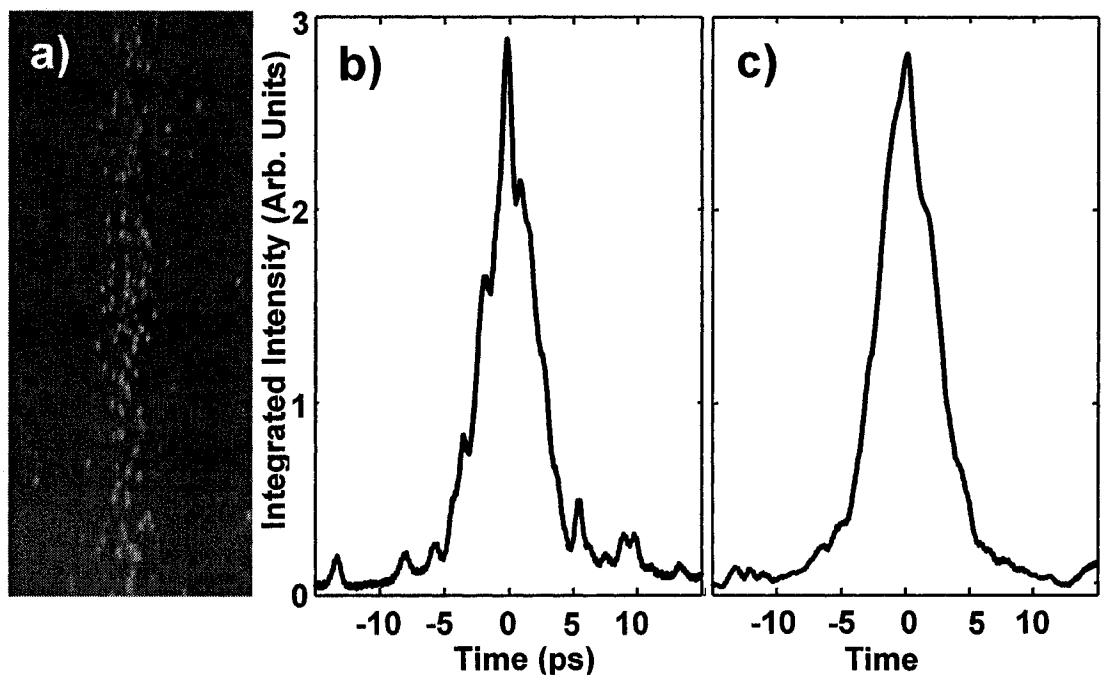

Figure 4.8 a) Single shot streak camera image of the 13.9 nm laser pulse. b) Lineout of the integrated laser line intensity vs time. c) Average corresponding to six laser shots. The measured FWHM width is 4.9 ps, and corresponding estimated true laser pulse duration is 4.6 ps. The laser was excited by a 6.7 ps duration pump pulse of 1 J energy impinging at a grazing incidence angle of 23 degrees with a pre-pulse to short pulse time delay of 250 ps.

Figure 4.8 shows a typical single streak measurement of the Ni-like Ag laser pulse for a short pump pulse of 6.7 ps duration and a time delay of 250 ps between the 350 mJ pre-pulse and the short pulse, pumping conditions that are nearly optimum for maximum soft x-ray laser output pulse energy generation. The left image shows a horizontal streak of the laser pulse. Each dot on the CCD image of the camera's phosphor screen is the result of a single photoelectron amplified on the internal multichannel plate. The curve on the center panel is the corresponding temporal profile of the x-ray laser, obtained by vertical integration of the image. Fig 4.8 (c) shows the time corresponding to an average of the six laser shots, and gives a measured FWHM trace width of (4.9±1.0) ps. The true laser pulse duration can be estimated to be (4.6±1.0) ps by deconvolution of the instrument smearing assuming a quadrature relationship. This soft x-ray pulse duration did not vary significantly and remained within the error of the measurement when the duration of the short pump pulse was reduced to 2.0 ps. The deconvoluted laser pulse duration for this case was (5.1±0.8) ps. The pulse duration of the Ni-like Ag x-ray laser was also measured as a function of delay between the prepulse and the short pump pulse, along the full range of operation of the laser [12].

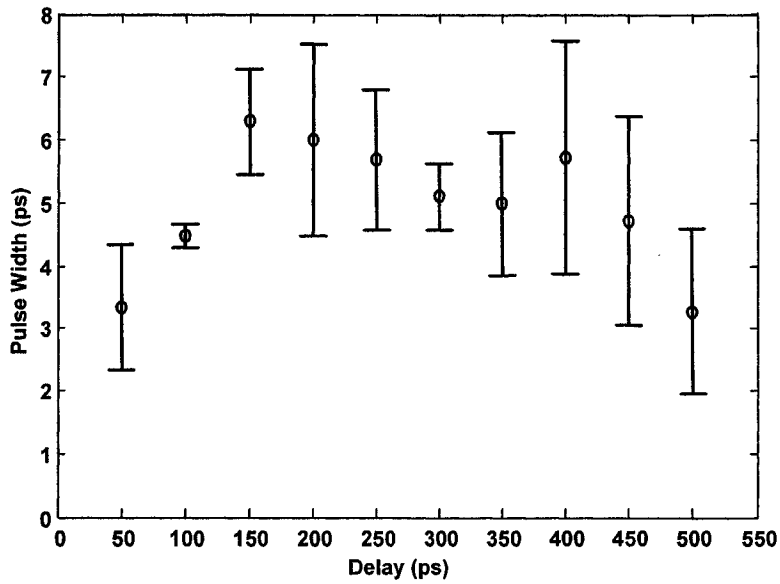

Figure 4.9 Measured variation of the 13.9 nm Ni-like Ag laser pulse width as a function of time delay between the 350 mJ pre-pulse and the 1 J pump pulse.

Figure 4.9 shows that the laser pulse duration remains relatively constant for time delays between about 150 ps and 450 ps, but it decreases outside this range as a result of a shorter duration of the gain for non-optimum delays. Model computations conducted with a hydrodynamic/atomic physics model developed in house shows a gain duration of about 15 ps for Ni-like Ag excited at the optimum pumping conditions. The exponential amplification of the amplified spontaneous emission is computed to decrease the laser pulse duration down to about 5 ps, followed by saturation re-broadening.

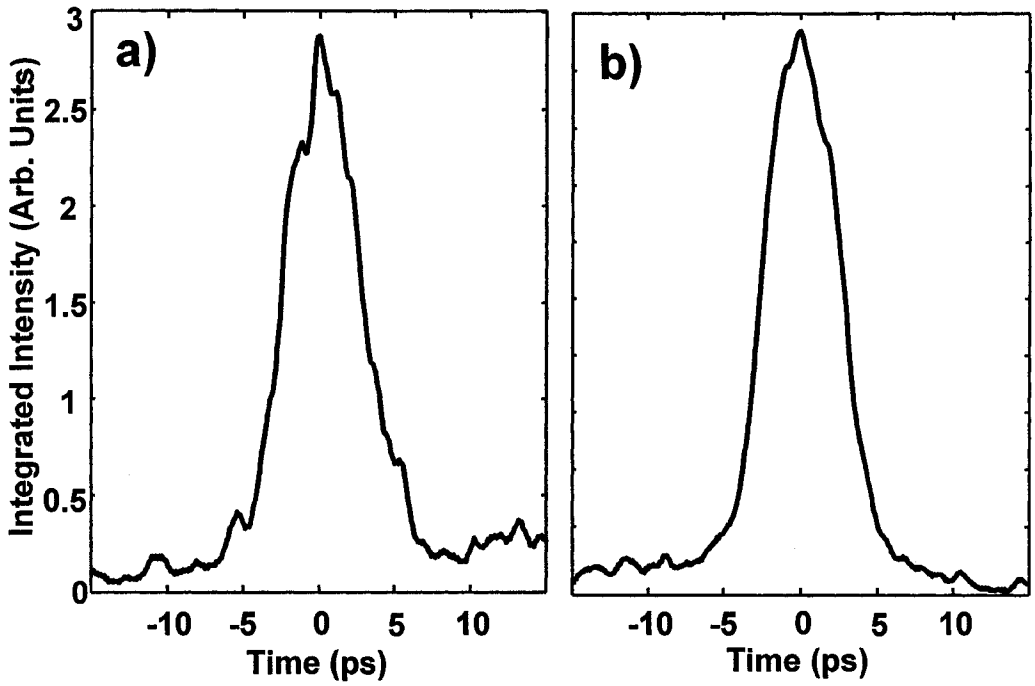

Figure 4.10 a) Lineout of a single-shot streak measurement of the 13.2 nm Ni-like Cd soft x-ray laser pulse. b) average of six laser shots, showing a deconvoluted FWHM pulse duration of 5.2 ps. The laser was excited by a 6.7 ps duration pump pulse of 1J energy impinging at a grazing incidence angle of 23 degrees for a pre-pulse to short pulse time delay of 100 ps.

We also measured a similar laser pulse duration for the 13.2 nm Ni-like Cd grazing incidence soft x-ray laser. Figure 4.10 (a) shows a single shot temporal profile and Fig. 4.10 (b) shows the average of six streak camera traces for the near optimum short pump pulse of 6.7 ps and time delay of 100 ps. The average measured FWHM pulse duration is (5.5 ± 0.3) ps (Fig. 4.10 (b)), and the deconvoluted FWHM pulse duration is (5.2 ±0.4) ps. Since from our model the linewidth of the output of these lasers after gain narrowing can be estimated to be $\Delta\nu \approx$ 2.5-3.0×10^{-5}, for the measured pulse duration of about 5 ps we can estimate $\Delta\nu \times \Delta t \sim 3$.

4.5 Conclusion

The divergence of the Ni-like Ag laser were measured to be 9 and 5 milliradians in the perpendicular and parallel directons respectively. The spatial coherence of a Ni-like Mo pumped at 20 degrees and Cd soft X-ray laser pumped at 23 degrees grazing incidence were measured in a series of Young's double-slit experiments. The equivalent incoherent source size is determined to be ~ 10 μm and the laser's peak spectral brightness ~ 3-10× 10^{23} photons sec^{-1} mm^{-2} $mrad^{-2}$ with 0.01% spectral bandwidth. Streak camera measurements show that the table-top Ni-like Ag and Cd transient lasers excited at grazing incidence have pulse durations of ~ 5 ps, corresponding to laser peak powers of up to 0.1-0.2 MW. Intense narrow bandwidth picosecond duration laser pulses in the 100 eV spectral region are available for the first time at high repetition rate for applications. The beam divergence, pulse duration and spatial coherence of the lasers were characterized.

An approach for producing soft x-ray lasers with smaller divergence and high coherence is high harmonic seeding of the pulse amplifier [13]. Chapter 5 will describes the demonstration of a high coherence soft x-ray amplifier in Ne-like Ti seeded by high harmonic pulses.

References

[1] Advanced Light Source, Lawrence Berkeley National Laboratory, courtesy Eric Gullikson.

[2] D. L. Matthews, P. L. Hagelstein, M. D. Rosen, M. J. Eckart, N. M. Ceglio, A. U. Hazi, H. Medecki, B. J. MacGowan, J. E. Trebes, B. L. Whitten, E. M. Campbell, C. W. Hatcher, A. M. Hawryluk, R. L. Kauffman, L. D. Pleasance, G. Rambach, J. H. Scofield, G. Stone, and T. A. Weaver, "Demonstration of a Soft X-Ray Amplifier," Phys. Rev. Lett. 54, 110 (1985)

[3] C. Macchietto, B. Benware, and J. Rocca, "Generation of millijoule-level soft-x-ray laser pulses at a 4-Hz repetition rate in a highly saturated tabletop capillary discharge amplifier," Opt. Lett. 24, 1115 (1999)

[4] J. Andruszkow, et al., "First Observation of Self-Amplified Spontaneous Emission in a Free-Electron Laser at 109 nm Wavelength," Phys. Rev. Lett. 85, 3825 (2000)

[5] M. Born and E. Wolf, Principles of Optics, 7th ed. Cambridge, U.K.:Cambridge Univ. Press, 1999, ch. X.

[6] R. A. London, M. Strauss and M. D. Rosen, "Modal analysis of x-ray laser coherence", Phys. Rev. Lett. **65**, 563-566 (1990)

[7] D.T. Attwood. Soft X-Rays and Extreme Ultraviolet Radiation: Principles and Applications. Cambridge University Press. (Cambridge, England, 1999)

[8] M.A. Larotonda, Y. Wang, M. Berrill, B.M. Luther, and J.J. Rocca, Mahendra Man Shakya, S. Gilbertson, and Zenghu Chang, "Pulse duration measurements of grazing incidence pumped high repetition rate Ni-like Ag and Cd transient soft x-ray lasers", Opt. Lett. **31**, 20, 3043 (2006)

[9] M. M. Shakya and Z. Chang, "Achieving 280 fs resolution with a streak camera by reducing the deflection dispersion," Appl. Phys. Lett. **87**, 041103 (2005).

[10] A. Klisnick, J. Kuba, D. Ros, R. Smith, G. Jamelot, C. Chenais-Popovics, R. Keenan, S. J. Topping, C. L. S. Lewis, F. Strati, G. J. Tallents, D. Neely, R. Clarke, J. Collier, A. G. MacPhee, F. Bortolotto, P. V. Nickles and K. A. Janulewicz, "Demonstration of a 2-ps transient x-ray laser", Phys. Rev. A 65, art. 033810 (2002).

[11] Y. Abou-Ali, G. J. Tallents, M. Edwards, R. E. King, G. J. Pert, S. J. Pestehe, F. Strati, R. Keenan, C. S. Lewis, S. Topping, O. Guilbaud, A. Klisnick, D. Ros, R. Clarke, D. Neely, M. Notley, A. Demir, "Measurement of the duration of X-ray lasing pumped by an optical laser pulse of picosecond duration", Opt. Commun. 215, 397-406 (2003).

[12] Y. Wang, M. A. Larotonda, B. M. Luther, M. C. Marconi, D. Alessi, M. Berrill, V. N. Shlyaptsev, and J. J. Rocca, "Demonstration of saturated high repetition rate tabletop soft X-ray lasers at wavelengths down to 13.9 nm," Phys. Rev. A., vol. 72, p. 053807, 2005.

[13] Y. Wang, E. Granados, M. A. Larotonda, M. Berrill, B. M. Luther, D. Patel, C. S. Menoni, and J. J. RoccaD. "High-brightness injection-seeded soft-x-yay-laser amplifier using a solid target," Phys. Rev. Lett. 97, 123901 (2006)

Chapter 5, High Harmonic Seeding of Ne-like Soft X-ray Laser Amplifier

5.1Introduction

For future applications of soft X-rays, there is a great interest in the generation of very high brightness beams of soft x-ray radiation. An emerging fourth generation synchrotron sources designed to provide highly coherent soft x-ray beams of greatly increased brightness will open new opportunities in science [1]. However, as discussed in the previous chapters, the widespread use of intense soft x-ray light requires the development of significantly more compact and less expensive coherent sources. With this objective significant efforts are presently focused in the development of table-top sources based on either the amplification of spontaneous emission in a plasma [2], or the non-linear up-conversion of optical laser light into soft x-ray light [3]. The first of these processes is a promising route for the generation of high energy soft x-ray laser pulses of high monochromaticity using table-top devices. The achievement of high brightness requires the demonstration of high spatial coherence. At a wavelength of 46.9 nm intense laser beams with essentially full spatial coherence have been produced in capillary discharge plasmas [4]. However, the self amplification of spontaneous emission in the much denser laser-created plasmas required to generate soft x-ray laser beams at shorter wavelengths normally generates beams of limited spatial coherence [5]. To overcome this limitation seeding of the soft x-ray laser amplifier with either the spatially filtered radiation from a second soft x-ray amplifier [6, 7] or with a high harmonic of an optical laser has been investigated [8-10]. The latter scheme has the advantage of

producing significantly shorter (sub-picosecond) laser pulses and also requires less laser pump energy to generate the seed pulse. Saturated amplification of the 25th harmonic of a Ti:Sa laser was recently demonstrated in a 32.8 nm Ni-like Kr optical field ionization (OFI) soft x-ray laser amplifier [9]. However, the comparatively low plasma density (< $1x10^{19}$ cm^{-3}) at which optimum lasing occurs in OFI lasers results in a relatively low saturation intensity, which will ultimately limit the maximum brightness possible using that scheme. Also at present the collisional pumped OFI lasers are limited to wavelength above 30 nm. Therefore there is much interest in the demonstration of high harmonic seeding of collisional soft x-ray laser amplifiers based on the dense plasmas created by laser heating of solid targets, which have been demonstrated to operate in the gain saturation regime at wavelengths as short at 5.9 nm [11]. The up to two orders of magnitude larger electron density in this type of plasma amplifier results in a significantly increased saturation intensity and a broader laser linewidth, opening a route that can lead to higher laser pulse intensities and shorter pulsewidths. An early experiment performed in a Ne-like Ga plasma amplifier pumped by overlapping three 200 J optical laser beams onto a solid gallium target demonstrated the amplification of the harmonic seed, but only by a factor of about 3× [7].

5.2 Seeded X-ray Laser Using High Harmonic Generation

This chapter describes the first demonstration of saturated amplification of a high harmonic seed in the high density plasma of a transient collisional soft x-ray laser created by heating a solid target. The 32.6 nm table-top soft x-ray laser amplifier operating in the $3p^1S_0 \rightarrow 3s^1P_1$ line of Ne-like Ti described in chapter 3 [12] was used

to amplify a seed pulse from the 25th harmonic of Ti:Sa into the gain saturation regime. The results were obtained with a table-top laser operating at a repetition rate of 5 Hz, showing this is a practical scheme to produce extremely high brightness soft x-ray beams for applications in a small laboratory environment. The result is scalable to produce extremely bright lasers at very short wavelength. We also demonstrated that the resulting soft x-ray beam is essentially fully spatially coherent. The experiment also demonstrated that in special cases it is possible to simultaneously seed more than one laser line to produce highly coherent soft x-ray laser beams at two different wavelengths. The 27th harmonic of Ti:Sa was simultaneously amplified in the 30.1 nm $3d^1P_1 \rightarrow 3p^1P_1$ line of Ne-like Ti in the same plasma. We discuss the measurements in comparison with modeling results that describe the dynamics of seeded amplification in a dense collisionally pumped soft x-ray laser amplifier. The model simulations indicate the soft x-ray laser pulses are sub-picosecond in duration.

5.3 Demonstration of a Seeded Ne-like Ti Soft x-ray Laser amplifier experiment setup

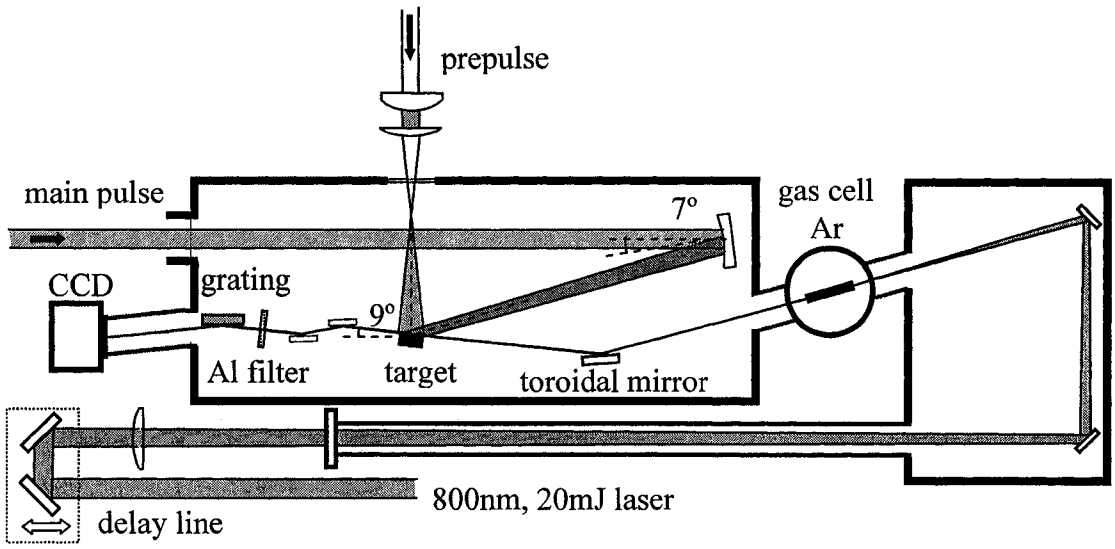

Figure 5.1 Experiment setup of the seeded soft x-ray laser amplifier, including high harmonic generation setup and solid target soft x-ray amplifier.

The experimental setup used to demonstrate seed amplification of a 32.6 nm solid target soft x-ray laser amplifier is schematically illustrated in Fig. 5.1. The Ti:Sa laser driver described in chapter 2 was operated operating at 5 Hz repetition rate both to create the harmonic seed pulse, and to pump the soft x-ray laser amplifier. A beam-splitter at the output of the second amplification stage was used to separate 30 mJ pulses for the generation of the harmonic seed. The pulses were compressed to about 50 fs within a grating compressor composed of two 1200 l/mm gold coated gratings. The rest of the energy was directed to the third amplification stage, where it was amplified to obtain a ~ 1.5 J pulse. As previously discussed, the soft x-ray laser amplifier consists of a line focus plasma of up to 4 mm in length generated by exciting a 2 mm thick polished Ti slab target. The plasma was formed by a 0.3 J pre-pulse, which arrives ~5 ns after a ~ 10 mJ pulse. The plasma is allowed to expand to reduce the density gradient and was subsequently rapidly heated by a ~800 mJ, 6.7 ps duration pulse impinging at a grazing incidence angle [13, 14] of 23 degrees onto the target. The pre-pulse beam was focused into a ~ 30 μm wide, 4.1 mm FWHM line focus. The short pulse was focused into a similar line focus utilizing a parabolic mirror of f = 76.2 cm positioned at 7 degrees from normal incidence. The target surface was tilted to form the grazing incidence angle of θ = 23 degrees with respect to the axis of the short pulse beam. At this angle of incidence $\theta = (n_e/n_c)^{1/2}$ refraction couples the pump beam energy into the plasma region where the electron density is $n_e = 2.6 \times 10^{20}$ cm^{-3}. High harmonic pulses of a few nJ energy were generated using 20 mJ drive pulses compressed to ~ 50 fs. These pulses were focused by a f = 5 m lens into an 8.8 cm long gas cell filled with 5 Torr of argon. The center wavelength of the

25th harmonic was matched to the 32.6 nm wavelength of the highest gain laser line in the Ti amplifier by adjusting the compressor. This broadened the duration of drive pulse to about 130 fs, reducing the energy of the seed pulse to 0.5-1 nJ. The harmonic seed beam exiting the gas cell was relay imaged onto a ~ 100 μm diameter spot at the entrance of the soft x-ray plasma amplifier using a gold coated toroidal mirror placed at a grazing angle of 9 degrees. A delay stage was placed before the 5 m focusing lens to adjust the delay time between the arrival of the harmonic pulses and main pump pulse. The output of the soft x-ray amplifier was analyzed using a flat field variable spaced 1200 lines/mm gold-coated spherical grating set at 3 degrees grazing incidence and a back-illuminated CCD detector placed 48 cm from the target. Two grazing incidence BK7 flats placed at grazing angle of 10 degrees were used to separate the soft x-ray laser from the Ti:Sa beam. Spectral filtering and attenuation was achieved using an Al filter.

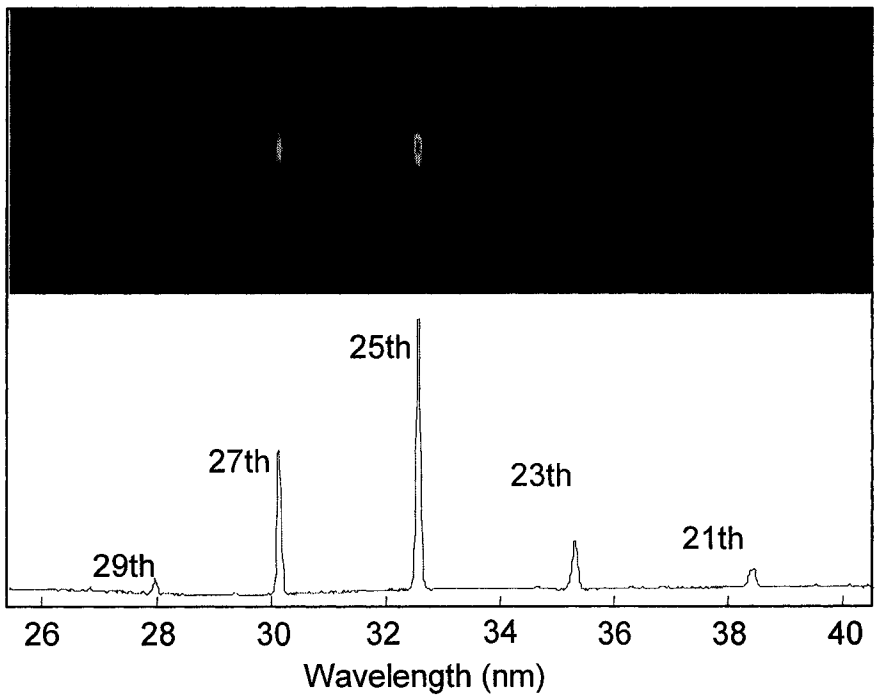

Figure 5.2 High harmonics generation in an 8.8 cm long Ar gas.

Figure 5.2 shows high harmonic spectrum generated using Ar gas. The Ar pressure we filled in gas cell is about 5.2 torr. With 50 fs pump pulses, we generated 1 nJ pulses at the 25^{th} order harmonic, corresponding to a wavelength of 32.2 nm. The wavelength of the 25^{th} order harmonic was tuned from 32.2 nm to 32.6 nm, to match the wavelength of Ne-like Ti laser [1], by moving the second grating in compressor 400 μm.

5.4 Results and Discussion

Figure 5.3 illustrates the dramatic increase in the output of a 3 mm long 32.6 nm Ne-like Ti amplifier and the large decrease in the beam divergence achieved by seeding the amplifier. The top frame (a) shows the spectra of the unseeded Ti soft x-ray laser amplifier, and the corresponding intensity distribution in the direction parallel to the target. The laser line at 32.6 nm dominates the spectra and has a divergence of about 10 mrad. The detection system can resolve the harmonic seed but not the laser linewidth of $\Delta\lambda/\lambda < 1\times10^{-4}$. Fig. 5.3 b shows the much lower divergence, about 1 mrad, but significantly broader spectra of the harmonic seed. The seeded amplifier output shown in Fig. 5.3 c consists of a highly monochromatic spectral line with an energy that is ~ 64 times larger that of the seed pulse. The FWHM beam divergence is observed to be about 2.2 mrad, considerably smaller than that of the unseeded laser.

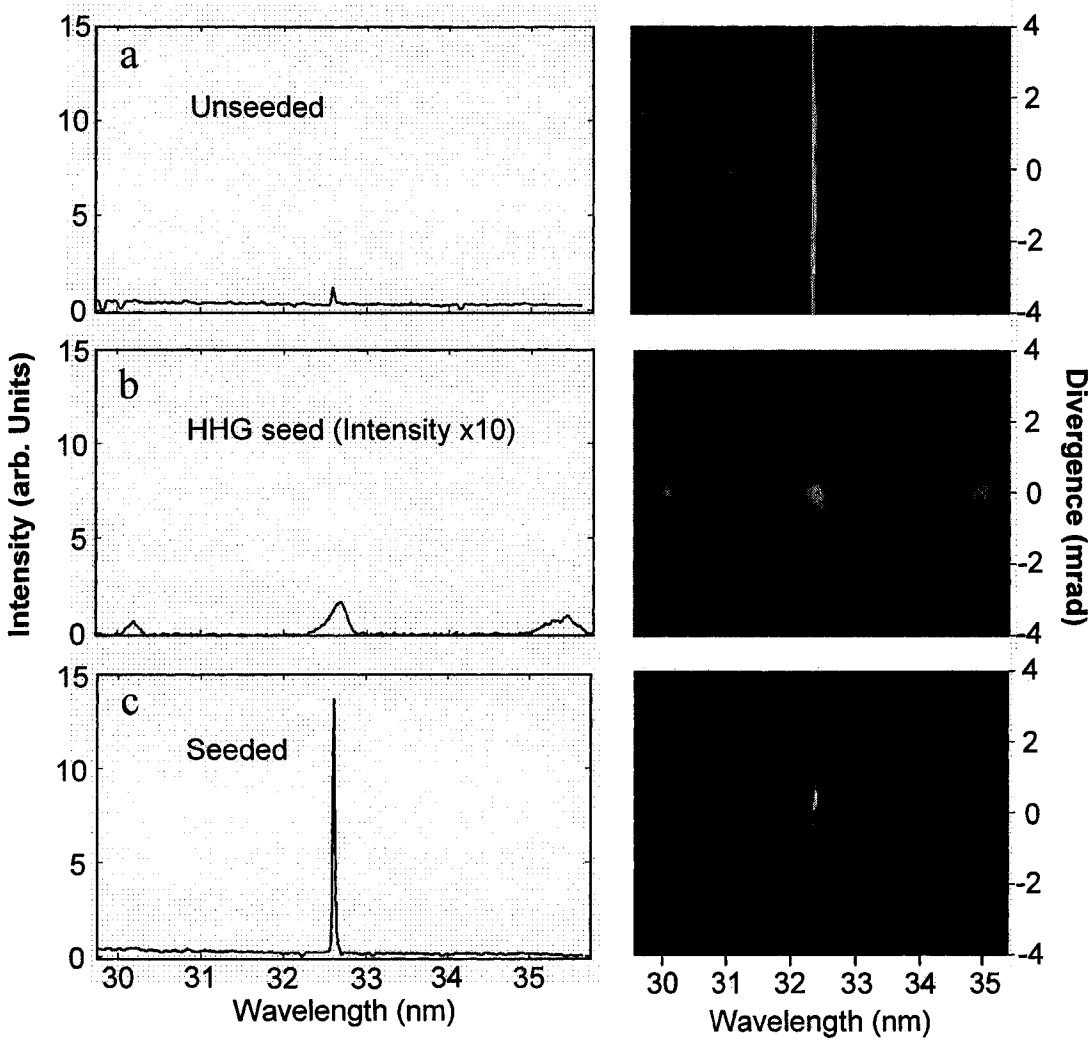

Figure 5.3 Spectra illustrating the relative intensity and beam divergence for; a) unseeded 32.6 nm soft x-ray laser amplifier; b) high harmonic seed pulse; c) seeded soft x-ray laser amplifier. The length of the plasma amplifier is 3 mm. The intensity scale of the seed pulse is magnified by 10 times.

Figure 5.4 shows the variation of the intensity of the amplified seed pulse as a function of delay between the 6.7 ps pump pulse and the arrival of the harmonic seed pulse. The time span during which the seed pulse is amplified is determined by the duration of the gain in the amplifier [15], and is about 5 ps. The maximum amplification is observed at delays between 2 and 4 ps.

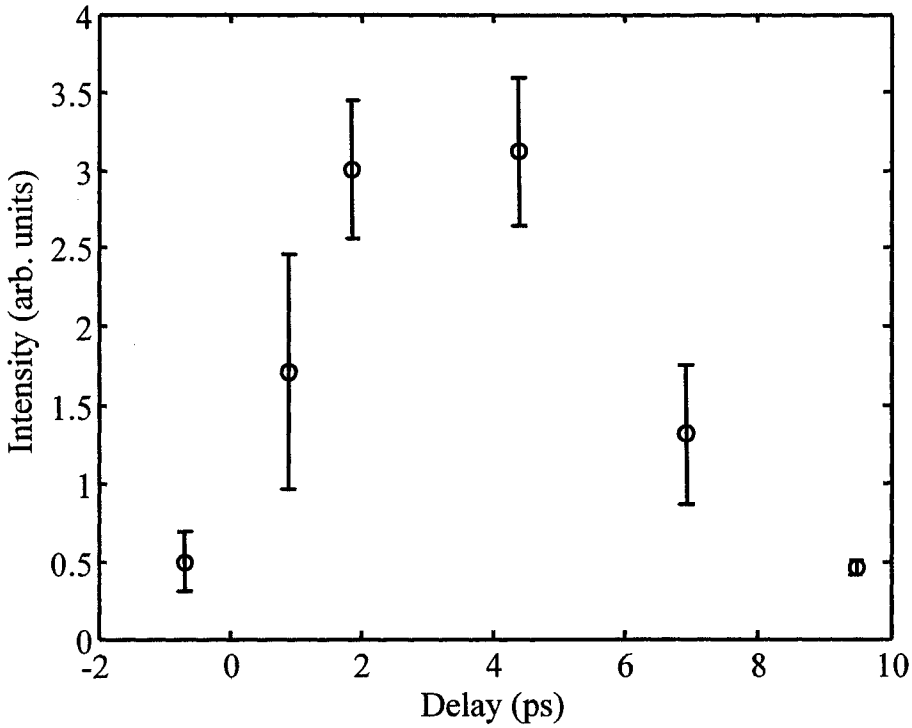

Figure 5.4 Variation of the intensity of the amplified seed pulse as a function of time delay between the peak of the 6.7 ps laser amplifier pump pulse and the arrival of the high harmonic seed pulse.

As illustrated in Fig. 5.5, we also observed it is possible to simultaneously inject seed two spectral lines. This is made possible by the fact that the wavelength separation between the 25^{th} and 27^{th} harmonics approximately matches the wavelength difference between the 32.6 nm and 30.1 nm lines of Ne-like Ti. For the pump conditions used in the experiment the unseeded output of the 30.1 nm laser line was observed to be very weak. However, when the wavelength of the harmonics was adjusted to simultaneously obtain sufficient overlap with the two laser lines, intense low divergence output was obtained for both lines.

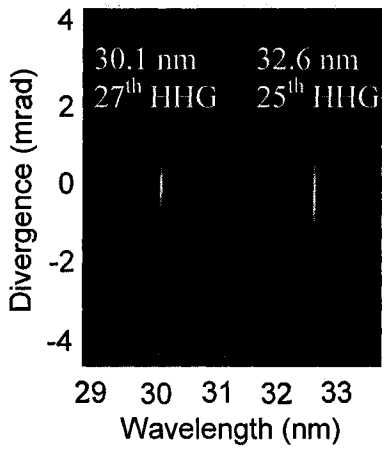

Figure 5.5 Spectra showing the simultaneous seeded amplification in the 32.6 nm and 30.1 nm lines of Ne-like Ti.

Figure 5.6 illustrates the measured energy increase of the energy of the 32.6 nm seed pulse as a function of amplifier length for a time delay of 4 ps. The data was obtained by varying the length of the target between 0 and 4 mm while maintaining both the seed pulse and the amplifier pump excitation conditions constant.

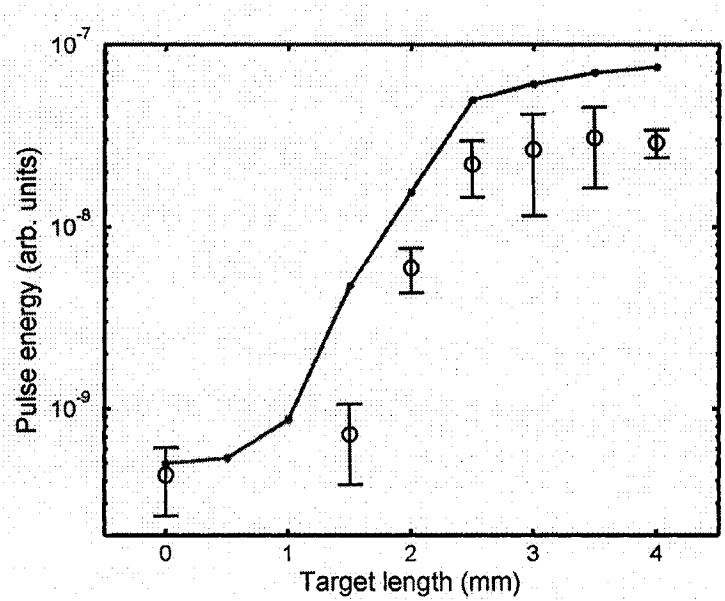

Figure 5.6 Measured and computed (continuous line) energy variation of the amplified seed pulse as a function of plasma amplifier length for the 32.6 nm line of Ne-like Ti. The measured beam reaches the saturation intensity after ~ 2.5 mm into the plasma.

The measurements are compared below with the results of model simulations in the same figure. The simulations were conducted using a 1½ dimension hydrodynamic/atomic physics code with multi-cell radiation transport to compute the evolution of the gain and plasma density profile of the Ne-like Ti amplifier [16]. The propagation and amplification of a 0.7 nJ seed pulse was computed using a ray tracing post processor code taking into account the effects of gain narrowing and gain saturation. The experimentally measured amplification behavior is very similar to that predicted by the code, and can be divided into three distinct phases. The first phase, which takes place in the first ~1 mm of the amplifier, is dominated by the gain narrowing of the seed pulse which initial 0.1 nm spectral bandwidth greatly exceeds that of the laser line. This leads to the amplification of only a fraction of its bandwidth, resulting in the observed slow initial seed pulse energy increase. When the seed pulse bandwidth narrows sufficiently to approach the laser linewidth, a second amplification phase starts in which a quasi-exponential increase in the energy of the seed pulse takes place. This rapid increase ends after about 2.5 mm into the amplifier. At this length, the measured amplified seed pulse energy reaches a value consistent with the computed saturation intensity for the 32.6 nm line of Ne-like Ti at a plasma density of 2.6×10^{20} electrons/cm^3. The third amplification phase corresponds to the gain saturated regime in which efficient energy extraction occurs. The maximum measured amplified seed pulse energy, 50-60 nJ, is similar to that predicted by the model. The model simulation of the pulse propagation in the amplifier predicts a pulse duration of 0.5-1 ps determined by the gain-narrowed

bandwidth of the amplified laser transition, which is an order of magnitude shorter than the amplifier gain lifetime.

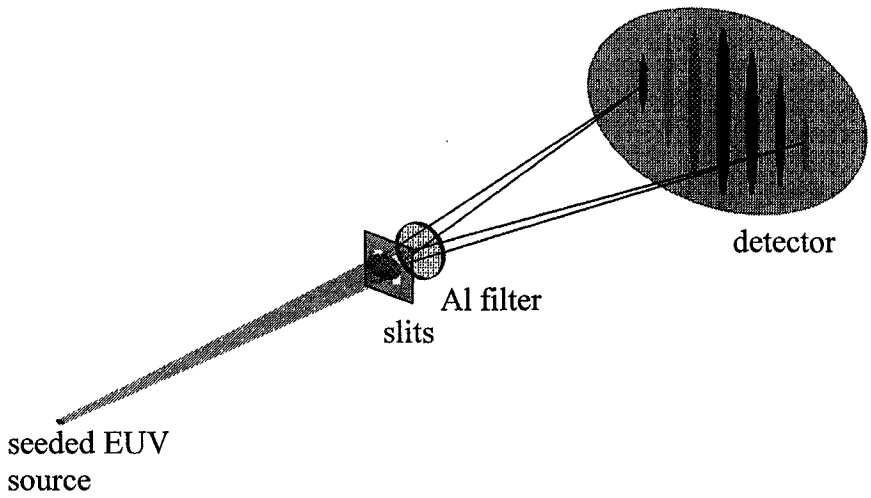

Figure 5.7 Schematic representation of the setup used to measure the spatial coherence of the seeded Ne-like Ti soft x-ray laser amplifier.

Measurements in grazing incidence transient collisional lasers have shown that the spatial coherence length is nearly an order of magnitude smaller than the beam diameter [5]. Pairs of 5 μm wide slits separated by 30, 75, 150 and 200 μm were placed at 10 cm from the exit of the amplifier, a location at which the FWHM beam diameter is about 200 μm (Fig. 5.7). These slits are same as what we used to measure spatial coherence of soft x-ray laser (ASE) in Chapter 4.

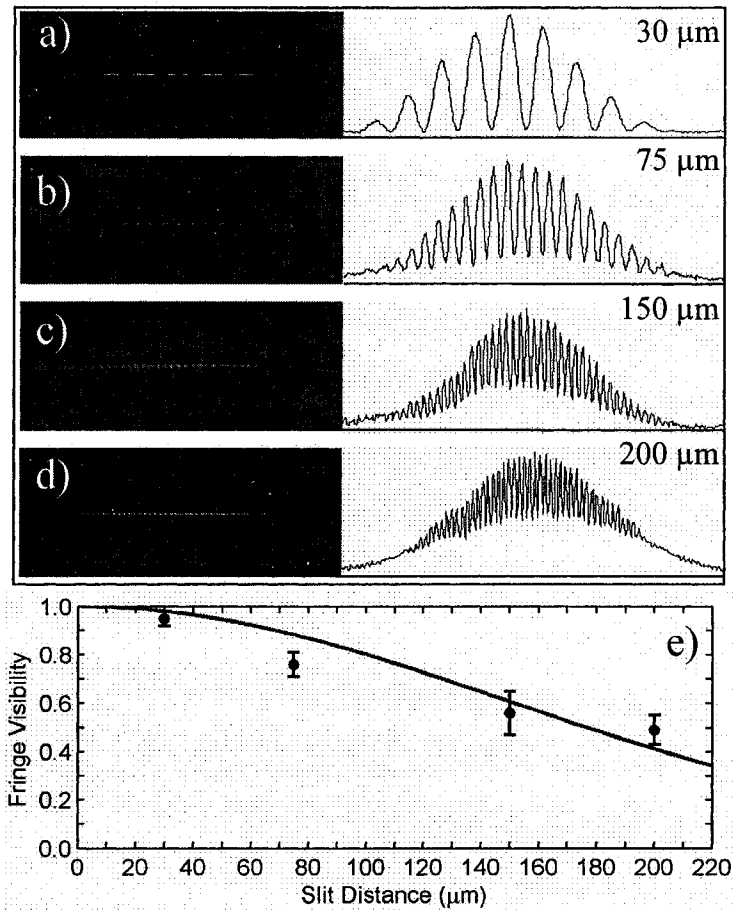

Figure 5.8 Results of Young's slit pair interference experiment for the output of the seeded 32.6 nm laser amplifier. a-d) Interferograms and their lineout for the slit separation indicated. e) Plot of the degree of coherence as a function of the slit separation.

The results of a Young's slit interference experiment illustrated in Fig. 5.8 show the degree of spatial coherence improves dramatically when the amplifier is seeded. The measured fringe visibility as a function of slit separation is illustrated in Fig. 5.8 e. A fit of the data with a Gaussian profile yields a coherent length of Lc = 150 um. The measurement shows the beam approaches full spatial coherence as the

majority of beam energy falls within a coherent length. The measured equivalent incoherent source diameter of this laser is about 6.9 μm.

Using the measured beam parameters mentioned above, and assuming a pulse duration of 0.5-1 ps and a horizontal divergence equal to half the vertical divergence, the peak spectral brightness of this source can be estimated to be $1.4\text{-}2.8\times10^{26}$ photons/(s mm^2 $mrad^2$ 0.01% bandwidth). Moreover, it should be noticed that the line width of this laser is nearly 20 times narrower than the 0.1 % bandwidth used to specify the brightness of synchrotrons and free electron lasers, an advantage in applications requiring high photon flux in a narrow bandwidth. With excellent temporal and spatial coherence these lasers are themselves attractive seed sources for mode control in free electron lasers.

5.5 Conclusion

In conclusion, we demonstrated the generation of an intense soft x-ray laser beam by saturated amplification of high harmonic seed pulses in a dense transient collisional soft x-ray laser plasma amplifier created by heating a titanium target. Amplification in the 32.6 nm line of Ne-like Ti generates laser pulses of sub-picosecond duration that are measured to approach full spatial coherence. The peak spectral brightness is estimated to be ~ 2×10^{26} photons s^{-1} mm^{-2} $mrad^{-2}$ (0.01% bandwidth). The scheme is scalable to produce extremely bright lasers at very short wavelength.

References

[1] V. Ayvazyan, N Baboi, J. Bahr, V. Balandin *et al*, "First operation of a free-electron laser generating GW power radiation at 32 nm wavelength," Eur. Phys. J. D **37**, 297, (2006).

[2] H. Daido, "Review of soft x-ray laser researches and developments," Rep. Prog. Phys, **65**, 1513, (2002); J. J. Rocca, Rev.Sci. Inst **70**, 3799, (1999).

[3] H. C. Kapteyn et al, "Extreme Nonlinear Optics: Coherent X Rays from Lasers," Physics Today 58, 39 (2005).

[4] Y. Liu, M. Seminario, F. G. Tomasel, C. Chang et al, "Achievement of Essentially Full Spatial Coherence in a High Average Power Soft X-Ray Laser," Phys. Rev. A **63**, 033802, (2001).

[5] M. A. Larotonda, B. M. Luther, Y. Wang. Y. Liu, "Characteristics of a Saturated 18.9 nm Tabletop Laser Operating at 5 Hz Repetition Rate", IEEE J. Sel. Top Quantum Electr. **10**, 1363 (2004).

[6] B. Rus, C. L. S. Lewis, G. F. Cairns *et al.* "Demonstration of amplification of a polarized soft-x-ray laser beam in a neonlike germanium plasma," Phys. Rev. A. **51**, 2316, (1995)

[7] M. Nishikino, M. Tanaka, K. Nagashima, M. Kishimoto, "Demosntration of an x-ray laser at 13.9 nm with full spatial coherence", Phys. Rev. A **68**, 061802(R), (2003).

[8] T. Ditmire, M. H. R. Hatchinson, M. H. Key, C. L. C. Lewis *et al*, "Amplification of XUV harmonic radiation in a gallium amplifier", Phys. Rev. A, **51**, R4337, (1995).

[9] P. Zeitoun, G. Faivre, S. Sebban, T. Mocek, "A high-intensity highly coherent soft X-ray femtosecond laser seeded by a high harmonic beam" Nature ,**431**, 426, (2004)

[10] T. Kawachi, K. Nagashima, M. Kishimoto, N. Hasagawa, "Recent progress in x-ray laser research in JAERI ". SPIE Vol. **5919**, 59190L, (2005).

[11] R. Smith, G. J. Tallents, J. Zhang *et al*, "Saturation behavior of two x-ray lasing transitions in Ni-like Dy," Phys. Rev. A 59, R47, (1999).

[12] D. Alessi, B. M. Luther, Y. Wang, M. A. Larotonda, M. Berrill, and J. J. Rocca, "High repetition rate operation of saturated tabletop soft x-ray lasers in transitions of neon-like ions near 30 nm," Opt. Express **13**, 2093 (2005).

[13] R. Keenan, J. Dunn, P. K. Patel *et al*, "High-Repetition-Rate Grazing-Incidence Pumped X-Ray Laser Operating at 18.9 nm," Phys. Rev. Lett. **94**, 103901, (2005).

[14] B. M. Luther, Y. Wang, M. Larotonda, D. Alessi, M. Berrill, M. Marconi, V. Shlyaptsev, J. J. Rocca, "Saturated high-repetition-rate 18.9-nm tabletop laser in nickellike molybdenum," Opt. Lett. **30** 165 (1999).

[15] T. Mocek, S. Sebban, G. Maynard *et al*, "Absolute Time-Resolved X-Ray Laser Gain Measurement," Phys. Rev. Lett. **95**, 173902, (2005).

[16] M. Berrill and J. J. Rocca, unpublished.

Chapter 6 Summary and Applications

This chapter summarizes the results of the soft x-ray laser development work discussed in the preceding part of this dissertation, and describes the one of these lasers in high resolution imaging. The chapter concludes with a brief discussion of future work opportunities.

6.1 Summary

The work conducted as part of this dissertation resulted in the demonstration of high repetition rate table top soft x-ray lasers for numerous wavelengths ranging from 32.6 nm to 10.9 nm. Of particular interest for applications is the first demonstration of 5 Hz repetition rate lasers operating in the gain saturated regime with average powers in excess of 1 μW for wavelengths as short as 13.2 nm.

The approach utilized to obtain these results consisted in the generation of large population inversions in plasmas heated at grazing incidence with picosecond laser pulses generated by a terawatt table-top Ti:sapphire laser system. The laser transitions excited correspond to transitions of Ni-like ions. Lasing in the gain-saturated regime was also obtained at wavelengths near 30 nm using transitions of Ne-like ions. The heating of a pre-created plasma with a fast optical laser pulse at grazing incidence allowed for very efficient heating of the plasma, making possible the operation these lasers in the gain-saturation regime with short pulse pump energies of no more than 1 J. The grazing incidence configuration takes advantage of the refraction of the pump beam in the plasma to efficiently deposit a large fraction of

its energy into a pre-selected region of the plasma with optimum electron density for amplification. A remarkable property of refraction is that it allows to precisely define this electron density based on only two parameters, the grazing incidence angle θ and the laser pump wavelength: $\theta = (n_e / n_{cp})^{1/2}$, where n_e is the maximum electron density within the amplification region and n_{cp} is the critical density at the wavelength of the pump. Hence when the grazing angle is changed, different parts of the density profile formed by the pre-pulse are preferentially heated. At a given incidence angle the pump beam is reflected at the point where it encounters the corresponding selected density n_e, significantly increasing the path length of the pump beam and therefore allowing for a large fraction of the pump energy (typically 20 to 50 percent) to be absorbed into the gain region. In addition, the fact that the grazing incidence pumping is intrinsically traveling wave for the range of incidence angles of interest simplifies the experimental set up. A new type of solid helicoidal target was also demonstrated, that will allow for uninterrupted 10 Hz operation for periods of a few hours.

The lasers were thoroughly characterized in term of small signal gain, output pulse energy, pulse duration, beam divergence and spatial coherence. Streak camera measurements for the 13.9 nm Ni-like Ag and 13.2 nm Ni-like Cd laser showed that the laser pulses produced have a pulse duration of about 5 ps. Young's interference measurements showed that the spatial coherence of these lasers is modest. While this is not a limitation for application such as high resolution imaging where high coherence is undesirable, it can impact other applications such as interferometry.

The desire to obtain high repetition rate table-top soft x-ray lasers with highest spectral brightness, shortest pulse duration, defined polarization and high spatial coherence motivated the seeding of the soft x-ray amplifiers with high harmonic pulses. Amplification of pulses from the 25^{th} harmonic pulses of Ti:sapphire laser in a 32.6 nm line of Ne-like Ti was demonstrated to generate highly monochromatic laser pulses of sub-picosecond duration that are measured to approach full spatial coherence. The peak spectral brightness is estimated to be $\sim 2\times10^{26}$ photons/(s mm^2 $mrad^2$ 0.01% bandwidth). The scheme is scalable to produce extremely bright lasers at very short wavelength.

These new lasers open the possibility of conducting numerous experiments requiring intense beams of soft x-ray light on a table-top. The next section summarized result of a high resolution soft x-ray microscopy experiment made possible by the demonstration of the 13.2 nm wavelength Ni-like Cd laser described in the previous chapters, with achieved record high resolution for a photon-based table-top broad area microscope.

6.2 Application to High Resolution Soft X-ray Imaging

An important application of soft x-ray lasers is microscopy. At present, the best spatial resolution for photon-based microscopes, 15 nm, has been obtained by using soft-x-ray illumination from a synchrotron source [1]. However, the widespread use of short wavelength microscopy requires the development of more compact and more widely accessible instruments. The new high repetition rate table-top lasers developed as the result of the work described in the previous chapters created a path

to the realization of very high-resolution tabletop imaging tools. By combining the output of the 13.2 nm Ni-like Cd laser with diffractive optics record high spatial resolution, better than 38 nm, was demonstrated obtained with exposures as short as several seconds [2].

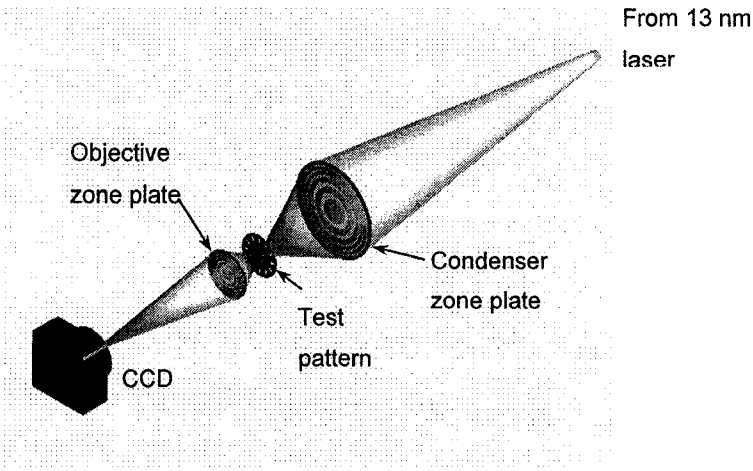

Figure. 6.1 Schematic diagram of the 13.2 nm wavelength imaging system

The soft x-ray laser microscope is schematically illustrated in Fig. 6.1. The illumination source is a 5 Hz repetition rate tabletop laser Ni-like Cd laser capable of generating highly monochromatic 13.2 nm wavelength light with microwatt average power [3]. A condenser zone plate collects the laser light and focuses it onto the test pattern, and an objective zone plate forms the image of the test pattern onto a back illuminated charge coupled detector (CCD). This compact microscope takes advantage of the high brightness, high monochromaticity, and directionality of the new tabletop soft-x-ray lasers to produce high resolution images.

The actual spatial resolution of the microscope was experimentally determined by imaging the portion of the test pattern containing the periodic lines and

spaces. Figure 6.2 shows an image of gratings with different periods, all of them with nominal 1:1 line/space ratio. The image was obtained with the Δr = 80 nm objective at λ = 13.9 nm using a 20 second exposure. The lines with 90, 75, and 60 nm half-periods are clearly resolved (Fig. 6.2 a). The lineout of the images reveals a modulation in the 73 – 87 % range. The best resolution was obtained using the objective with Δr = 50 nm and λ=13.2 nm illumination from the Ni-like Cd laser. Similar images of the smallest available for these experiments, lines and spaces with 38 nm half-period, resulted in ~ 70 % intensity modulation (Fig. 6.2 b). This result clearly demonstrates that the spatial resolution of the microscope is better than 38 nm.

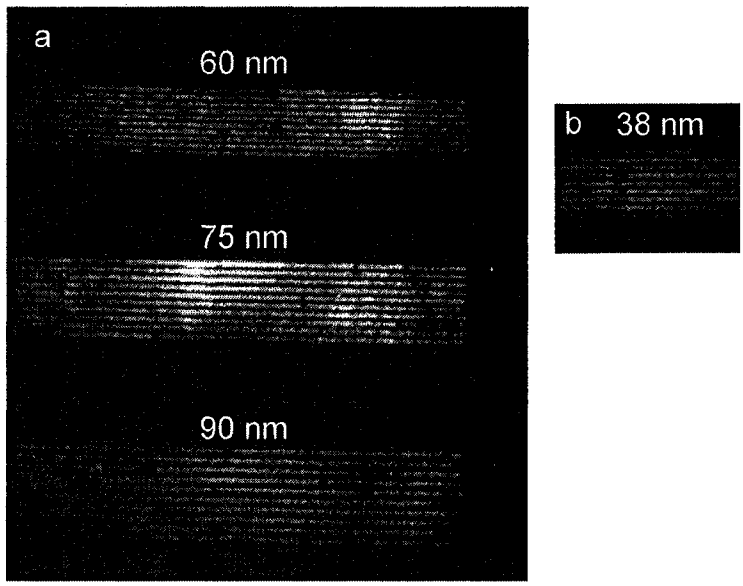

Figure 6.2. a) 90, 75, and 60 nm half-period line patterns are well resolved with the 13.9 nm wavelength microscope. This image was obtained with Δr = 80 nm zone plate and 20 sec exposure time. b) 38 nm half-period line patterns are resolved with the 13.2 nm wavelength, with Δr = 50 nm zone plate and 20 sec exposure time.

6.3 Future Work

The results presented here open numerous opportunities and challenges for the future. These include the optimization of these sources to produce unprecedented high average powers of coherent soft x-ray light on a table-top set up. Of significant interest is also the extension of the results to shorter wavelengths, in particular the demonstration of high coherence, high brightness seeded amplifiers operation at 13 nm and beyond.

Aside from the microscopy application described above, these sources are of interest for several other applications. These include the metrology necessary for the implementation of extreme ultraviolet lithography as a fabrication tool for the fabrication of the future generations of integrated circuits. Specifically, the wavelength of the Ni-like Cd laser, 13.2 nm, is within the bandwidth of the Mo-Si multilayer coatings of the mirrors and masks that will be used for extreme ultraviolet lithography. This makes possible the implementation of interferometry tools to inspect and align the lithography projection optics as well as the possible implementation of defect inspection tools. This is just one example, as the opportunities opened by these new high repetition rate soft x-ray lasers also include surface physics, photochemestry and photophysics both in the gas phase and on surfaces, and plasma studies.

References

[1] W. Chao, B. D. Harteneck, J. A. Liddle, E. H. Anderson, and D. T. Attwood, "Soft X-ray microscopy at a spatial resolution better than 15nm." Nature 435, 1210 (2005).

[2] G. Vaschenko, C. Brewer, F. Brizuela, Y. Wang, M. A. Larotonda, B. M. Luther, M. C. Marconi, J. J. Rocca, C. S. Menoni, E. H. Anderson, W. Chao, B. D. Harteneck, J. A. Liddle, Y. Liu, and D. T. Attwood "Sub-38 nm resolution tabletop microscopy with 13 nm wavelength laser light." Opt. Lett. 31, 1214 (2006).

[3] K. Goldberg, P. P. Naulleau, P. E. Denham, S. B. Rekawa, K. Jackson, E. Anderson, and J. A. Liddle, "At-wavelength alignment and testing of the 0.3 NA MET optic" J.Vac. Sci. Technol. B 22, 2956 (2004).